FLUIDIZED SYSTEMS: A STUDY OF REACTION RATES

(The Reduction of a Lead Sinter by Hydrogen)

by

J.C. LILL, B.E.

of the

Department of Mining, Metallurgical and Chemical Engineering

A THESIS

Submitted for the Degree of Doctor of Philosophy

in the

Faculty of Engineering of the University of Adelaide

August

1961

ACKNOWLEDGEMENTS

The author is indebted to Professor E.C.R. Spooner, who initiated this project, for his continuous interest in the work, and to Dr. R.V. Culver for his advice and encouragement during the investigation.

He also wishes to thank Mr. G. Armstrong who assisted in part of the experimental work and the Departmental workshop staff for their assistance in the construction of apparatus.

The assistance of the Australian Atomic Energy Commission, which provided financial support for the project in the form of a Studentship and an Equipment Grant, is also gratefully acknowledged.

TABLE OF CONTENTS

TABLE OF CONTENTS (contd.)

TABLE OF CONTENTS (contd.)

TABLE OF CONTENTS (contd.)

TABLE OF CONTENTS (contd.)

TABLE OF CONTENTS (contd.)

TABLE OF CONTENTS (contd.)

TABLE OF CONTENTS (contd.)

LIST OF TABLES

LIST OF FIGURES

LIST OF FIGURES (contd.)

LIST OF FIGURES (contd.)

SUMMARY

This thesis deals with the reduction of a typical updraught lead sinter by hydrogen in fluidized systems, and the project forms part of a fundamental investigation of a proposed new process for the production of metallic lead.

A literature review established that there was no published information relating to the reduction of lead oxide in fluidized systems, although the kinetics of the hydrogen reduction of pure lead monoxide have been extensively studied in a differential, fixed bed, reactor.

The chemical and physical structures of lead sinters are unknown and are very complex. However, a thermodynamic analysis of a simplified system of reactions, based on reported data relating to the composition of lead sinters, suggests that equilibrium considerations are unlikely to affect the measured reaction rates.

Lead sinter contains a number of compounds reducible by hydrogen, but, experimentally, the overall reaction rate indicated by the rate of water formation is a satisfactory measure of the rate of reduction of the oxidized lead compounds. This overall reaction rate is increased by decreasing the particle size and increasing the reaction temperature. The measured reaction rate is approximately proportional to the twelfth power of the absolute temperature, and the time required for a given reduction is dependent on the initial surface area; this initial surface area is directly related to the average particle size.

For equivalent system conditions the reaction rate is faster in a fluidized bed than in a fixed bed; the efficiency of gas-solid

contact is increased by the intense agitation and circulation which occurs in the fluidized beds. However, the fluidization technique is unsuitable for the reduction of a material such as lead sinter.

A preliminary study of the reaction in a small vertical flow reactor indicates that a transport system may provide the most favourable method of reducing lead oxide by hydrogen. Fine particles of lead sinter (-200 +325 # B.S.S.) can be almost completely reduced at 900°C during passage through a 1 in. diameter tube, 11 ft long.

I hereby certify that this Thesis contains no material which has been accepted for the award of any other Degree or Diploma in any University and that, to the best of my knowledge and belief, this Thesis contains no material previously published or written by another person except when due reference is made in the text of the Thesis.

J.C. LILL

1. INTRODUCTION

This thesis, which is concerned with the reduction of impure lead oxide by hydrogen in fixed and fluidized reactors, deals with one aspect of a general investigation in progress within this Department. The aim of this programme is to examine a possible alternative to the present method of producing metallic lead from finely divided lead flotation concentrates.

The conventional procedure is based on the lead blast furnace, which was designed originally to handle lump, oxidized, ores, the deposits of which are now almost exhausted. Consequently, the material delivered to the smelters now consists almost exclusively of flotation concentrates and it is necessary to convert this finely divided lead sulphide into an oxidized, agglomerated, condition suitable for use as a blast furnace feed. The existing extraction process therefore involves the two stages of

(a) simultaneous roasting and sintering, and

(b) smelting,

and in the sintering process granulated slag and other diluent materials are added to the high grade lead concentrates. This procedure also possesses other undesirable features.

The proposed alternative method, which is based on roasting with air and smelting with H_2 or CO in fluidized systems, avoids both the sintering process and the undesirable dilution of the relatively pure flotation concentrates. It also enables the inherently high reaction rates obtained with small particle sizes to be utilized.

The roasting of lead sulphide will be the subject of two future investigations - one aimed at elucidating the kinetic mechanisms and the other involving a study of the oxidation reaction in fluidized bed reactors. Similarly, the present investigation deals with the reduction of lead oxide

in fluidized systems and is complementary to a concurrent study of the kinetics of the reduction of pure lead oxide in fixed beds.

Since lead oxide tends to stick at temperatures below 800°C and reduction converts the solids to liquid lead the study of the reduction of pure lead oxide in fluidized systems presents obvious difficulties. Consequently, an impure form of lead oxide is more suitable for the present investigation; the presence of inert material decreases the tendency to stick and provides a supporting matrix for the liquid lead formed. The material used in the experimental work is obtained by crushing and grinding a bulk sample of a typical updraught lead sinter containing 42.0 mass per cent lead. This is readily obtainable and, in addition, data relating to the reactivity and surface areas of various size fractions of this sinter are available as a result of a concurrent investigation proceeding within the Department. Hydrogen has been used as the reducing agent in preference to CO because of its ready availability and non-toxic properties.

The use of an impure form of lead oxide decreases the practical difficulties associated with a study of the rate of reduction of PbO in fluidized systems; however, it presents additional theoretical problems. Firstly, lead sinter has a complex chemical composition and contains a number of compounds reducible by hydrogen. Consequently, the kinetic data obtained for pure lead monoxide are not directly applicable to the present case. Secondly, the general technique used to obtain kinetic data for heterogenous reactions, viz., measurement of the mass flow rate of the reducing gas before and after passage through an isothermal bed of the solid reactants, will measure the overall reaction rate in the present case; therefore, since the investigation is basically concerned with the reduction of lead oxide, it is essential to establish the relation between the reduction

of the oxidized lead compounds to metallic lead and the overall sinter reduction.

The first part of the experimental programme, which involves a study of the reduction of lead sinter by hydrogen in a differential bed reactor, provides a basis for evaluating the results obtained in the fluidized reactors, and has as its main objectives

(1) the measurement of kinetic data for comparison with the results obtained in the fluidized bed reactor,

(2) the determination of the relation between the overall reaction rate and the rate of reduction of the oxidized lead compounds,

and (3) the provision of a basis for relating results obtained in the present investigation to the data available on the kinetics of the reduction of pure lead oxide.

The remaining experimental work relates to the study of the reduction of the lead sinter in fluidized reactors and deals with the effect of system variables such as temperature and particle size on the rate of reaction.

The thesis may be separated into five broad divisions, namely, a thermodynamic investigation of the reactions occurring during the reduction of a lead sinter by hydrogen followed by a summary of the relevant literature, the study of the reaction in a fixed bed reactor, the determination of reaction rates in fluidized systems, and, finally, a summary and conclusions; these aspects are dealt with in turn.

2. THERMODYNAMIC CONSIDERATIONS IN THE HYDROGEN REDUCTION OF LEAD SINTERS

Lead sinter is a heterogeneous solid containing many chemical compounds which may or may not be reducible by hydrogen under a given set of system conditions, and it is necessary to have some basis for selecting the reactions which can occur within a given range of temperature and pressure. In the absence of experimental data the classic method of attacking this problem involves a thermodynamic analysis of the system, and this application of thermodynamics is described in various texts [1,2], (1950) and (1943). Basically, the method consists of obtaining the relation between the change in free energy, designated by ΔF, and the temperature for all the possible chemical equations which can be formulated from the system components. The magnitude of ΔF is dictated by the reaction temperature and the activities of the participating substances, and this change in free energy is a measure of the tendency for the reaction to proceed at the specified conditions [3] (1950). In this respect, it is generally true [4] (1948) that significant decrease in free energy for a high temperature reaction indicates that the reaction will occur. Conversely, an increase in free energy suggests that the reaction will probably not take place to any great extent.

2.1 Physical and Chemical Structure of Typical Updraught Lead Sinters

The primary requirement for the application of thermodynamic laws to a heterogeneous solid is a firm knowledge of the chemical composition and physical state of the various compounds existing in the solid. This Section, which summarizes the available information relating to the physical and chemical structure of lead sinters, provides a basis for the selection of equations to represent the reactions which may take place during the hydrogen reduction of a lead sinter.

The mechanisms involved in the sintering process are complex and only slightly understood. Briefly, the technique employed at Port Pirie can be described as follows: lead flotation concentrates are mixed with other materials in the following approximate proportions,

lead concentrate	= 62.0 mass percent
lead-bearing siliceous ore	= 1.0
limesand	= 5.5
Siliceous sand	= 1.0
ironstone	= 2.5
zinc plant residue	= 3.0
plant sludges	= 3.0
return granulated blast furnace slag	= 20.5
flue dust	= 1.5

This raw feed is mixed with return, crushed, lead sinter in approximately 1:1 proportion by weight and about 2 per cent of coke fines are added; this mixture is then charged to the sintering machine. During updraught sintering a hot reaction zone travels from the bottom to the top of the bed and numerous reactions take place between the compounds present. The mechanisms are unknown, but it is probable that the primary reaction is the oxidation of PbS to PbO. This lead oxide may then react with more PbS to produce metallic lead which may, in turn, be oxidized to PbO [5] (1958). While these chemical reactions are taking place melts are produced which bond the bed particles together. At the same time volatile compounds such as PbO, PbS and ZnS vaporize in the hot zone and condense in the cold zones above the hot zone [6] (1958).

Manson [7] (1958), concludes from microscopic examinations of thin sections and polished specimens of updraught sinters that part of the charge attains a high degree of fusion while some of the feed material is retained in its original form in a matrix of fused material. The major altered components in the sinter are litharge and lead oxide compounds, and metallic lead, spinels and ferrites of variable composition, and melitites can also be identified. The litharge, which frequently occurs in patches around metallic lead particles, is observed to grade off into a yellow-green matrix of lead oxide and lead silicate compounds which form most of the sinter bond.

Woods and Harris [6] (1958), who studied the factors affecting the production of lead-zinc sinters, conclude that $ZnSO_4$, $PbSO_4$, and $CaSO_4$ are unstable in air containing 1% SO_2 by volume above the temperatures shown, viz.,

$ZnSO_4$	—	805°C
$PbSO_4$	—	1004°C
$CaCO_4$	—	1255°C

The peak temperature reached in hard sintering is approximately 1300°C, and it is therefore likely that $CaSO_4$ is the only normal sulphate present in the sinter. However, there may be various basic sulphates present, since basic lead sulphates in particular are often more stable than the normal form. Also, provided the temperature does not exceed 1350°C, the iron oxides will be in the form of hematite, Fe_2O_3, rather than magnetite, Fe_3O_4 [6, 8] (1958).

The preceding discussion reveals that lead sinter has a complex physical and chemical structure; physically it consists of unaltered feed material, which may be hard or soft, held in a matrix of fused compounds of

indeterminate character; chemically the composition varies from unaltered materials such as limesand, siliceous sand, ironstone, blast furnace slag and lead sulphide to fused materials of varying composition such as lead oxide and lead silicate compounds and a wide range of spinels, ferrites, and melitites.

2.2 Possible Reactions in the Reduction of Lead Sinters

The following analysis of the system has been based on the presumption that if the hydrogen reduction of two oxides such as CaO and SiO_2 is thermodynamically unlikely then the reduction of compounds of the two oxides such as $CaO.hSiO_2$ is also unlikely to proceed. Conversely if PbO is reducible by hydrogen, then it is assumed that lead silicates are also likely to reduce under the same conditions. The necessity to assign chemical compositions to such compounds as zinc ferrite and lead silicate is therefore avoided and the major elements in lead sinter are considered to exist in the combined state as oxides, sulphates and sulphides.

By considering the above assumptions in conjunction with the data on the composition of updraught lead sinters cited in Section 2.1 the following equations have been selected to represent the possible reactions occurring during the reduction of a lead sinter by hydrogen:

$$PbO + H_2 \rightleftharpoons Pb + H_2O \qquad (1)$$

$$PbS + H_2 \rightleftharpoons Pb + H_2S \qquad (2)$$

$$ZnO + H_2 \rightleftharpoons Zn + H_2O \qquad (3)$$

$$3Fe_2O_3 + H_2 \rightleftharpoons 2Fe_3O_4 + H_2O \qquad (4)$$

$$Fe_3O_4 + H_2 \rightleftharpoons 3FeO + H_2O \qquad (5)$$

$$FeO + H_2 \rightleftharpoons Fe + H_2O \qquad (6)$$

$$\tfrac{1}{4}CaSO_4 + H_2 \rightleftharpoons \tfrac{1}{4}CaS + H_2O \qquad (7)$$

$$CaO + H_2 \rightleftharpoons Ca + H_2O \quad \text{——————(8)}$$

$$\tfrac{1}{2}SiO_2 + H_2 \rightleftharpoons \tfrac{1}{2}Si + H_2O \quad \text{——————(9)}$$

$$MnO + H_2 \rightleftharpoons Mn + H_2O \quad \text{——————(10)}$$

$$\tfrac{2}{3}Al_2O_3 + H_2 \rightleftharpoons \tfrac{4}{3}Al + H_2O \quad \text{——————(11)}$$

The so-called "roast reaction", $2PbO + PbS \rightleftharpoons 3Pb + SO_2$, which occurs in the solid state at the temperatures concerned in the present investigation, is considered unlikely to proceed and is omitted from the possible reactions.

In the main the standard free energy changes, $\triangle F^\circ_T$, for these reactions have been calculated from data presented by Richardson and Jeffes[4] (1948) and Osborn [3] (1950). Values obtained from other sources are specifically referred to in TABLE 1, which lists the values of $\triangle F^\circ_T$ for each reaction at temperatures in the range 400°C to 1000°C.

TABLE 1

THE EFFECT OF TEMPERATURE ON THE CALCULATED FREE ENERGY CHANGE FOR POSSIBLE REACTIONS DURING THE REDUCTION OF LEAD SINTER

Reaction	Standard Free Energy Change, $\triangle F^\circ_T$, k cal/ g. mole H_2						
	400°C	500°C	600°C	700°C	800°C	900°C	1000°C
$PbO+H_2$ —— $Pb+H_2O$ [9]	-14.10	-15.10	-16.12	-17.15	-18.18	-19.20	-20.20
$PbS+H_2$ —— $Pb+H_2S$	11.75	11.0	10.25	9.5	8.75	8.00	7.25
$ZnO+H_2$ —— $Zn+H_2O$ [10]	29.90	26.0	22.24	18.44	14.64	10.70	7.0
$3Fe_2O_3+H_2$——$2Fe_3O_4+H_2O$ [11]	-18.10	-19.3	-20.60	-22.02	-23.5	-25.25	-28.0
$Fe_3O_4+H_2$——$3FeO+H_2O$ [11]	4.0	2.85	1.68	0.50	-0.63	-1.82	-2.95
$FeO+H_2$——$Fe+H_2O$ [11]	2.30	2.05	1.82	1.60	1.38	1.18	0.93

TABLE 1 (cont.)

Reaction	Standard Free Energy Change, ΔF°_T, k cal/g. mole H_2						
	400°C	500°C	600°C	700°C	800°C	900°C	1000°C
$\frac{1}{4}CaSO_4 + H_2 \rightarrow \frac{1}{4}CaS + H_2O$	-7.8	-8.58	-9.35	-10.10	-10.8	-11.5	-12.2
$CaO + H_2 \rightarrow Ca + H_2O$	85.4	84.4	83.37	82.32	81.3	80.3	79.3
$\frac{1}{2}SiO_2 + H_2 \rightarrow \frac{1}{2}Si + H_2O$	39.55	38.75	37.95	37.10	36.27	35.5	34.7
$MnO + H_2 \rightarrow Mn + H_2O$	30.31	29.91	29.52	29.13	28.73	28.33	27.93
$\frac{2}{3}Al_2O_3 + H_2 \rightarrow \frac{4}{3}Al + H_2O$	64.20	63.30	62.40	61.60	60.70	59.80	58.90

Now, as Osborn [3] (1950) points out, the relation between the actual free energy change, ΔF_T, and the standard free energy change is

$$\Delta F_T = \Delta F^\circ_T + RT \ln \frac{a_M^m \cdot a_N^n}{a_A^a \cdot a_B^b} \qquad \text{——————(12)}$$

for a reaction of the general type

$$aA_{solid} + bB_{gas} \rightleftharpoons mM_{solid} + nN_{gas} \qquad \text{——————(13)}$$

At equilibrium $\Delta F_T = 0$, and hence

$$\Delta F^\circ_T = -RT \ln \frac{a_M^m \cdot a_N^n}{a_A^a \cdot a_B^b} \qquad \text{——————(14)}$$

Normally, for the reduction of oxides, the solid reactants and products are mutually insoluble and the solid state activities are taken as unity. Under these conditions equation (14) reduces to

$$\Delta F^\circ_T = -RT \ln K_p \qquad \text{——————(15)}$$

where K_p = gas phase equilibrium constant.

Now, for the reaction given in equation (13), K_p is approximately equal to the ratio of the partial pressures, i.e. $(p_N)^n/(P_B)^b$. Consequently, the calculated standard free energy change can be used to estimate the equilibrium gas composition at a given temperature. However, in the present case, the basic approach outlined above must be modified to allow for the facts that

(i) the solid reactants may be in the form of solid solutions, and

(ii) the system has been simplified by assuming that the reduction of compounds such as lead silicate and zinc ferrite is equivalent to reducing the constituent compounds separately.

The formation of a solid solution decreases the activity of a solid and it follows from equation (14) that the equilibrium gas phase composition $(p_N{}^n/P_B{}^b)$ is lower for a solid solution than for a pure phase. In the second case, because the free energy of a stable compound is more negative than the sum of the free energies of its constituent compounds, the overall reaction has a lower equilibrium gas phase composition than the composition calculated as the product of the equilibrium ratios for the reduction of the pure constituent compounds.

The magnitude of the decrease in equilibrium constant due to the above effects cannot be estimated; consequently, the data presented in Tables 2 and 3, which are calculated from the ΔF°_T values listed in Table 1, only suggest the magnitude of the equilibrium gas composition for a given reaction.

TABLE 2

EQUILIBRIUM PARTIAL PRESSURE OF WATER VAPOUR FOR REACTIONS OCCURRING DURING THE HYDROGEN REDUCTION OF A LEAD SINTER

Reaction	Equilibrium Partial Pressure of Water Vapour, atm.					
	500°C	600°C	700°C	800°C	900°C	1000°C
$PbO+H_2 \longrightarrow Pb+H_2O$	0.9999	0.9999	0.9998	0.9998	0.9997	0.9996
$3Fe_2O_3+H_2 \longrightarrow 2Fe_2O_3+H_2O$	0.9999	0.9999	0.9999	0.9999	0.9999	0.9999
$Fe_3O_4+H_2 \longrightarrow 3FeO+H_2O$	0.135	0.276	0.436	0.573	0.685	0.762
$FeO+H_2 \longrightarrow Fe+H_2O$	0.209	0.260	0.304	0.344	0.377	0.409
$CaSO_4+4H_2 \longrightarrow CaS+4H_2O$	0.996	0.996	0.9945	0.9936	0.9916	0.9915
$CaO+H_2 \longrightarrow Ca+H_2O$	1.6×10^{-24}	1.4×10^{-21}	3.2×10^{-19}	2.8×10^{-17}	1.3×10^{-17}	2.5×10^{-14}
$SiO_2+2H_2 \longrightarrow Si+2H_2O$	1.12×10^{-11}	3.16×10^{-10}	4.46×10^{-9}	4.07×10^{-8}	2.51×10^{-7}	1.12×10^{-6}
$MnO+H_2 \longrightarrow Mn+H_2O$	3.54×10^{-9}	4.0×10^{-8}	2.88×10^{-7}	1.41×10^{-6}	5.36×10^{-6}	1.59×10^{-5}
$Al_2O_3+3H_2 \longrightarrow 2Al+3H_2O$	1.26×10^{-18}	2.5×10^{-16}	1.6×10^{-14}	5.0×10^{-13}	8.0×10^{-12}	8.0×10^{-11}

The values given in Table 2 are calculated for a system pressure of 1 atmosphere from the relation $p_{H_2} + p_{H_2O} = 1$. For reactions (2) and (3) the equilibrium constant is expressed by p_{H_2S}/p_{H_2} and $p_{Zn}.p_{H_2O}/p_{H_2}$, respectively, and the effect of temperature on these ratios is shown in Table 3.

TABLE 3

EQUILIBRIUM CONSTANTS FOR THE REDUCTION OF PbS and ZnO BY HYDROGEN

Reaction	Equilibrium Constant, Kp					
	500°C	600°C	700°C	800°C	900°C	1000°C
$PbS+H_2 \rightleftharpoons Pb+H_2S$	4.46×10^{-8}	2.46×10^{-6}	7.1×10^{-5}	10.5×10^{-3}	1.02×10^{-3}	6.3×10^{-2}
$ZnO+H_2 \rightleftharpoons Zn+H_2O$	7.76×10^{-4}	2.69×10^{-3}	7.25×10^{-3}	1.66×10^{-2}	3.24×10^{-2}	5.75×10^{-2}

Referring to Tables 2 and 3 it is apparent that the system conditions of temperature and gas composition determine which reactions may occur. Consequently, reactions such as reaction (4) may not proceed until other, more favourable, reactions are almost completed. In particular, the extremely low equilibrium partial pressure of water vapour shown in Table 2 reveals that the reduction of the refractory oxides is negligible in the temperature range investigated.

2.3 Conclusions

The physical and chemical structure of a lead sinter is complex and only slightly understood. However, by making certain assumptions, it is possible to formulate a system of reactions which approximates the chemical behaviour of a lead sinter during reduction by hydrogen. A

thermodynamic analysis of the possible reactions in this system suggests that

(1) the reactions which may occur at a given temperature are determined by the gas phase composition,

(2) within the limitations imposed by the lack of knowledge of the physical and chemical structure of sinter it appears that the reduction of lead oxide, lead silicate, calcium sulphate and ferric oxide may proceed even at high water vapour partial pressures. The reduction of Fe_3O_4 and FeO may only occur at relatively low H_2O/H_2 ratios. The reaction of PbS with hydrogen is not affected by the H_2O partial pressure, but is controlled by the small equilibrium partial pressure of H_2S. The reduction of ZnO can proceed for all H_2O partial pressures, but the equilibrium value of p_{Zn} may only become significantly large at low H_2O/H_2 ratios.

(3) the reduction of the refractory oxides can be neglected for the temperature range investigated.

Finally, it must be emphasized that the thermodynamic approach deals only with equilibria and thus provides no information on the rates of the various reactions; the system kinetics may therefore affect the above conclusions.

3. LITERATURE SURVEY

This review summarizes the information available in the literature which is relevant to the present investigation and deals with the following topics: firstly, the kinetics of reactions occurring during the hydrogen reduction of a lead sinter are discussed, secondly, the experimental determination of heterogeneous reaction rates is considered, and, finally, the remaining Sections deal with the analytical techniques used to determine lead oxide in the presence of other lead compounds, a brief outline of the mechanics of fluidization, and a discussion of the comparison of reaction rates in fixed and fluidized beds.

3.1 Kinetics of Reactions Occurring during the Hydrogen Reduction of Lead Sinter

A simplified version of the possible reactions occurring during the reduction of lead sinter by hydrogen is presented in Section 2. Thermodynamic analysis of this system suggests that the compounds most likely to contribute to the overall rate of water formation are lead oxide and lead silicates, calcium sulphate, ferric oxides and, to a lesser extent, zinc oxides.

The kinetics of the reaction of primary importance in this investigation - the reduction of lead monoxide - have been the subject of a comprehensive study by Matthew [9] (1959). A literature survey revealed a paucity of published information; the only available data related to the temperature at which reduction commenced and dealt with the rate-determining step at temperatures below 400°C. In view of this Matthew measured the rate of reaction between pure lead oxide spheres and hydrogen over a wide range of temperature, particle size and hydrogen

pressure in a differential flow reactor. The reaction was strongly dependent on the temperature - the value of the exponent "n" in the relation

$$R = CT^n \qquad (16)$$

where

R = reaction rate, g.H_2O formed/(g mat.), (min),

T = absolute temperature, ^oK, and

C and n are constants,

was 21.5 $\pm$ 2 for hydrogen and hydrogen-nitrogen mixtures, and 18.4 for hydrogen-water vapour mixtures. In particular, -7 +10 # (B.S.S.) spheres were completely reduced in 30 minutes at 775°C while the same material was only 20% reduced in 180 minutes at 475°C. The reaction rate was also affected by the particle size; at 575°C, -7 +10 # (B.S.S.) spheres were reduced in 230 minutes whereas, under the same conditions, -36 +52 # (B.S.S.) spheres were totally reduced in 120 minutes.

The effect of water vapour on the reaction rate was determined for water vapour partial pressures up to 0.9 atmospheres. The presence of water vapour depressed the reaction rate; with pure hydrogen and hydrogen-nitrogen mixtures the reaction rate was approximately proportional to p_{H_2}, whereas with hydrogen-water vapour mixtures the rate was proportional to $(p_{H_2})^{1.36}$.

Oldright and Miller [12] (1932) have summarized the published data relating to the reduction of lead silicates by hydrogen. The reduction of compounds containing less than 21% SiO_2 is said to commence at 240°C while the reaction rate for more acidic silicates becomes appreciable at 300°C. Both $2PbO.SiO_2$ and $PbO.SiO_2$ are reduced by

hydrogen at 350°C and complete reduction to metallic lead occurs at 650°C. These results agree with the data of McIntosh [13] (1927) who also states that lead silicates produced at high temperatures are more readily reduced than silicates formed at low temperatures.

The reduction of calcium sulphate by hydrogen has not been subjected to intensive study and none of the available data relates to recent work. Zawadski et al. [14] (1926) investigated the reduction of $CaSO_4$ by hydrogen, hydrogen sulphide, carbon monoxide and carbon. At 800°C, using hydrogen as the reducing gas, the reduction was almost complete and the reaction rate was fast.

The kinetics of the reduction of iron oxides by hydrogen and carbon monoxide have been widely studied. Edström [15] (1953) who summarizes the available data, measured the rate of reaction between single crystals of Fe_2O_3 and Fe_3O_4 and hydrogen at temperatures in the range 450°C to 800°C; the results confirm the previous conclusion that the reaction rate shows a minimum between 600°C and 800°C. This effect is considered to result from the formation of a dense layer of wüsstite which retards the reaction rate by decreasing the rate of gas diffusion in the solid phase. Stalhane and Malmberg [16] (1930) show that the rate-controlling step in the hydrogen reduction of iron oxides is the reduction of wüsstite to metallic iron and that small amounts of water vapour strongly retard this reaction.

The production of metallic iron by gaseous reduction of its oxides has also been investigated in various fluidized systems. Ezz [17] (1960) states that the tendency for iron oxides to become sticky during reduction at high temperatures has limited the available

kinetic data to low temperature, high pressure, investigations. However, he measures the rate of reduction of Fe_2O_3 and Fe_3O_4 at 500°C, 600°C and 700°C, and concludes that the rate-controlling factor is the rate of supply of reducing gas. The data also show the effect of temperature on the reaction rate; approximately 72 # (B.S.S.) particles are totally reduced in 15 minutes at 700°C, whereas the same material requires 60 minutes for complete reduction at 600°C. The data of Lloyd and Amundson [18] (1961) and Dalla Lana and Amundson [19] (1961) relate to the reduction of iron oxides in vertical flow reactors. Using this apparatus the problem of sticking is minimised and, as the technique is fundamentally suited to the use of fine material, very fast reaction rates are obtained; -325 # (B.S.S.) Fe_2O_3 is 90% reduced to metallic iron in 10 seconds at 500°C. Lloyd and Amundson [18] (1961) state that the reduction rate for powdered iron oxides is limited in fixed and fluidised beds by the mass velocity of the reducing gas. Dalla Lana and Amundson [19] (1961) also claim that the reaction sequence involves the reduction of wüstite above 570°C, whereas below this temperature Fe_3O_4 is directly reduced to metallic iron. This mechanism is used to explain the observed decrease in reaction rate between 550°C and 600°C.

There appears to be little published information relating to the kinetics of the reaction between ZnO and hydrogen. Olmer [20] (1943) states that the reduction commences at 315°C in the presence of an excess of pure hydrogen; however, the rate of reaction is not significantly fast until the temperature exceeds 500°C.

3.2 Experimental Determination of Reaction Rates

The determination of heterogeneous reaction rates may be carried out in two distinct experimental systems, viz., static and dynamic. However, since the study of reaction rates in a fluidized bed involves the use of a dynamic, rather than a static, system, it is desirable to use a flow reactor to obtain kinetic data in the fixed-bed. Consequently, this Section deals with the use of dynamic systems to study reaction rates in fixed and fluidized beds. The extent of the survey is limited by restricting the discussion of the fixed-bed data to reactions involving H_2 and CO.

3.2.1 Fixed Beds

Parravano [21] (1952) described a constant volume apparatus used to study the reduction of nickel oxide by hydrogen. After the sample is degassed, a known volume of hydrogen is admitted to the system and circulated at a high velocity through the oxide bed. The water vapour is removed from the gases leaving the bed and the reaction rate is determined from the change in system pressure.

Baba [22] (1956) uses a dynamic system is conjunction with a thermobalance to investigate the reduction of germanium dioxide by hydrogen. The sample is suspended in a stream of H_2 and the reaction rate is followed by measuring the weight lost by the sample; differentiation of the graph of cumulative weight lost against time then gives a measure of the rate of reduction.

In the method which has found widest application in dynamic systems a known volume of reducing gas of fixed composition is passed through a bed of the solids; since the change in

composition of the reducing gas is directly related to the reaction rate, the progress of the reaction is followed by measuring the composition of the exit gases. This is the technique used by Pease and Taylor [23] (1921) for the reduction of copper oxide by hydrogen, by Benton and Emmett [24] (1924) for the reduction of nickel and ferric oxides, by Gadsby, Hinshelwood and Sykes [25] (1946) for the steam-carbon reaction, by Culver, Hamdorf and Spooner [26] (1958) for the reduction of barytes, and by Matthew [9] (1959) for the reduction of lead oxide.

The apparatus used by Edström [15] (1953) to study the reduction of iron oxides differs from the general arrangement in that the hydrogen passes over a silica boat which contains the iron oxide sample; however, this technique is of doubtful value with small particles since it may introduce an additional resistance to reaction - the necessity for gas diffusion through the bed of solids.

3.2.2 Fluidized Beds

The techniques used to measure the rate of reaction between solids and gases in fluidized beds are essentially similar to those employed in fixed beds.

Kivnick and Hixson [26] (1952), in a study of the reduction of nickel oxide by H_2-N_2 mixtures, follow the pregress of the reaction by performing a continuous hydrogen analysis on the exit gases; the reaction rate over a given time interval is then calculated from the difference in hydrogen concentration from inlet to outlet.

The measured change in composition of fluidizing gas which results from passage through a bed of solids is used by Lewis,

Gilliland and Reed [27] (1949) to study the reaction between copper oxide and methane, by Lewis, Gilliland and McBride [28] (1949) to study the rate of gasification of carbon by CO_2, and by Johnstone, Batchelor and Shen [29] (1955) for the oxidation of ammonia.

Ezz [17] (1960) describes an investigation of the reduction of iron oxides by hydrogen, in which the reaction rate is measured by absorbing the reaction product - in this case, H_2O - in weighed drying tubes filled with $CaCl_2$.

In an investigation of the gasification of carbon using metal oxides as the oxygen carrier, Lewis, Gilliland and Sweeney [30] (1951) use a constant pressure, constant volume, system. A constant volume of CO_2 is admitted to the system at the start of an experiment and recycled by means of a pump. The additional CO_2 formed by reaction is exhausted to atmosphere via a mercury check valve and a wet-test meter. The exhaust gas is also analyzed, and these data may be used in conjunction with carbon and oxygen mass balances over short time intervals to calculate the reaction rates. Culver, Hamdorf and Spooner [31] (1958), who study the reduction of barytes by H_2, also use a constant volume, constant pressure, system. The reaction product, i.e., water vapour, is continuously removed from the system and the reaction rate is followed by measuring the rate of make-up hydrogen necessary to maintain the constant circulating volume.

3.3 Analytical Techniques

The composition of a lead sinter is complex and ideally the rate of reduction should be followed by chemical analysis of the reduced solids. However, as this investigation is primarily

concerned with the rate of metallic lead formation, this Section is limited to a discussion of the various techniques used to separate the total lead content of a sample into the constituent lead compounds.

Several workers, after investigating the selective solution of various lead compounds from lead slags and sinters, have published summaries of their experimental methods. Collee [32] (1956) has extended the earlier work of Krossin [33] (1948), in which only the total lead and the lead oxide were directly determined. He suggests an analytical procedure in which each lead compound normally encountered in slags and sinters can be determined by direct analysis. The lead oxide and lead silicate are dissolved in hot ricinoleic acid and the residual solids are attacked with boiling ammonium acetate which selectively dissolves the lead sulphate. The remaining solids, containing any metallic lead and lead sulphide present are then treated with boiling hydrogen peroxide and the original lead sulphide content is determined by extracting the resulting lead sulphate with ammonium acetate. The residual lead in the sample - estimated in the normal way by solution in aqua regia - is reported as metallic lead. This method has the advantage that once the selectivity of the various solvents is established the accuracy of the experimental results can be subjected to a partial check by equating the total lead determined in the normal way against the sum of the lead present in the individual compounds.

An alternative method is described by Oldright and Miller [34] (1929). The lead oxide and lead sulphate are extracted with ammonium acetate, and the residual solids are attacked with cold, 10 per cent,

silver nitrate solution. This reagent selectively dissolves any metallic lead in the sample and the residual solids contain any lead initially present as sulphide and silicate. The lead sulphide is determined by dissolution in a ferric chloride-sodium chloride solution and the residue is analysed for lead, this being reported as the silicate.

Each of these methods is applicable to the present investigation, but there is considerable disagreement about the selectivity of the reagents. The experimental result obtained by Collee [32] (1956) - that ammonium acetate selectively dissolves the lead oxide, silicate, and sulphide in a given sample - is supported by Low, Weinig and Schoder [35] (1948) who state that the only lead compounds insoluble in this reagent are the sulphide and the chromate. However, Read [36] claims that artificial silicates prepared by fusing lead oxide and silica at high temperatures are almost insoluble in ammonium acetate. He also suggests that metallic lead is appreciably soluble in this reagent. The preferential solution of metallic lead in silver nitrate is also criticised by Read [36] on the basis of results obtained from artificial mixtures; lead sulphide appeared to be partially soluble in this reagent. McIntosh [37] (1927), who separates the oxidized lead compounds from the free lead and lead sulphide by solution in caustic soda, also suggests that prolonged contact favours the solution of lead sulphide in silver nitrate. However, this conclusion is not confirmed by Oldright and Miller [34] (1929). They experienced a loss of lead sulphide, but found that the metallic lead content was also too low; these discrepancies were attributed to oxidation during the ammonium acetate extraction.

3.4 Mechanics of Fluidization

This Section deals with the theoretical aspects of the fluidization technique, and its scope is limited to the system applicable to the present investigation, viz., the fluidization of granular solids by gases.

3.4.1 General Description of Fluidization

Consider the effect of passing a stream of gas at a gradually increasing rate through a bed of crushed solids free to move in a vertical direction. At first the pressure drop increases without bed expansion until the flow rate is sufficiently large to provide a pressure gradient across the bed equal to the buoyant weight of solids per unit cross sectional area; this is the point of incipient fluidization. Further increase in flow rate causes the bed to expand, but the pressure drop remains substantially constant. On increasing the gas flow beyond the point of incipient fluidization gas bubbles appear and the bed becomes fully fluidized as the solids circulate and mix; continued increase in the flow rate causes larger bubbles to pass through the bed with increasing frequency. Consequently, a fluidized bed is not homogeneous with respect to the concetration of solids, but may be considered to contain two distinct phases,

(i) a dilute phase consisting of the gas in excess of the volume required for incipient fluidization passing through the bed in the form of bubbles, and

(ii) a dense phase having a porosity equal to the porosity of the bed at the point of incipient fluidization wherein the gas is in intimate contact with the solids.

The relative proportion of these two phases varies with the flow rate.

The prevailing particle movement during fluidization is upwards in the centre and then towards and down along the walls of the containing vessel. Some local side mixing may also take place [38,39,40] (1949), (1950) and (1951) with the result that the solids composition is relatively uniform throughout the bed. It has also been shown that some back-mixing and radial mixing occurs in the gas phase in fluid beds [41,42,43] (1951), (1952) and (1952). However, it is unlikely that complete mixing takes place, even at low superficial gas velocities.

3.4.2 Deviations from Ideal Fluidization

The ease with which a fluid bed may be formed depends to a large extent on the physical properties of the solid, and the uniformity of the bed is a function of the size, shape, and surface properties of the fluidizing particles as well as the dimensions of the bed [40] (1951). For these reasons, the ideal behaviour described in Section 3.4.1 seldom exists in practice, and the two most common deviations from ideal fluidization which occur in gas-fluidized beds are channelling and slugging. Both these effects decrease the contact area between the solids and gas and are therefore very undesirable.

(i) Channelling

Chanelling occurs when the fluidizing gas passes through the bed along a few paths rather than as a uniform distribution across the whole bed area. Such a flow pattern offers less resistance to flow than uniform fluidization and the pressure drop across the bed is decreased. Comparison of the theoretical pressure drop based on the bed weight with the observed pressure drop across the bed therefore

provides a reliable indication of the uniformity of fluidization.

(ii) Slugging

The term "slugging" describes the condition in which bubbles of the supporting fluid coalesce and eventually occupy the whole diameter of the containing vessel; the mass of particles supported by the carrier gas then moves upwards in a piston-like fashion. This effect is encouraged by the use of deep, small diameter, beds [44,45] (1951) and (1949), and the tendency to slug also appears to increase with particle size and density [44,45,46] (1951), (1949) and (1947). High superficial gas velocities also increase the possibility of slugging [46] (1947).

The presence of slugging in a fluid bed may be predicted from the magnitude of the fluctuations in the pressure drop across the bed [40,46] (1951) and (1947); with good fluidization the fluctuation is small, but with slugging fluidization the pressure drop varies between quite wide limits [47] (1956).

3.4.3 Effect of Physical Properties of Gas and Solids on Fluidization

The properties of a fluid bed are often markedly influenced by the physical properties of the solids and the fluidizing gas, and this Section summarizes the rather limited information relating to the effect of some of these physical properties.

(a) Gas density

An increase in gas density decreases the free-falling velocity of the bed particles and the point of incipient fluidization may occur at a lower gas velocity [47] (1956).

(b) Gas viscosity

It is probable that an increase in viscosity tends to decrease the ease with which gas may leave the dense phase. Experimental evidence [44,48] (1951) and (1955) on the fluidization of a bed using different gases indicates that both density and viscosity, but mainly density, affect the flow through a fluidized bed.

(c) Particle size

In the fluidization of solids by gases it appears that particle size may be the most important single factor influencing the quality of fluidization and the utility of the technique. Small particles (< 40 u) are often difficult to fluidize [45,46,47] (1949), (1947) and (1956) and tend to agglomerate and channel [46] (1947). Alternatively, large particles may require an uneconomically high gas velocity to initiate fluidization.

The effect of particle size distribution is not clearly understood. Theoretically, a narrow size range would be expected to have ideal fluidizing properties; however, practically, it is observed that there is generally an optimum size range for good fluidization and that this size range includes large and small particles [40,47] (1951) and (1956).

3.4.4 Estimation of Physical Properties of Fluid Beds

The basic calculations required for the design and operation of fluidized bed reactors and the interpretation of kinetic data are

(i) the fluidization pressure drop, $\triangle P$,

(ii) the minimum fluidizing velocity, V_{mf}, and

(iii) the height of the expanded bed, L_f.

3.4.4.1 Fluidization Pressure Drop

The pressure drop across a fluidized bed is basically constant and independent of the gas velocity. Leva [44] (1951) derives the following expression for the pressure drop,

$$\Delta P = L(1-\varepsilon)(\rho_s - \rho) \qquad \text{---------- (17)}$$

where the voidage, ε, and the bed height, L, are measured at the same bed condition. For gas-solid fluidization this simplifies to

$$\Delta P = L(1-\varepsilon)\rho_s \qquad \text{---------- (18)}$$

and

$$\Delta P = \frac{\text{weight of material in bed}}{\text{bed area}} \qquad \text{---------- (19)}$$

3.4.4.2 Minimum Fluidizing Velocity

The fluid velocity required to initiate fluidization may be calculated from an equation for the pressure drop across a fixed bed. The variation of the pressure drop with the gas velocity in a fixed bed has been extensively studied, and one of the most widely used correlations, developed by Carman [49] (1937), is

$$f = \Delta P \cdot d \cdot \rho_g \cdot \varepsilon^3 / L \cdot 2G^2 \cdot (1-\varepsilon)^2 \cdot \beta \qquad \text{---------- (20)}$$

where

f = friction factor (dimensionless),

ΔP = pressure drop across the bed (lb force/ft^2),

L = bed depth (ft),

d = particle diameter (ft),

G = mass flow of bas gased on superficial area (lb/(ft^2),(hr)),

ρ_g = gas density (lb/ft^3)

ε = bed porosity (dimensionless), and

β = shape factor (dimensionless).

This equation has been applied at the point of incipient fluidization by several investigators [50,51,52,53] giving a relation of the form

$$G_o = k.\varepsilon_o^3.d^2(\rho_s - \rho_g).\rho_g.\ g_c/\mu_g.\ (1 - \varepsilon_o). \qquad \text{——————(21)}$$

where

G_o = mass velocity at incipient fluidization (lb/(ft^2),(hr)),

ρ_s = density of solid particles (lb/ft^3),

g_c = gravitational constant (ft/sec^2),

μ_g = gas viscosity (lb mass/(ft),(hr),),and

ε_o = maximum bed porosity (dimensionless).

Each investigator has obtained a slightly different value for constant, k, in this equation, viz.,

Leva et al. [50] (1948)	k = 0.005,
Miller and Logwinuk [51] (1951)	k = 0.006,
van Heerden et al. [52] (1952)	k = 0.065, and
Cathala [53] (1953)	k = 0.0055 (from theoretical grounds)

van Heerden et al. [52] (1952) have extended this equation to predict the onset of fluidization for beds containing mixtures of particle sizes. The effective diameter of the particles is defined as "the diameter of a sphere which would give the same number of particles per unit volume of bed as the material under consideration (both counted at maximum porosity)". Using this diameter the commencement of fluidization may be estimated with reasonable accuracy for powdered solids by the following equation

$$G_o = 0.00123\ \rho_g.\rho_{bm}.\ g_c.\ d_e^2/B_e.\ \mu_g \qquad \text{——————(22)}$$

where

ρ_{bm} = bed density at maximum porosity (dimensionless),

B_e = generalised shape factor,

and the other symbols have the same meaning as before. This equation is only true for gas flows in the viscous range. An alternative approach which may be applied to turbulent flows has been presented by Leva [44] (1951).

All investigators agree that the value of the bed density and the bed porosity are correctly obtained by fluidizing the material and slowly reducing the flow rate until the bed is quiescent; the volume occupied by a known weight of solids may then be measured at the loosest stable packing. However, as both Leva [50] (1948) and van Heerden et al. [52] (1952) point out, little error is involved in determining the bed density by pouring the material into a measuring cylinder; Leva [50] (1948) found that porosities measured in this manner were only about 5% lower than those obtained by the more complicated method.

The shape factor, B_e, in equation (22) may be defined as a measure of the departure of the particles from the ideal spherical shape. For spheres $B_e = 1$, but for all other particles $B_e > 1$. Most particles have shape factors of about 1.3 to 1.5, but for very irregular particles B_e may exceed 1.75 [44] (1951).

3.4.4.3 Height of Expanded Beds

The expansion of a fluidized bed at a mass flow exceeding the minimum fluidizing flow is difficult to evaluate, but it can be estimated from data presented by Leva [44] (1951)

3.5 Comparison of Reaction Rates in Fixed and Fluidized Beds

The general approach to the study of heterogenous reaction rates is to view the overall reaction as consisting of a number of distinct steps. These steps may be considered separately and the relative rate of each step influences the distribution of concentrations in the system and determines the overall rate of reaction [54] (1956).

In the present case the overall reaction may be divided into the following steps:

(1) Mass transfer of the reactant gas through the gas film to the exterior surface of the solid.

(2) Diffusion of the reactant gas through the solid to reaction interface.

(3) Chemical reaction at the interface.

(4) Diffusion of the gaseous product from the interface to the surface of the solid.

(5) Mass transfer of the product gas through the gas film to the bulk of the gas.

Now, steps (2), (3) and (4) are specific functions of the properties of the reactants and products, and of the reaction temperature; consequently, the rates of these steps are unaffected by the system used to study the overall reaction rate. Therefore, as Othmer [54] (1956) states, any difference in reaction rate between a thick, fixed, bed and the same bed in the fluidized state results mainly from the difference in rate of mass transfer through the fluid film surrounding the particles; the difference in uniformity of temperature control also affects the relative magnitude of the reaction rates to some extent.

The preceding discussion relates to thick beds but does not mention the possible effect of the gaseous reaction product on the reaction rate; if the reaction is inhibited by the presence of the reaction product, then the fluidized bed reaction rate may exhibit a gas velocity dependence which is due to kinetic, rather than diffusional, effects.

In thin bed reactors the composition of the reducing gas in contact with the solids may be taken as the arithmetic average of the inlet and outlet compositions, and, except in the initial stages of reaction, this average composition is almost equal to the inlet composition. Consequently, to relate the rate of reaction obtained in a differential bed reactor to the reaction rate in an integral reactor, either fixed or fluidized, it is necessary to know the effect of the reaction product on the reaction rate.

There are very few published investigations in which the rate of reaction measured in a fluidized bed is related to kinetic data obtained in fixed beds. Culver, Hamdorf and Spooner [31] (1958), in a study of the reduction of $BaSO_4$ by hydrogen, used rate data obtained in a differential reactor to predict the behaviour of deep, fixed beds under similar conditions. In a previous paper [55] (1958) it was shown that the reduction rate was comparatively insensitive tovariations in H_2O partial pressure, and the authors conclude that the differential reactor data should be applicable to a thick, fixed, bed. However, at 1100°C the reaction is limited by the rate of supply of hydrogen to the bed and it is not possible to compare the predicted rate curve with the experimental data until 79% reduction

has occurred; the agreement is satisfactory, but the prediction is not tested for high H_2O partial pressures. At 1000°C the performance of the thick, fixed, bed falls considerably below the differential bed and this is attributed to the presence of the reaction products. No attempt is made to relate the fluidized bed data to the results obtained in the fixed bed. However, it appears that the gas velocity may influence the reaction rate; the reduction of -10 +14 # (B.S.S.) barytes is faster at 1000°C in a 1500 g. bed fluidized by 220 l. s.t.p./min. of hydrogen than in the equivalent fixed bed at a gas flow rate of 120 l. s.t.p./min.

Johnstone, Batchelor and Shen [29] (1955) used the low temperature, catalytic, oxidation of ammonia to investigate the effect of fluidization on the reaction rate obtained in fixed beds. For the system conditions chosen the reaction rate was a function of time only, and the space velocity, or contact time, was held constant for the fixed and fluidized beds; this was achieved by increasing the bed depth in the fluidized system. The results suggest that the faster reaction rate obtained in the fluidized bed may be separated into two parts: the part that is related to the chemical kinetics may be predicted from the fixed bed data; the part that depends on mass transfer to the discontinuous phase is a function of gas velocity and is relatively independent of particle size. For non-zero order reactions the authors also note that by-passing of the gas as bubbles, or gas mixing, cause the fluidized bed reaction rate to be less than the rate in the equivalent thick, fixed, bed.

The reduction of nickel oxide by hydrogen has been investigated by Kivnick and Hixson [26] (1952) in a fluidized bed, and the reaction rate is observed to increase with increasing gas velocity at each reduction temperature. The possible causes of the velocity dependence are discussed in some detail. By-passing of the gas tends to decrease the reaction rate, while Benton and Emmett [24] (1924), working with a fixed bed, established that water vapour only slightly affected the reaction rate. Calculations based on data presented by Skapski and Dabrowski [56] (1932) also revealed that the overall gas composition was vastly different from the equilibrium value for this reaction. Consequently, the authors conclude that the velocity effect resulted from mass transfer effects. The rate of diffusion through the gas film surrounding the particles is shown by calculation to be much greater than the overall reaction rate, and, because of this, the observed velocity effect is explained on the basis of the two-phase fluidization theory. Toomey and Johnstone [57] (1952), who developed this theory, consider that the bulk of the reaction takes place in the highly turbulent region adjacent to the bubbles passing through the smoothly fluidized part of the bed. An increase in gas flow rate increases the proportion of gas in the discontinuous phase which

(i) increases the turbulence in the bed with a consequent increase in the area available for mass transfer and reaction, and

(ii) improves the mass transfer coefficient in the turbulent region.

Both these effects tend to increase the rate of mass transfer.

4. ANALYTICAL PROCEDURES

A detailed description of the methods of chemical analysis used in this investigation is set out in Appendix I, together with a discussion of the development of the technique used to determine the amount of various lead compounds present in a complex material.

In broad outline the method used to determine the "forms of lead" in samples which may contain lead oxide, lead silicate, lead sulphate, lead sulphide and metallic lead is as follows: a weighed sample of crushed material is attacked for six hours with boiling ammonium acetate. The mixture is then filtered and the residue subjected to a second attack; the lead present in the filtrates is determined either gravimetrically or volumetrically and reported as lead oxide, lead silicate and lead sulphate. This procedure is repeated until the filtrate from the acetate extraction is free from lead. In general, boiling for six hours is sufficient to extract all the acetate-soluble lead. The remaining solids are shaken intermittently with 10% silver nitrate solution for two hours, and again separated into a filtrate and a residue; the filtrate is treated with sulphuric acid, and the nitrate soluble lead - reported as metallic lead - is determined gravimetrically as the sulphate. A chloride reagent is added to the residue which is then allowed to stand, with intermittent shaking, for 15 hours. The mixture is then filtered and the residual solids discarded. The filtrate is treated with sulphuric acid and the chloride-soluble lead - determined gravimetrically as the sulphate - is reported as lead sulphide.

The total lead and total zinc contents of the various

samples are determined by the standard methods outlined in Scott and Furman [58] (1939).

5. RAW MATERIALS

5.1 Gases

The nitrogen and hydrogen were of commercial quality supplied in cylinders. Apart from variable amounts of water vapour, the most important impurity in each gas was oxygen. Analyses showed that the oxygen content was less than 0.2 volume per cent in the case of nitrogen and less than 0.1 volume per cent for the hydrogen.

5.2 Lead Sinter

The material used in the experimental work was obtained from a typical sample of updraught sinter supplied as -4 in. lumps by Broken Hill Associated Smelters Limited, Port Pirie. The analysis received with this sample gave the composition as:

Pb	= 41.7 (weight percent basis)
Zn	= 10.1
FeO	= 12.7
CaO	= 7.6
SiO_2	= 8.3
Al_2O_3	= 3.1
MnO	= 1.9
Total sulphur	= 1.7
Sulphate sulphur	= 0.6

The material unaccounted for (12.9%) consists mainly of combined oxygen together with the various trace elements present.

5.2.1 Preparation of Samples

The -4 in. lumps were crushed in a set of rolls, and the +14 # (B.S.S.) material in the product was recirculated. The -14 # (B.S.S.) product was dry-screened for 20 minutes in a nest of screens

on a Rotap and the main size fractions required for the experimental work, viz., -25 +36#, -36 +52#, -52 +72#, and -72 +100# (B.S.S.) were collected; the -100 +150# and -200 +325# (B.S.S.) fractions in the undersize material were collected and the -14 +25# material was dry-ground in a small tumbling mill and then rescreened. The various size fractions were then wet-screened to remove slimes and the product immediately dried in an oven at 104°C. The material produced in this manner was then stored in air-tight containers until required.

5.2.2 Physical Properties of Samples

Microscopic examinationof the various size fractions reveals that the particles are irregular in shape with a tendency to be long, thin, flakes rather than spheres, and the shape of the particles is similar for each size fraction. The specific gravity, which is also constant for the various particle sizes, is 5.63.

The B.E.T. surface area was measured for each size fraction by the normal krypton adsorption technique and these results are shown in Table 4.

TABLE 4

THE SURFACE AREA OF VARIOUS SINTER SIZE FRACTIONS

Size Fraction (B.S.S.)	-25 +36	-36 +52	-52 +72	-72 +100
Surface Area ($cm^2/g.$)	3250	3900	4600	5400

5.2.3 Chemical Analysis of Samples

The size fractions used in the experimental work were analysed for total lead and total zinc by the standard methods set out in Scott

and Furman [58] (1939), and the total lead content of each sample was separated into the constituent compounds by the method described in Appendix I.2. The results of these analyses, expressed as mass percentages, are set out in Table 5.

A complete analysis of the -72 +100 # (B.S.S.) fraction revealed that apart from the lead and zinc contents the composition was essentially similar to the values reported for the original sample; consequently, the remaining size fractions were only analysed for total lead, total zinc, and the constituent lead compounds.

TABLE 5

CHEMICAL COMPOSITION OF THE VARIOUS SINTER SIZE FRACTIONS

Size Fraction (B.S.S.)	Total Zn	Total Pb	Lead Oxide, Lead sulphate, lead silicate	Metallic lead	Lead sulphide
- 25 + 36	10.11	40.9	38.8	0.1	1.3
- 36 + 52	9.61	39.0	36.7	0.4	1.6
- 52 + 72	10.20	38.3	36.1	0.2	1.7
- 72 +100	9.89	38.9	36.9	-	1.8
-100 +150		39.3	37.0	0.2	1.8
-200 +325		42.2	39.3	1.0	1.3

6. THE REDUCTION OF LEAD SINTER IN A FIXED-BED REACTOR

The stated aim of this project is to study the reduction of impure lead oxide by hydrogen in fluidized reactors, and the results obtained in fluidized systems are generally interpreted on the basis of kinetic data obtained in a fixed-bed reactor.

The kinetics of the reduction of pure lead oxide have been studied by Matthew [9] (1959), but the use of impure lead oxide in the present investigation precludes the direct application of these data. Consequently, it is necessary to investigate the kinetics of the reduction of lead sinter by hydrogen in a fixed bed and this study involves the determination of the effect of system variables on the reaction rate; in particular, sufficient data must be obtained on the effect of water vapour partial pressure and reducing gas velocity to permit comparison of the fixed-bed reaction rates with the rates obtained in the fluidized reactors.

The complex chemical composition of lead sinter introduces the possibility that the rate of reduction of the oxidized lead compounds may differ from the overall reaction rate. In this eventuality the rate of reaction should be followed by chemical analysis of the reduced solids, but, as shown in Section 6.1, this technique is impracticable. Consequently, an experimental relation between the overall reaction rate and the rate of reduction of the lead compounds must be established.

This Section deals with a study of the rate of reaction between lead sinter and hydrogen in a fixed bed which has as its

main objectives,

(i) the determination of the relation between the overall reaction rate and the rate of reduction of the oxidized lead compounds to metallic lead, and

(ii) the measurement of the effect of system variables, in particular, H_2O partial pressure and gas velocity, on the rate of reaction.

6.1 Selection of Operating Conditions and Experimental Technique

The proposed comparison of the fixed-bed data with the results obtained in the fluidized bed reactor makes it essential to use a dynamic system for the measurement of reaction rates. In addition, the requirements of the overall experimental programme indicate the use of a differential, rather than an integral, bed reactor. With an integral bed the gas composition varies from point to point within the bed and the effect of water vapour on the reaction rate is not readily obtained. However, a differential reactor employs a thin bed of solids, and the gas composition in contact with the solids may be taken as the arithmetic mean of the inlet and outlet compositions without serious error.

Consequently, the effect of water vapour partial pressure on the reaction rate may be directly determined by altering the inlet gas composition.

The selected experimental technique must be suitable for measuring the reaction rate for a wide range of system conditions. Firstly, it must be capable of measuring reaction rates in the range 500°C to 800°C. At temperatures below 500°C the rate of reduction of

pure lead oxide is extremely slow [9] (1959), and Fe_2O_3 is only slowly reduced at this temperature [59] (1960). Also, the reduction of ZnO commences at 315°C, but the reaction rate is not significantly fast until the temperature exceeds 500°C [20] (1943). Therefore, the overall reaction rate is likely to be slow and difficult to measure accurately at temperatures below 500°C. Higher temperatures increase the rate of reaction, but volatilization of lead oxide becomes serious at 800°C; although it appears that SiO_2 and Fe_2O_3 lower the tendency for lead oxide to vapourize, Mostowitsch [60] (1907) concludes that volatilization commences at 700°C and is marked at 800°C. Vapour phases reactions are extremely fast and any significant volatilization will introduce large errors into the determination of the fixed-bed reaction rate. Secondly, the technique must be suitable for studying the effect of water vapour on the reaction rate over the range of H_2O partial pressures likely to occur in the fluidized bed reductions. The maximum H_2O/H_2 ratio anticipated in the fluidized bed is approximately 0.10, and the rate of reaction in the fixed-bed will be measured for inlet gas compositions varying from pure hydrogen (p_{H_2} = 1 atm.) to H_2-H_2O mixtures where p_{H_2} = 0.9 atm. Finally, the experimental procedure must be suitable for preparing samples of partially reduced sinter for which the overall per cent reduction is known.

In the present case the experimental techniques which warrant consideration are

(i) measurement of the volume of hydrogen consumed by reaction,

(ii) measurement of the weight of water formed by reaction, and

(iii) chemical analysis of the solid phase.

Now, lead sinter contains a number of compounds which are reducible by hydrogen and the overall reaction rate measured by the rate of water formation may not be the correct value to assign to the rate of reduction of the oxidized lead compounds. Consequently, the basic method which should be applied in the present case is to follow the rate of reduction by chemical analysis of the residual solids. In this approach the degree of reduction is determined from the oxidized lead content of the reduced solids; the curve of per cent reduction against time may then be constructed from a knowledge of the compositions of a series of samples reduced for various, known, times. The differential of this curve is the rate of reduction. This method is obviously extremely time-consuming since the construction of a satisfactory curve requires approximately eight points and each point represents an experimental run followed by three analyses. Consequently, this technique is not suitable for use in an investigation involving a large number of tests and it is desirable to apply the more easily measured overall reaction rate to the study of the rate of reaction between impure lead oxide and hydrogen. Therefore, the initial step in the experimental programme must be to establish the conditions under which the overall reaction rate may be used to represent the rate of reduction of the oxidized lead compounds. However, since this relation is obtained by chemical analysis of reduced solids from which a known weight of water has been formed, any technique suitable for measuring the overall reaction rate may be used.

The literature survey (Section 3.2.1) reveals that the most commonly used technique when the reducing gas is nominally pure hydrogen

is to measure the change in composition of the inlet gases which results from passage through a thin bed of the solid reactant. This method is applicable to the present investigation and is selected in preference to method (i) above. The change in gas composition is most simply obtained by measuring the weight gained by an efficient dessicant placed in the exit gas stream; the weight increment is the sum of the water produced by reaction and the water content of the inlet gases. The water entering the reactor results from incomplete removal of oxygen or incomplete drying, and is likely to be small in comparison to the water formed by reaction except towards the end of the reaction; when the reaction is completed, the water picked up by the drying tube is equal to the water content of the inlet gas and the previous weight increments may be corrected on the basis of this final "carry-over" value.

The main disadvantage of this method is the high analytical precision necessary to measure accurately the relatively small amounts of water formed from the small sample weight used in the differential bed. It is this difficulty which limits the use of the technique to inlet gas compositions approaching pure hydrogen; for H_2-H_2O mixtures the increment in gas composition due to the water formed by reaction is too small in comparison to the composition of the inlet gas to be measured accurately. Consequently, experimental data on the rate of reaction between lead sinter and H_2-H_2O mixtures must be obtained by chemical analysis of the reduced solids; this method is briefly outlined above.

6.2 The Experimental Apparatus and Procedure

The apparatus used with pure hydrogen is based on the arrangement developed by Matthew [9] (1959) to study the reduction of lead monoxide. However, when the reducing gas is a hydrogen-water vapour mixture the initial apparatus is modified by the inclusion of a constant temperature water bath containing a hydrogen saturator placed in the hydrogen line between the flowrator and the bottom of the preheater. The two apparatuses are described in Sections 6.2.1 and 6.2.3, and the experimental methods are set out in Sections 6.2.2 and 6.2.4.

6.2.1 The Experimental Apparatus for use with Hydrogen

A line diagram of the apparatus is shown in Figure 1, and a detailed description of the components is given in Appendix II. Two photographs of the apparatus are shown in Figure 2.

Hydrogen enters the apparatus through the needle valve, V_2, and passes through a heated bed of copper turnings, O_2, where any oxygen is converted to water vapour. The gas is cooled in a spiral condenser, C_2, and dried in a train comprising two towers containing silica gel, S_2, a copper tube packed with "molecular sieves", M, and two towers containing magnesium perchlorate dispersed on glass wool, D_2. The temperature and flow rate are measured with the thermometer, t, and the rotameter, F_1, and the gas is heated to the reaction temperature in the preheater, P. During a run the hydrogen flows through a ground silica joint into the reactor, R, and then out to atmosphere via the gas distributor, Q, and the drying tubes, B. The reactor and the preheater are constructed from silica tubing, but the reactor

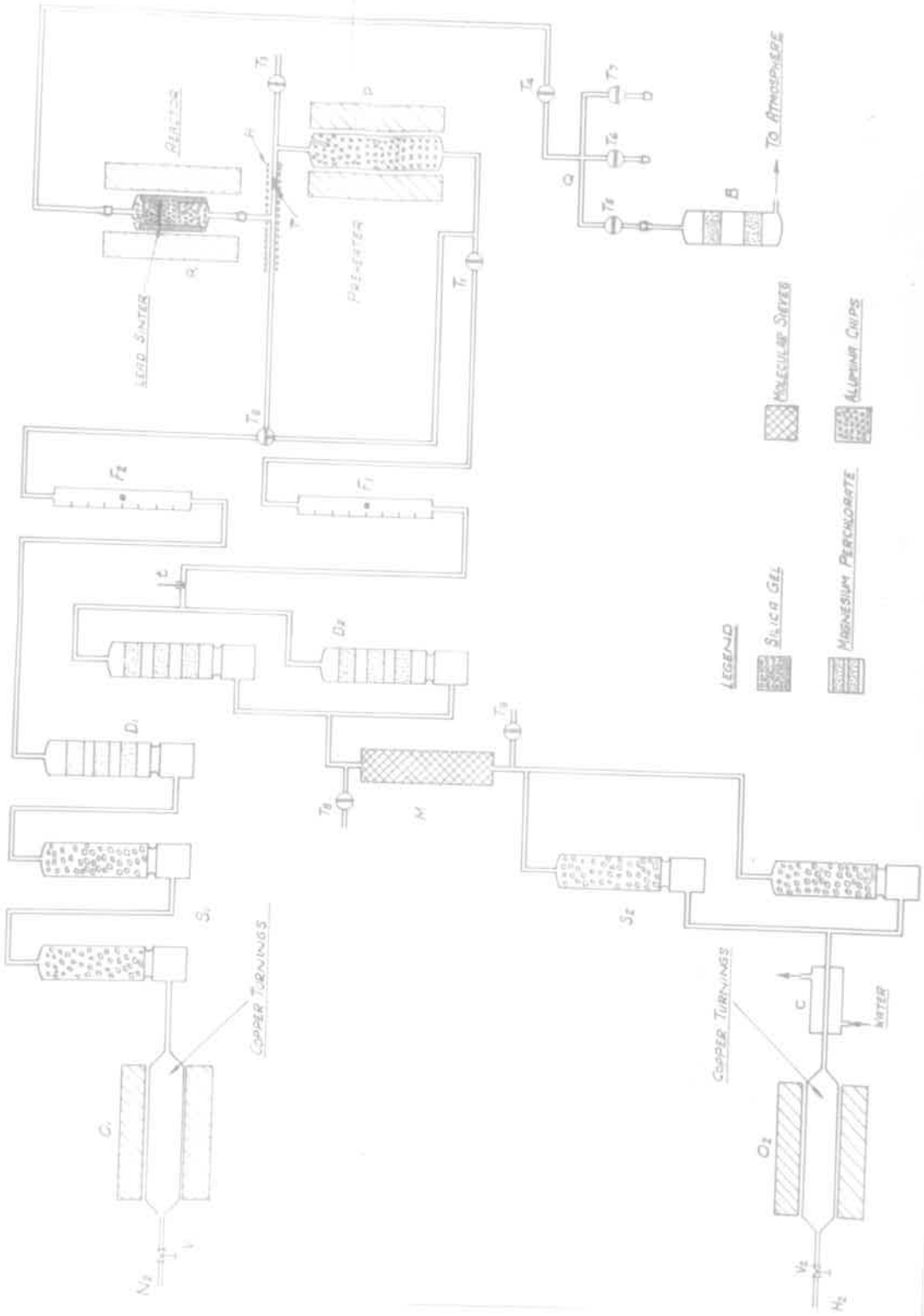

Fig. 1 - Line Diagram of Fixed Bed Apparatus

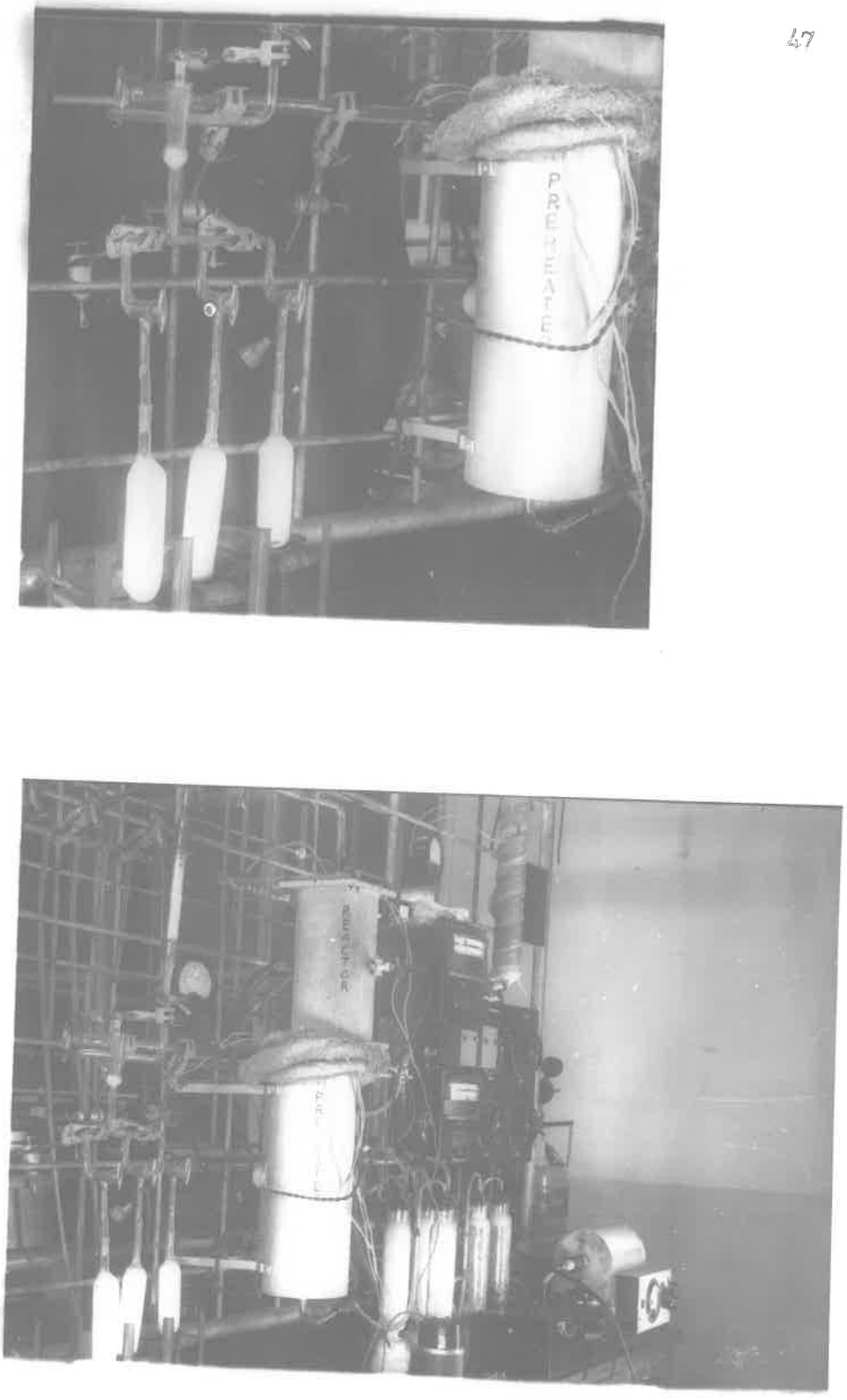

Fig. 2 - Photographs of Fixed-Bed Apparatus for reduction with pure Hydrogen

contains a thermal alumina liner to prevent slagging between the lead sinter and the reactor walls. The reactor and preheater furnace temperatures are controlled by "Pyrovane" controllers; the circuit diagrams for these control loops are presented in Figure 35, Appendix II. During the temperature stabilization period preceding each run, the hydrogen, together with a backflow of nitrogen passing through the deoxidizing furnace, O_1, the drying towers S_1 and D_1, the flowmeter F_2, and the constriction r, passes out to atmosphere via the tap T_3; the nitrogen flow prevents diffusion of hydrogen into the reactor.

6.2.2 The Experimental Procedure using Hydrogen as the Reducing Gas

The experimental procedure used to measure the rate of reduction of lead sinter by pure hydrogen, and to prepare samples reduced by a known amount, is described by the following steps:

(i) 15 g. of lead sinter is held in the middle of the reactor by alumina chips placed above and below the differential bed of reducible material. The alumina chips are supported with silica wool at the bottom of the reactor and the bed is held in place by packing the free space at the top of the reactor with silica wool.

(ii) The nitrogen and hydrogen deoxidizing furnaces, O_1 and O_2, are turned on, and the nitrogen flow is started by opening V_1 and connecting T_2 to the line leading to the bottom of the preheater.

(iii) The reactor is weighed. Then the silica cone and socket on the reactor, by means of which the reactor is joined

to the analysis system and the preheater, are smeared with a silicone grease suitable for high temperature work and the reactor is placed in the furnace.

(iv) The system is purged with a slow stream of oxygen-free, dry, nitrogen by connecting T_2 to the bottom of the preheater with T_3 open and T_1 and T_4 closed. The furnaces and the auxiliary heating winding H are switched on, and the reactor and the preheater are slowly brought up to the set temperature for the run.

(v) A weighed drying tube is placed in position B and when the temperature reaches 100°C T_4 and T_5 are opened and T_3 is closed so that the nitrogen purge passes through the reactor and out to atmosphere via the drying tube.

(vi) When the reactor and preheater reach the set temperature the drying tube is removed and reweighed. The weight change represents water driven off from the sinter and the preheater-reactor system together with any residual water in the nitrogen stream.

(vii) Tap T_3 is opened and T_4 closed and the nitrogen flow is diverted to the reactor side of the restriction r by means of T_2. The flow is adjusted to approximately 10 l. s.t.p./min. by the needle valve V_1 and, with T_1 open, the hydrogen flow, which is measured by the rotameter F_1 and controlled by the needle valve V_2, is started. At

this stage hydrogen is passing through the preheater but is prevented from entering the reactor by the nitrogen stream flowing through the restriction r and out to atmosphere via tap T_3.

(viii) The hydrogen flow is set at the desired value - normally 10 l. s.t.p./min. - and the reactor and the preheater temperatures are controlled at the set value for the run. The nitrogen is turned off by closing V_1 and T_2, and after T_4 and T_5 are opened T_3 is shut. A stockclock is started immediately T_3 is closed and the hydrogen flow is readjusted to the set value.

(ix) The drying tubes are removed at measured time intervals, purged with nitrogen, and reweighed. This procedure is continued until the reaction is complete or the rate of reaction is very slow. In the preparation of samples of partially reduced sinter the water leaving the reactor is collected in a single drying tube which is reweighed when the predetermined reduction time has elapsed.

(x) The magnitude of the carryover water is determined; this represents the water vapour content of the inlet gas stream and results from a combination of incomplete oxygen removal and inefficient drying of the incoming gas. Normally, the carryover is measured after the reaction is completed and is taken as the average of the gain in weight per minute of three drying tubes in

succession. However, this method is not always applicable. Firstly, the reaction rate at temperatures below 700°C is such that an excessively long time is needed to reach 100% reduction, and, secondly, this investigation requires the preparation of some partially reduced samples. In each of these cases the carryover value is measured in a separate test. A blank run is performed under identical conditions with the exception that the reactor does not contain a bed of lead sinter and the carryover value obtained in this manner is applied to the results of the previous experimental run.

(xi) At the end of the run the hydrogen is turned off and V_1 and T_2 are closed. The system is then purged of hydrogen by opening V_1 and adjusting T_2 to pass a slow stream of nitrogen through the preheater and the reactor. The reactor, the preheater, and the hydrogen deoxidizing furnace, O_2, are then switched off, and the system allowed to cool.

(xii) When the reactor temperature reaches about 250°C the nitrogen flow is turned off and tap T_4 is closed to isolate the system from the atmosphere. The system then cools overnight to room temperature. The furnace O_1 is also turned off.

(xiii) The reactor is reweighed and then the reaction mass is removed and stored in an air-tight container.

(xiv) The reactor is boiled in aqua-regia for 4 hours to remove any remaining sinter particles, and then dried before re-use.

(xv) The experimental data are used to calculate the per cent. reduction and the reaction rate at various times. The amount of water formed by reaction in a given time interval is the measured gain in weight of the drying tube less the weight gain resulting from the carryover water. The reaction rate is calculated as the weight of water formed by reaction divided by the measured time interval and this average reaction rate is considered to occur at the mid-point of the measurement period. The cumulative water formed by reaction is also obtained and the per cent reduction at any time is equal to the cumulative water formed divided by the amount of water corresponding to 100% reduction.

6.2.3 The Experimental Apparatus for use with Hydrogen-Water Vapour Mixtures

The apparatus used with hydrogen-water vapour mixtures is essentially similar to the arrangement described in Section 6.2.1 for use with pure hydrogen.

A controlled ratio of hydrogen to water vapour is obtained by bubbling the hydrogen stream through distilled water held at a constant temperature. Theoretically, the H_2O/H_2 ratio obtained in this way depends only on the water temperature, but, in practice, the ratio also depends on the efficiency of the saturator. However, the hydrogen flow rate is controlled at 9 l. s.t.p./min., and therefore the degree of

saturation and the H_2O/H_2 ratio are constant for a given water temperature.

The additions to the apparatus used with pure hydrogen shown in Figure 1 are as follows:

(i) A heating tape wrapped around the hydrogen line leading from the saturator to the bottom of the preheater. This prevents condensation of the hydrogen-water vapour mixture produced in the saturator, and the heat input to this winding is controlled by a 1 kW "Variac" autotransformer.

(ii) A constant-temperature water bath containing a hydrogen saturator placed in the hydrogen line between the flowmeter F_1 and the stopcock T_1. The water bath temperature is controlled by a mercury regulator actuating a Sunvic Hot-wire Vacuum Switch to within $\pm$ 0.1°C of the set point. The hydrogen saturator consists of two glass jars, 4 in. diameter x 15 in. high, in parallel, filled with distilled water to a height of 10 in., and each containing two bubblers. The bubblers consist of a piece of 1 in. diameter, porosity 1, sintered glass. The hydrogen flow is heated to the water bath temperature in 15 ft. of $\frac{3}{8}$ in. diameter copper tube placed in the bath before the saturators.

6.2.4 <u>The Experimental Procedure for use with Hydrogen-Water Vapour Mixtures</u>

The procedure is the same as that described in Section 6.2.2

for reduction by pure hydrogen.

The desired H_2O/H_2 ratio is obtained by adjusting the water bath temperature; an initial series of tests established the relation between the water bath temperature and the H_2O/H_2 ratio for the hydrogen flow of 9 l. s.t.p./min. used throughout the tests. It was then assumed that the H_2O/H_2 ratio was constant for a given water temperature.

Normally, the samples were reduced for a known, set, time and the water formed was not collected. However, in the initial stages of the reaction the water formed by reaction is quite a large fraction of the total water content of the gases leaving the reactor, and an approximate measure of the reaction rate may be obtained in the normal way by absorbing the water in the drying tubes. However, in general, the amount of reduction is calculated from the chemical analysis of the reduced solids by the method set out in Section 6.5.2.2.

6.3 Accuracy of Results

A detailed discussion of the accuracy of the data obtained in the fixed-bed apparatus is presented in Appendix VI.1.

For the A series of runs, in which the overall reaction rate is determined at various times, the accuracy of the measured reaction rate decreases as the reaction proceeds; however, it is claimed that the accuracy of the reported reaction rates exceeds ± 10% for the major part of the reaction.

In the C to F Series the per cent reduction of the sample is calculated from the chemical analysis of the reduced samples. The percentage accuracy of the fraction reduced increases as the reduction increases, but the actual deviation from the true value is larger at

the high per cent reductions; however, it is considered that the maximum deviation from the true per cent reduction does not exceed $\pm$ 5 per cent reduction.

The accuracy of the calculated overall per cent reduction varies with the degree of reduction, but it is claimed that the per cent reductions calculated from data obtained in the A, C, D and E Series of tests are correct to within $\pm$ 2.0 and $\pm$ 0.5 per cent reduction, respectively.

6.4 Experimental Programme

The experimental work carried out in the fixed-bed reactor is summarized in Tables 6 and 7, which set out the experimental conditions for each test.

6.4.1 The A Series of Runs

These runs were performed using pure hydrogen as the reducing gas. The amount of water formed was measured at various time intervals to enable the overall rate curve to be drawn. The experimental apparatus and procedure detailed in Sections 6.2.1 and 6.2.2 were used for each run in this series. The experimental conditions are shown in Table 6, and the detailed results are given in Appendix VII.2.

TABLE 6

EXPERIMENTAL CONDITIONS FOR THE A SERIES OF RUNS

Run No.	Size fraction (B.S.S.)	Temperature (°C)	Gas flow rate (l. s.t.p./min.)
A:1	-25 +36	600 ± 3	5.0
A:2	-25 +36	600 ± 5	10.0
A:3	-25 +36	700 ± 4	5.0
A:4	-25 +36	700 ± 5	10.0
A:5	-25 +36	800 ± 5	5.0
A:6	-25 +36	800 ± 2	10.0
A:7	-25 +36	800 ± 5	13.0
A:8	-25 +36	500 ± 6	10.0
A:9	-72 +100	700 ± 4	10.0
A:10	-72 +100	700 ± 4	13.0
A:11	-72 +100	500 ± 2	10.0
A:12	-72 +100	600 ± 4	10.0
A:13	-72 +100	800 ± 6	13.0
A:14	-52 +72	500 ± 4	10.0
A:15	-52 +72	600 ± 5	10.0
A:16	-52 +72	700 ± 5	10.0
A:17	-36 +52	500 ± 2	10.0
A:18	-36 +52	600 ± 6	10.0
A:19	-36 +52	700 ± 8	10.0

6.4.2 The C to E Series of Runs

These series were carried out with pure hydrogen as the reducing gas using the experimental apparatus and procedure described in Sections 6.2.1 and 6.2.2. However, the aim of these tests was to produce a series of samples of partially reduced sinter, and in each test the sample was reduced for a set time. The total water formed during this time was measured, and the samples were analyzed by the methods set out in Appendix I.2. The experimental conditions are given in Table 7, and the detailed results are set out in Appendix VII.3. The hydrogen flow rate was 10 l. s.t.p./min. in each case.

TABLE 7

EXPERIMENTAL CONDITIONS FOR THE C TO E SERIES OF RUNS

Run No.	Size fraction (B.S.S.)	Temperature (°C)	Reduction time (min.)
C:1	-25 +36	600	5
C:2	-25 +36	600	11
C:3	-25 +36	600	20
C:4	-25 +36	600	35
C:5	-25 +36	600	60
C:6	-25 +36	600	90
C:7	-25 +36	600	240
C:8	-25 +36	600	2
D:1	-52 +72	700	1
D:2	-52 +72	700	3
D:3	-52 +72	700	7
D:4	-52 +72	700	15
D:5	-52 +72	700	30
D:6	-52 +72	700	60
E:1	-52 +72	500	12
E:2	-52 +72	500	24
E:3	-52 +72	500	45
E:4	-52 +72	500	90

6.4.3 The F Series of Runs

In these tests samples of -52 +72 # (B.S.S.) lead sinter were reduced for various, known, times by a hydrogen-water vapour mixture containing 9 per cent H_2O by volume. This was equivalent to a hydrogen partial pressure of 0.91 atm., and the hydrogen flow rate was 9 l. s.t.p./min. The experimental apparatus and procedure used in this Series are described in Sections 6.2.3 and 6.2.4, respectively, and the experimental conditions are listed in Table 8. The samples prepared in these tests were analysed by the methods described in Appendix I.2, and the results are set out in Appendix VII.3.

TABLE 8

EXPERIMENTAL CONDITIONS FOR THE F SERIES OF RUNS

Run No.	Reduction time (min.)	Temperature (°C)
F:1	1	700
F:2	3	700
F:3	7	700
F:4	11	700
F:5	2	600
F:6	11	600
F:7	20	600

6.5 Discussion of Results

6.5.1 The Weight Lost by the Sinter during Reduction

The data presented in Appendix VI.2 may be used to estimate the amount of material, apart from oxygen, which is removed from the sinter during reduction. The difference between the measured loss in weight of the reactor and the weight of oxygen associated with the water formed represents the weight of material lost by the sinter. Now, although Mostowitsch [60] (1907) concluded that lead oxide was volatile at 700°C, the vapour pressure data presented by Perry [61] (1950) indicate that lead oxide, lead sulphide and metallic lead are unlikely to vapourize to any significant extent at temperatures below 900°C. However, the vapour pressure of metallic zinc is quite high (60 mm. Hg) at 700°C, and volatilization losses may be appreciable. The experimental results confirm these conclusions; the decrease in total lead content observed in some cases is within the limit of sampling and analytical errors, but the total zinc content is markedly decreased as the per cent reduction and the reduction time increases. For example, the reduced sample produced in Run A:13 [-72 +100# (B.S.S.) sinter reduced at 800°C] contains 38.6 mass per cent lead and 3.7 mass per cent zinc; the total lead and total zinc contents of the unreduced material are 38.9% and 9.9%, respectively. In Table 9 the loss in weight of the sinter (excluding oxygen removed as water) is compared with the calculated weight loss due to vapourization of zinc; the data are obtained from the C, D and E series of runs (see Appendix VII.3).

TABLE 9

MATERIALS BALANCE ON THE DIFFERENTIAL REACTOR

Run No.	Total Wt. Loss (g.)	Oxygen Removed (g.)	Difference (g.)	Wt. of Zn Lost (g.)
C:8	0.0884	0.0955	-	0.087
C:1	0.2776	0.2565	0.021	-
C:2	0.4409	0.4035	0.037	0.0315
C:3	0.6197	0.5500	0.070	0.0615
C:4	0.8579	0.745	0.113	0.0315
C:5	0.9975	0.861	0.1365	0.1060
C:6	1.1766	0.990	0.187	0.137
C:7	1.5511	1.312	0.2391	0.286
D:1	0.2855	0.220	0.0655	0.082
D:2	0.4843	0.446	0.038	0.075
D:3	0.6922	0.637	0.055	0.075
D:4	1.0254	0.947	0.078	0.012
D:5	1.2237	1.080	0.144	0.128
D:6	1.6000	1.330	0.270	0.338
E:1	0.1946	0.180	0.015	-
E:2	0.3566	0.356	-	0.030
E:3	0.4933	0.482	0.011	0.015
E:4	0.6728	0.651	0.022	0.045

The data presented in Table 9 do not constitute a complete mass balance since the loss in weight due to the removal of material such as lead and sulphur is not considered. In addition, the accuracy of the reported values is limited by

(i) the difficulty associated with the selection of a small representative sample of reduced material,

(ii) the limited accuracy of the measured change in reactor weight, and

(iii) to a lesser extent, the analytical errors.

However, despite these facts, an examination of Table 9 reveals that the loss in sinter weight attributed to vapourization is essentially due to the removal of zinc. Also, the loss of zinc is not significant until approximately 50% overall reduction has occurred (Runs C:4 and D:4), and this indicates

(i) zinc is vapourized as the metal rather than as the oxide or sulphide, and

(ii) the reduction of the zinc compounds does not occur in the initial stages of the reaction.

6.5.2 Calculation of Per Cent Reduction

The experimental results obtained under a given set of experimental conditions relate the reduction time to the weight of water formed and the change in composition of the lead compounds in the sinter. However, in this form, the results of various tests cannot be conveniently compared and evaluated, and it is desirable to convert the measured quantities of water formed and change in chemical composition to percentage reductions.

6.5.2.1 Overall per cent reduction

The amount of oxygen removed from the sinter is directly related to the amount of water formed, and it is assumed that the overall reduction is measured by the amount of water formed by reaction.

The reaction rates associated with the removal of the last traces of oxygen from the sinter are very slow and it is difficult to ascertain the total water which may be formed from a given sample. Also, the various size fractions have slightly different compositions and therefore the total water formed by reaction is probably different for each particle size. However, a consideration of the experimental results obtained at 700°C and 800°C, which are presented in Appendix VII.2, reveals that the maximum amount of water formed for all particle sizes may be taken as 1.70 g./15 g. sinter without serious error. Consequently, this value has been arbitrarily chosen to represent the completion of reaction at all temperatures and the overall per cent reductions are calculated on the basis that 1.70 g. H_2O/15 g. sinter is equivalent to 100 per cent reduction.

6.5.2.2 Chemical per cent Reduction

The per cent reduction calculated from the chemical composition may be based on the metallic lead, or the acetate-soluble lead, content of the sample.

The experimental data show that lead sulphide is formed during the reaction. This results from the reduction of oxidized lead compounds containing sulphur, e.g., lead sulphate, and causes the per cent reduction based on the metallic lead content to be less than the per cent reduction calculated from the oxidized lead content. Therefore,

the selection of the calculation basis for the chemical per cent reduction depends on the requirements of the investigation; a theoretical comparison of the overall per cent reduction with the chemical per cent reduction indicates the use of the oxidized lead content, but in a technological investigation the important factor is the amount of metallic lead formed. In the present case the semi-technical nature of the investigation indicates that both per cent reductions should be considered.

The chemical per cent reductions are calculated as follows. Firstly, the oxidized lead contents of the unreduced size fractions reported in Table 5 are taken to represent 100 per cent oxidized lead reduction. Secondly, the total combined lead in the unreduced samples may theoretically be reduced to metallic lead, and the metallic lead values corresponding to 100% reduction are chosen as the difference between the total lead contents and the initial metallic lead contents reported in Table 5. The reduction of a sample is therefore calculated as the measured increase in metallic lead content, or decrease in oxidized lead content, divided by the value corresponding to complete reduction.

In Section 6.5.1 it was established that the vapourization losses consisted mainly of zinc. The total lead content of a sample is therefore almost unaltered during reduction, and the accuracy of the calculated chemical per cent reduction depends only on the analytical accuracy and the sampling technique.

6.5.3 The Relation Between the Reduction of the Lead Compounds and the Overall Reduction

The relation between the overall reduction, based on the water formed, and the chemical reduction, based on

(i) the decrease in oxidized lead content, and

(ii) the increase in metallic lead content,

was determined for -52 +72 # (B.S.S.) particles at 500°C and 700°C, and for -25 +36 # (B.S.S.) particles at 600°C. These tests formed the C, D and E Series of runs and the detailed experimental data are tabulated in Appendix VII.3. The samples were prepared by the method discussed in Section 6.2.2 and the reduced samples were analysed by the techniques described in Appendix I.2. The results are summarized in Table 10, and the per cent reductions reported in this Table are calculated by the procedure set out in Section 6.5.2.

TABLE 10

SUMMARY OF EXPERIMENTAL RESULTS FOR THE C, D AND E SERIES

Run No.	Temperature (°C)	Reduction (min.)	Per Cent Reduction		
			Overall	Oxidized Lead	Metallic Lead
C.8		2	6.3	0.5	-
C.1		5	17.0	13.9	10.6
C.2		11	26.7	31.0	27.0
C.3	600°C	20	36.4	45.6	39.0
C.4		35	49.3	57.6	45.1
C.5		60	57.0	68.0	55.6

TABLE 10 (contd.)

Run No.	Temperature (°C)	Reduction (min.)	Per Cent Reduction		
			Overall	Oxidized lead	Metallic lead
C.6		90	65.5	73.0	61.7
C.7		240	86.9	83.1	70.9
D.1	700°C	1	14.6	5.8	5.0
D.2		3	29.5	25.2	20.0
D.3		7	42.2	42.6	36.5
D.4		15	62.6	67.5	58.0
D.5		30	71.5	80.9	68.6
D.6		60	88.0	90.0	73.0
E.1	500°C	12	11.9	5.3	6.0
E.2		24	23.6	19.7	16.3
E.3		45	31.9	33.2	31.0
E.4		90	43.1	48.4	41.5

The results presented in Table 10 are illustrated in Figure 3 as graphs of per cent reduction against time for reduction at 500°C, 600°C, and 700°C. These plots indicate the relation between the overall reduction based on the water formed and the chemical reduction based on

(i) the decrease in oxidized lead content, and

(ii) the increase in metallic lead content,

at each temperature used in the experimental work. If required,

the overall reaction rate measured experimentally may be converted to the rate of reduction of the lead compounds on the basis of these graphs. However, reference to Figure 3 suggests that the overall reduction is a satisfactory measure of the reduction of the lead compounds up to 70% reduction. Above this value the oxidized lead content decreases much more quickly than the metallic lead content increases. This may be attributed to the reduction of compounds such as $PbSO_4$, and an examination of the experimental data presented in Appendix VII.3 confirms this conclusion; the measured lead sulphide content increases quite significantly in the latter stages of the reaction.

Now, the results obtained at 700°C show that towards the end of the reaction the per cent reductions based on the change in oxidized lead content approximate the values obtained for the overall reduction. Therefore, it may be concluded that the overall reduction indicates the degree of oxygen removal from the lead compounds throughout the reaction. However, the lead compounds are not reduced entirely to metallic lead. After approximately 70% reduction the reduction of compounds such as $PbSO_4$ apparently commences; these compounds contribute to the overall reaction without necessarily increasing the amount of metallic lead formed.

The results discussed above are strictly only applicable to the specific conditions of particle size, gas flow rate, and gas composition used in the preparation of the reduced samples. Now, it is unlikely that the gas flow rate and the particle size influence the

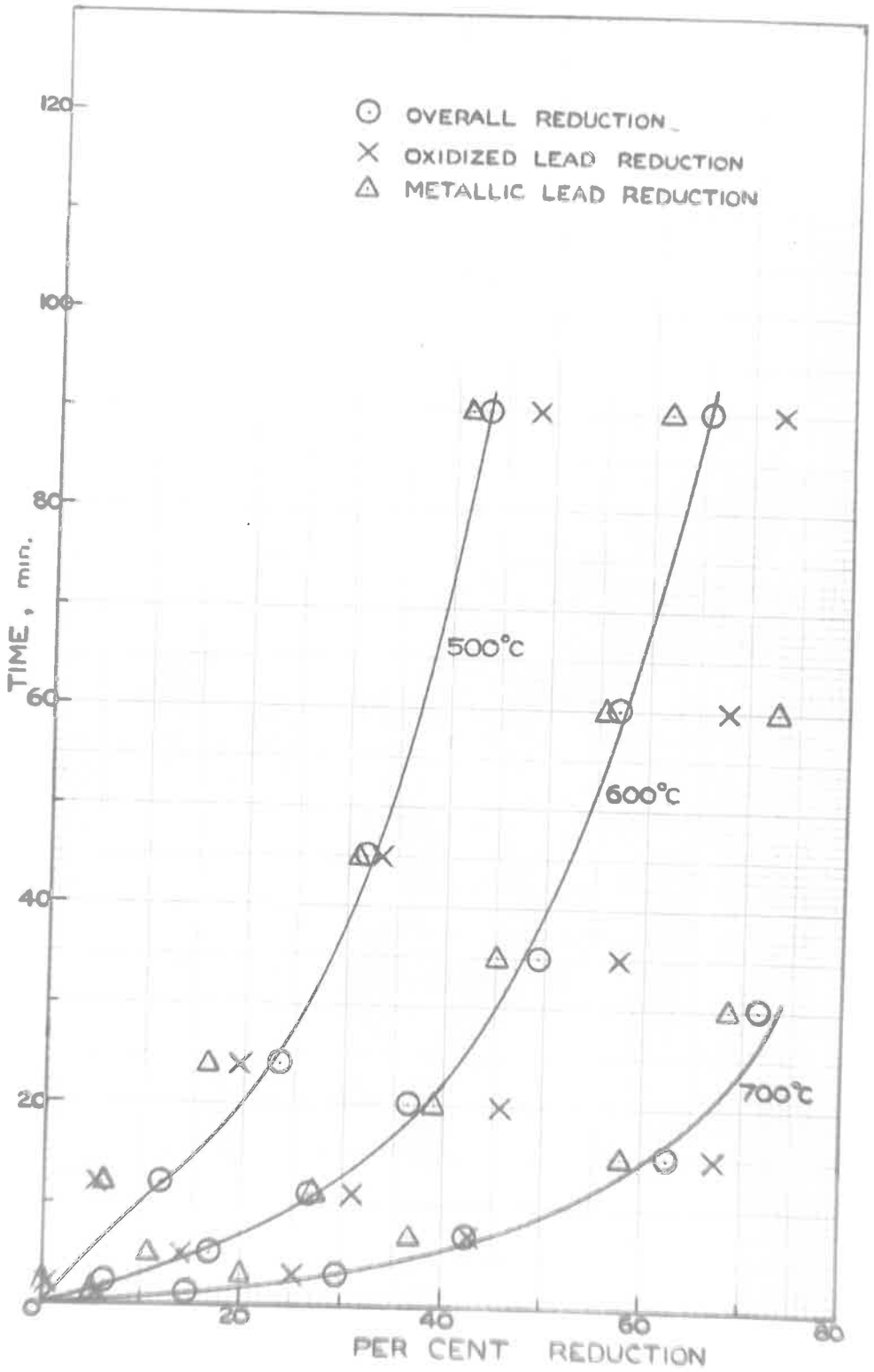

Fig. 3 - The Relation between the Overall Per Cent Reduction and the Reduction of the Lead Compounds at 500°C, 600°C, and 700°C.

experimental relations presented in Figure 3, but the presence of water vapour may have some effect. However, it is impossible to establish the effect of water vapour with the available apparatus since the overall reduction can not be measured accurately for reduction by H_2-H_2O mixtures (see Section 6.1). Therefore, it is necessary to assume that the data reported in Table 10 may be applied to other systems and other system conditions, and it is considered that this assumption will not introduce serious errors.

Figure 3 also shows that reduction of the lead compounds does not commence until approximately 10% overall reduction has occurred; this suggests preferential reduction of a compound other than the oxidized lead compounds and indicates that the behaviour of lead sinter is not completely homogeneous during reduction.

6.5.4 The Effect of System Variables

In the present investigation the important system variables are the reducing gas velocity, the reduction temperature, the particle size, and the H_2O/H_2 ratio in the reducing gas, and the effects of these factors on the overall reaction rate are discussed in turn.

6.5.4.1 Gas Velocity

In a differential, fixed-bed, reactor the gas velocity may only influence the overall reaction rate under conditions such that the reaction rate is controlled by the rate of diffusion through the inert gas film. The other factors which may control the overall reaction rate are the rate of mass transfer of the gaseous reactants and products

through the solid phase and the rate of the chemical reaction.

In general, the chemical reaction rate is increased by increasing the system temperature, and the resistance of the solid phase to mass transfer is decreased by decreasing the particle size; gas-film diffusion control is therefore normally favoured by high temperatures and small particle sizes. Now, the experimental conditions covered in the fluidization experiments involve temperatures in the range 500°C to 700°C and particle size fractions varying from -25 +36 # (B.S.S.) to -72 +100 # (B.S.S.). Consequently, it should be sufficient for the needs of the present investigation to study the effect of gas velocity on the rate of reduction of -72 +100 # (B.S.S.) particles at 700°C.

The effect of gas velocity on the rate of reaction between -72 +100 # (B.S.S.) particles and hydrogen at 700°C is shown in Figure 4, which is a plot of per cent reduction against $\log_{10}$ (reaction rate). An examination of this Figure discloses that increasing the gas flow from 10 to 13 l. s.t.p./min. does not increase the rate of reaction. Therefore, it is probable that the rate of mass transfer through the inert gas film does not control the overall reaction rate at gas flow rates of 10 l. s.t.p./min. and above. This conclusion is supported by the additional data presented in Figure 5, which refer to -25 +36 # (B.S.S.) particles reduced at 600°C and 800°C. At 600°C the rate curves obtained at 5 and 10 l. s.t.p./min. are almost identical. At 800°C the reaction rate curve measured at a gas flow of 5 l. s.t.p./min. is always less than the rate curve obtained at a gas flow of 10 l. s.t.p./min.; however, the values obtained at 10 and

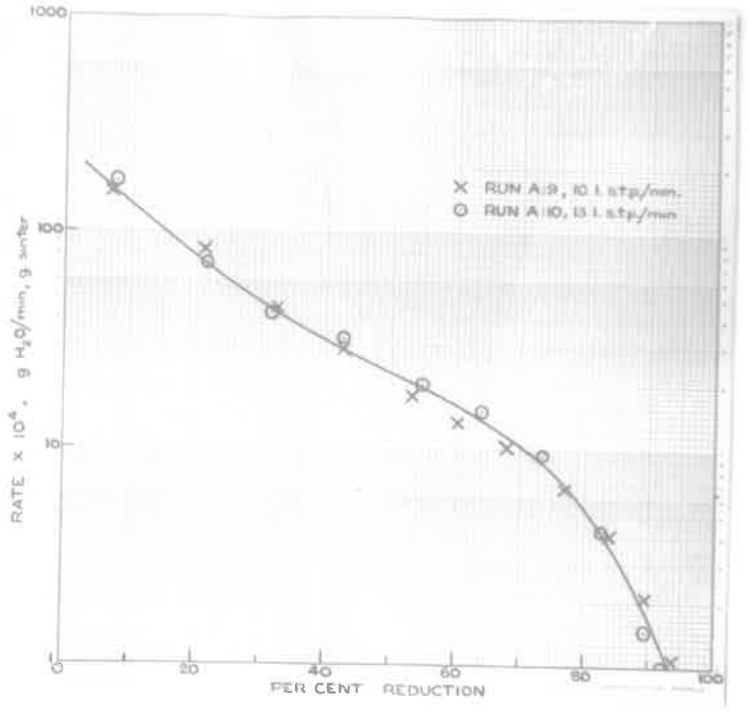

Fig. 4 - The Effect of Gas Velocity on the Rate of Reaction for -72 +100 # (B.S.S.) particles reduced at 700°C in a Fixed Bed

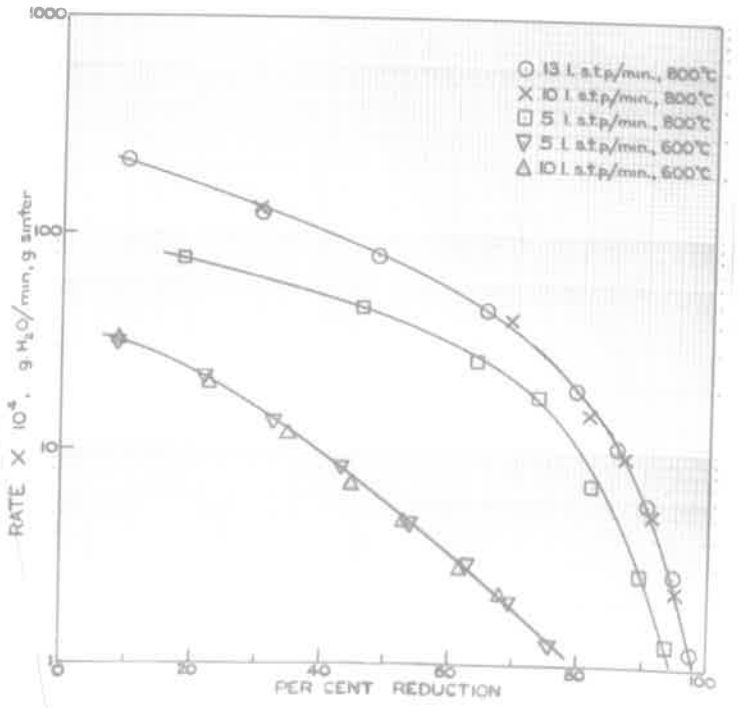

Fig. 5 - The Effect of Gas Velocity on the Rate of Reduction of -25 +36 # (B.S.S.) particles reduced at 600°C and 800°C in a Fixed Bed

13 l. s.t.p./min. lie on a single curve. Consequently, it may be concluded that for temperatures up to 700°C control of the overall reaction rate by gas-film diffusion may be prevented for particle size fractions down to -72 +100 # (B.S.S.) by using a gas flow rate of 10 l. s.t.p./min. The effect of gas velocity at 800°C has not been fully established; however, a flow rate of 10 l. s.t.p./min. is satisfactory for -25 +36 # particles (see Figure 5).

6.5.4.2 Reduction Temperature

The rate of reaction was measured at temperatures in the range 500°C to 800°C for particle size fractions varying from -25 +36 # (B.S.S.) to -72 +100 # (B.S.S.). The gas flow rate used in these tests was 10 l. s.t.p./min. of hydrogen. The results are illustrated in Figures 6 to 9, which are plots of log (reaction rate) against per cent reduction for the different size fractions.

These curves clearly show the strong temperature dependence of the reaction rate; at 20% reduction increasing the temperature from 500°C to 800°C produces a twenty-five fold increase in reaction rate, and the time required for 80% reduction of -25 +36 # (B.S.S.) particles is decreased from 180 minutes to 15 minutes by increasing the temperature from 600°C to 800°C.

The order of the temperature dependence of the reaction rate is given by the value of the index "n" in equation (16). This equation may be rewritten as

$$\log R = \log C + n \log T \qquad \text{----------(23)}$$

where

R = reaction rate (g. H_2O/g. sinter, min.),

T = absolute temperature (°K), and

C and n = constants

A typical plog of log R against log T is shown in Figure 10, and it can be seen that the points at each per cent reduction lie on different straight lines. The slope of these lines is equal to the index "n", and the values obtained from the experimental data are listed in Table 11.

TABLE 11

EFFECT OF THE DEGREE OF REDUCTION ON THE TEMPERATURE DEPENDENCE OF THE OVERALL REACTION RATE

Size Fraction (B.S.S.)	Value of n at different overall per cent reductions				
	10%	20%	40%	60%	80%
-25 +36	9.4	9.8	12.3	13.9	14.8
-36 +52	9.2	10.0	12.8	13.6	15.1
-52 +72	9.7	10.1	12.3	13.9	16.0
-72 +100	10.0	9.2	11.1	13.1	15.6

Table 11 reveals that the value of the index "n" increases with increasing per cent reduction, e.g., at 10% reduction the average value of n is 9.7 whereas at 80% reduction the average value is 15.5. This change in temperature dependence of the overall reaction rate indicates that the reaction mechanism changes as the reaction proceeds, and suggests that the sinter is not reducing as a homogeneous solid, i.e. the significance of the contributions of each of the reactions to the overall reaction rate depends on the amount of reduction.

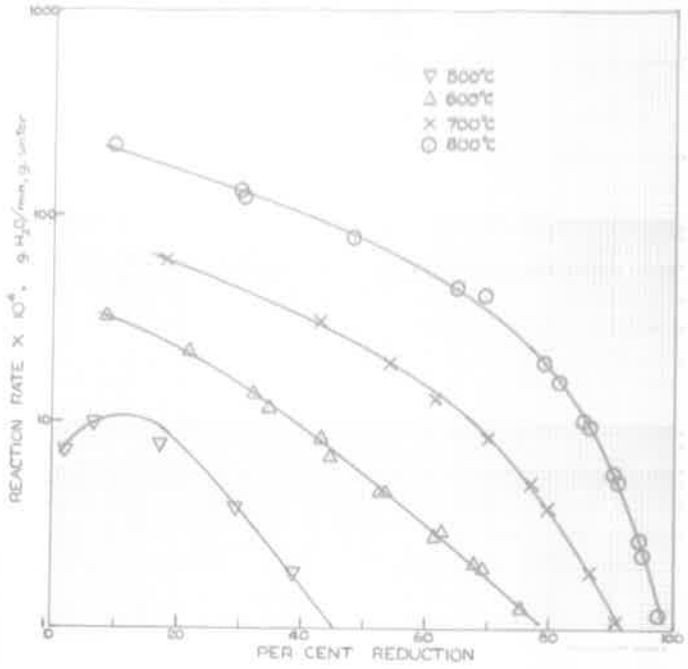

Fig. 6 - The Effect of Temperature on the Rate of Reduction of -25 +36 # (B.S.S.) particles in a Fixed Bed

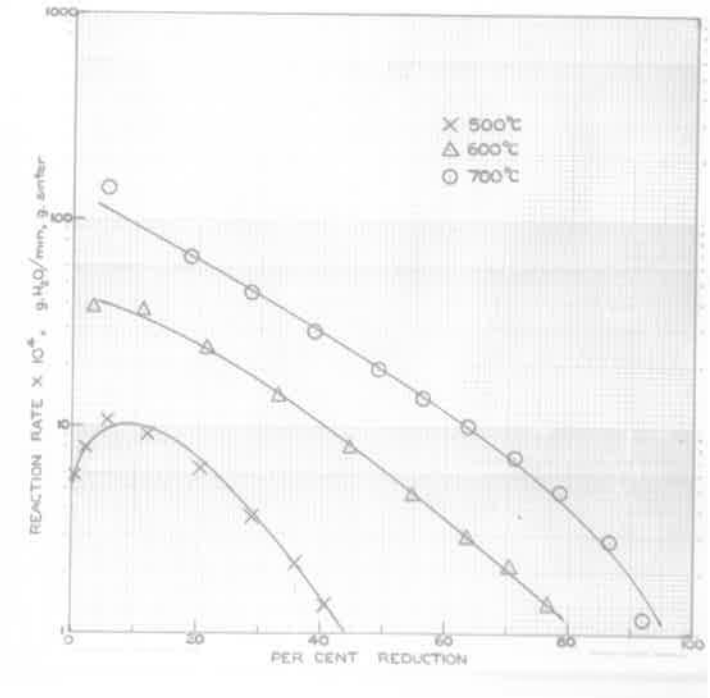

Fig. 7 - The Effect of Temperature on the Rate of Reduction of -36 +52 # (B.S.S.) Particles in a Fixed Bed

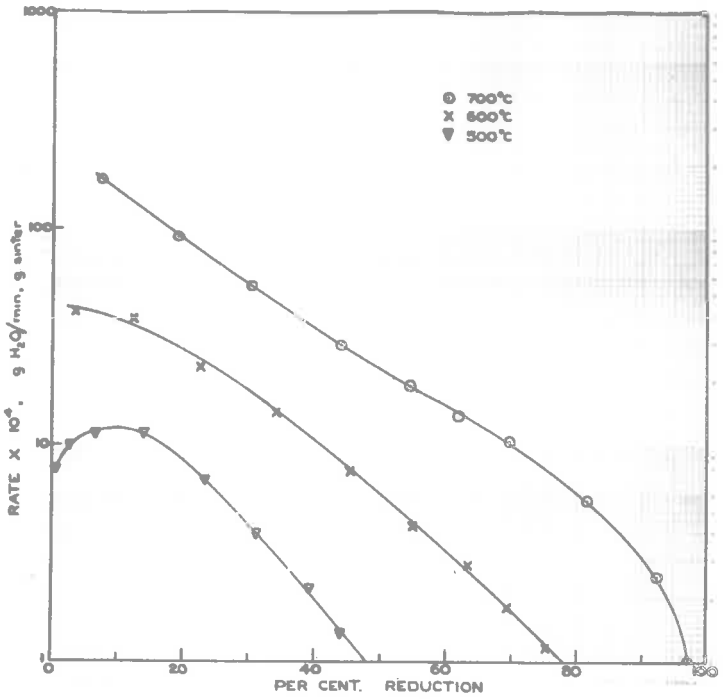

Fig. 8 - The Effect of Temperature on the Rate of Reduction of -52 +72 # (B.S.S.) Particles in a Fixed Bed

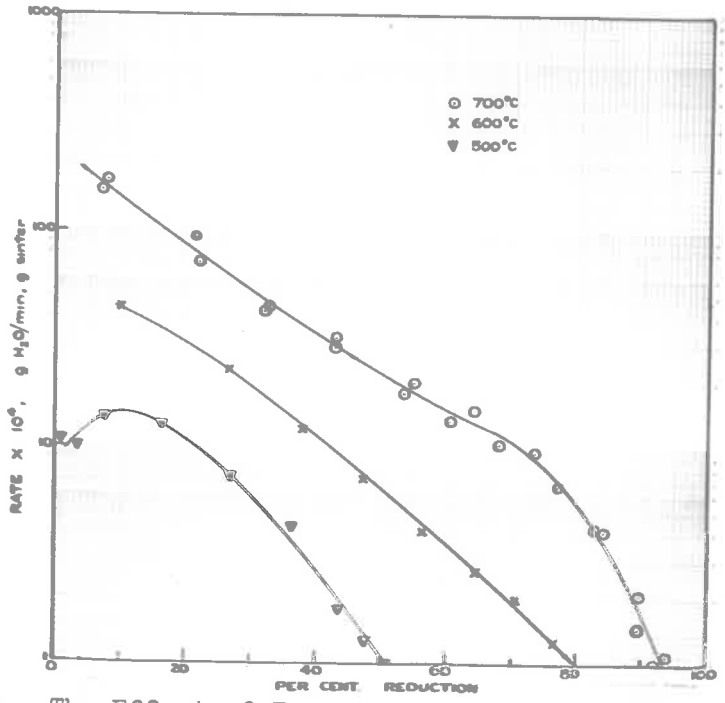

Fig. 9 - The Effect of Temperature on the Rate of Reduction of -72 +100 # (B.S.S.) Particles in a Fixed Bed

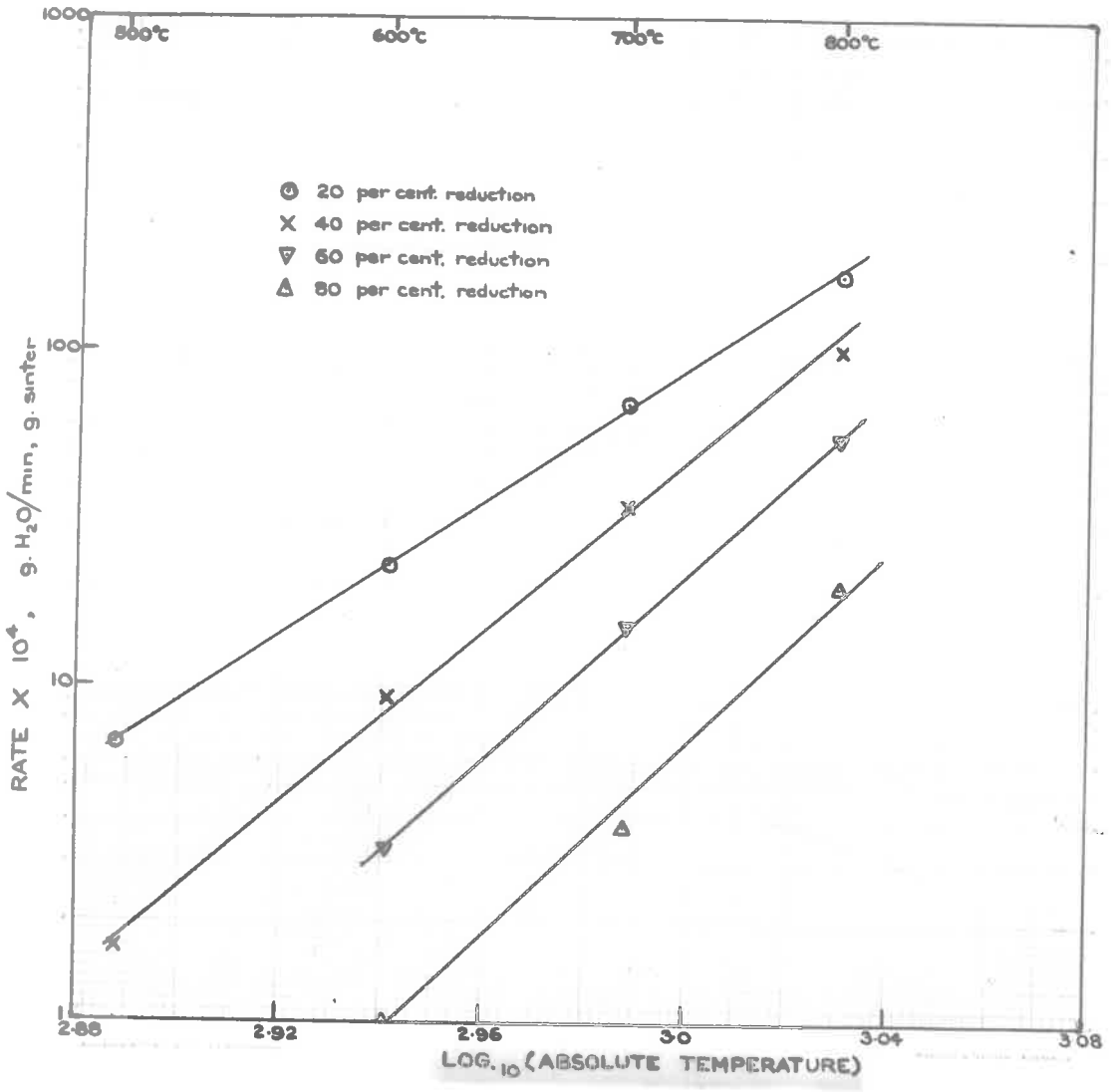

Fig. 10 - The Temperature Dependence of the Overall Fixed-Bed Reaction Rate for -25 +36 # (B.S.S.) particles

The shape of the curves obtained at 500°C is typical of an autocatalytic reaction, and many oxides exhibit this behaviour on reduction, viz., copper oxide [23] (1921), nickel oxide [24,26] (1924) and (1952), germanium dioxide [22] (1956), and iron oxide [59] (1960). Now, Matthew [9] (1959) has established that auto-catalysis does not occur in the reduction of pure lead monoxide by hydrogen and H_2-H_2O mixtures. Also, it is shown in Section 6.5.1 that reduction of the zinc compounds does not occur in the initial stages of the reaction. Therefore, in the absence of data on the reduction of $CaSO_4$, it is tentatively suggested that the auto-catalytic effect results from the reduction of iron oxide.

6.5.4.3 Particle Size

The overall rates of reaction for -25 +36 #, -36 +52 #, -52 +72 #, and -72 +100 # (B.S.S.) particles reduced by hydrogen at 500°C, 600°C, and 700°C, are plotted against the overall per cent reduction in Figure 11.

The initial reaction rate, R_o, may be estimated by extrapolating these curves to zero per cent reduction, and these values may be used to establish the effect of the initial specific surface, A_o. The initial surface areas are presented in Table 4, Section 5.2, and the effect of surface area on the initial reaction rate is shown in Table 12.

TABLE 12

THE EFFECT OF SURFACE AREA ON THE INITIAL OVERALL REACTION RATE

Size Fraction (B.S.S.)	Temperature (°C)	R_o g. H_2O/min., g. sinter	R_o/A_o g. H_2O/min., cm^2
-25 +36	500	5.3×10^{-4}	1.63×10^{-7}
-36 +52		6.1×10^{-4}	1.57×10^{-7}
-52 +72		7.2×10^{-4}	1.57×10^{-7}
-72 +100		9.4×10^{-4}	1.74×10^{-7}
-25 +36	600	3.8×10^{-3}	1.17×10^{-6}
-36 +52		4.45×10^{-3}	1.14×10^{-6}
-52 +72		4.90×10^{-3}	1.07×10^{-6}
-72 +100		6.60×10^{-3}	1.22×10^{-6}
-25 +36	700	1.45×10^{-2}	4.45×10^{-5}
-36 +52		1.70×10^{-2}	4.36×10^{-5}
-52 +72		2.05×10^{-2}	4.45×10^{-5}
-72 +100		2.25×10^{-2}	4.17×10^{-5}

An examination of this Table reveals that the initial reaction rate is determined by the initial surface area. Now, the rate per unit area cannot be estimated at various per cent reductions because it is impossible to measure the interfacial surface area. However, the curves presented in Figure 12, which relate the initial surface area to the time required for various per cent reductions, show that the

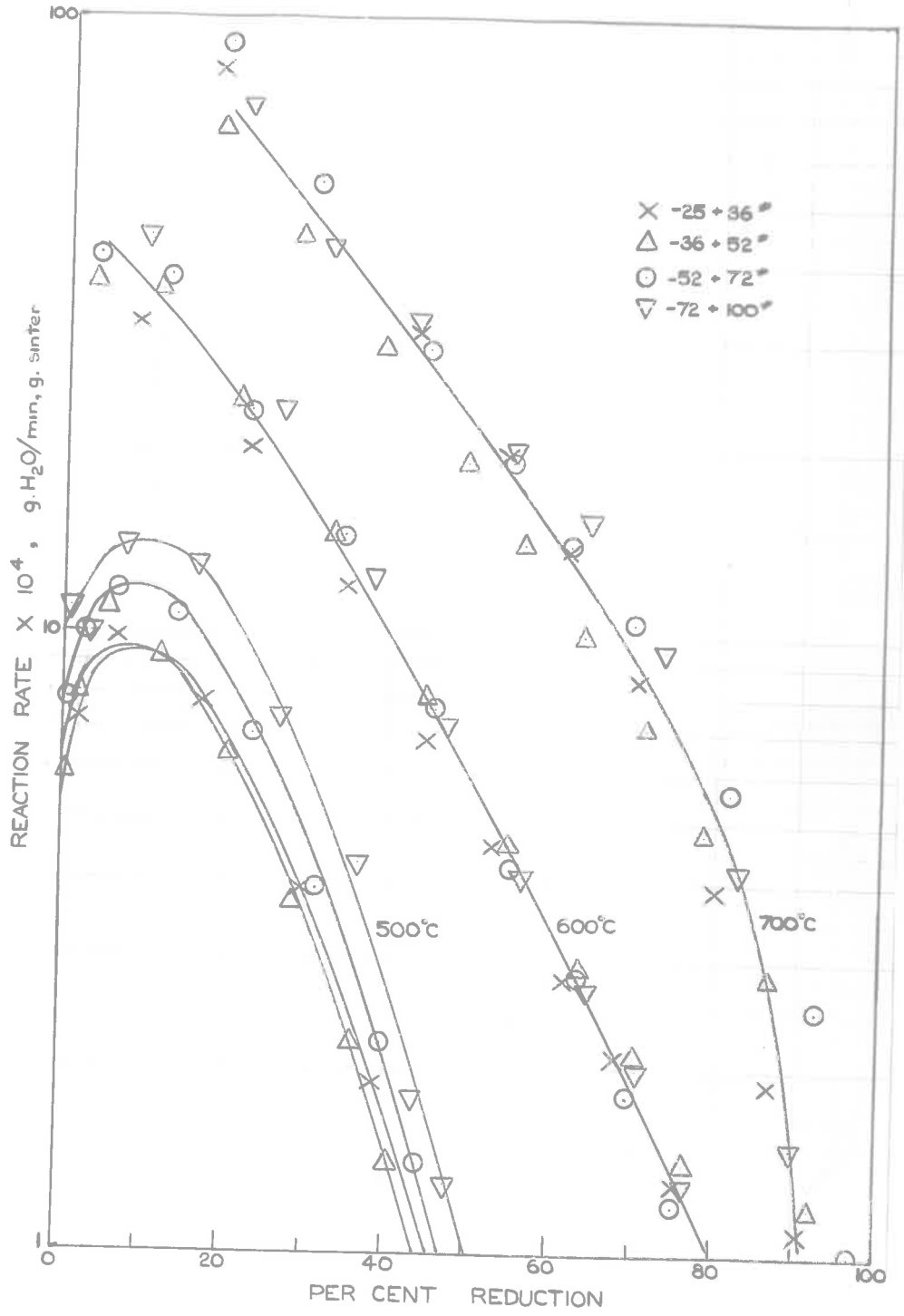

Fig. 11 - The Effect of Particle Size on the Fixed Bed Reaction Rate at 500°C, 600°C, and 700°C

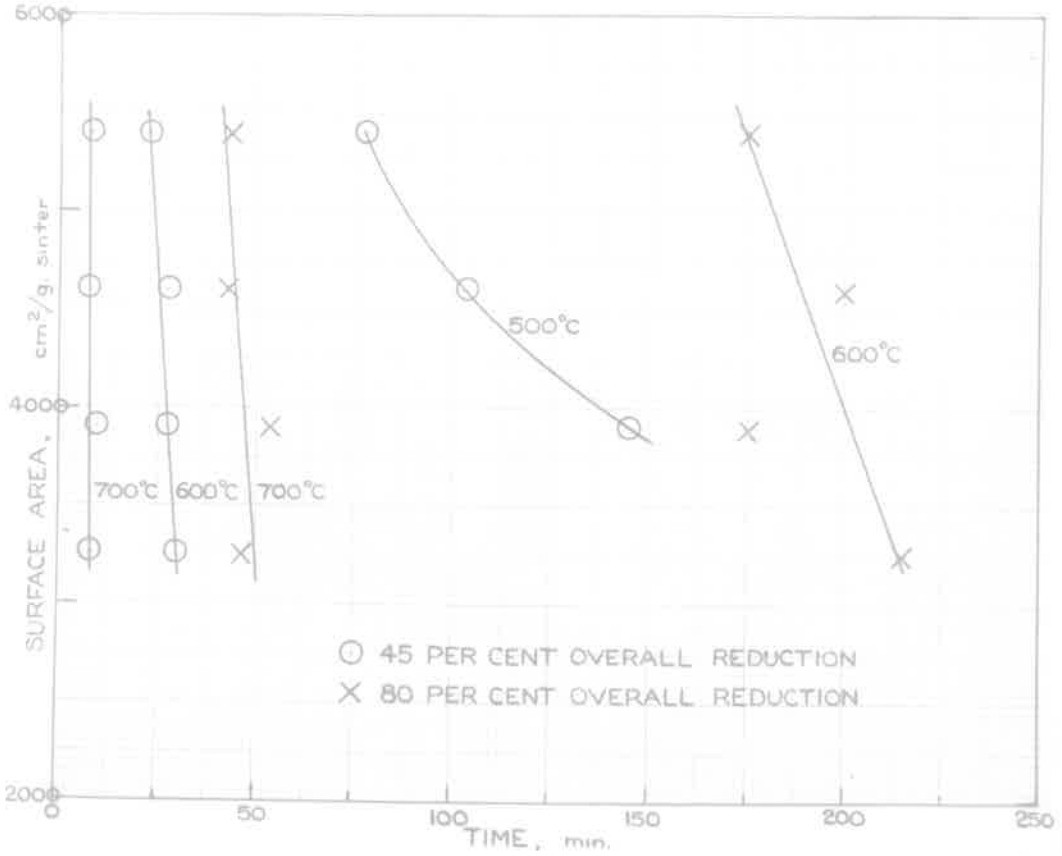

Fig. 12 - The Effect of Initial Specific Area on the Time Required for 45% and 80% Overall Reduction in the Fixed Bed

effect of specific surface decreases as the reduction temperature increases. At 500°C, the time required for 45 per cent overall reduction is directly proportional to the initial specific surface area, whereas at 700°C it is independent of this variable. Similarly, the effect of initial surface area on the time required for 80% reduction is less at 700°C than at 600°C.

There are several factors, such as an increase in the rate of diffusion through the solids and an increased tendency for the particles to crack, which may cause the effect of particle size to diminish with increasing reduction temperature. However, the relatively strong temperature dependence of the overall reaction rate indicates that solid-phase diffusion is not the rate-controlling factor, and also it is unlikely that cracking and fissuring of the particles at higher temperatures could obscure the particle size effect observed at 500°C. Now, the sinter particles removed from the reactor after reduction at 600°C and 700°C are partially fused together whereas particles reduced at 500°C still retain their original identity. Partial fusion of the bed of solids would tend to make the gas-solid contact area independent of the particle size, and it is therefore considered that the effect of particle size is masked in the fixed-bed reactor by partial fusion of the particles which occurs at temperatures of 600°C and above. However, the effect of particle size is apparently quite important, and relatively fast reaction rates may be obtained by decreasing the particle size provided the tendency to agglomerate is overcome.

6.5.4.4 Reduction by H_2-H_2O Mixtures

The overall reaction rate can not be measured accurately during reduction by H_2-H_2O mixtures (see Section 6.1), and the effect of water vapour on the reaction rate may strictly only be determined from analysis of the reduced solids. The experimental data therefore relate the per cent reduction of the lead compounds to the reduction time.

The reduction of -52 +72 # (B.S.S.) particles by a H_2O-H_2 mixture containing 9% H_2O by volume (p_{H_2} = 0.91 atm.) was investigated at 600°C and 700°C. The apparatus and experimental technique described in Sections 6.2.3 and 6.2.4, respectively, were used, and these tests constituted the F Series of runs. The detailed results are presented in Appendix VII.3.4, and these results, which are summarized in Table 13, are compared with data obtained using pure hydrogen in Figure 13.

TABLE 13

SUMMARY OF EXPERIMENTAL RESULTS FOR THE F SERIES

Run No.	Temperature (°C)	Reduction time (min.)	Per Cent Reduction	
			Oxidized Lead	Metallic Lead
F.1	700	1	5.0	3.7
F.2		3	21.6	18.0
F.3		7	38.5	33.0
F.4		11	50.1	44.2

TABLE 13 (contd.)

Run No.	Temperature (°C)	Reduction time (min.)	Per Cent Reduction	
			Oxidized Lead	Metallic Lead
F.5	600	2	1.7	-
F.6		11	28.0	23.0
F.7		20	41.9	36.6

Reference to Figure 13, which is a plot of reduction time against chemical per cent reduction, shows that the reduction of the lead compounds is retarded by the presence of water vapour; this effect is, however, only small. These results agree with the data obtained by Matthew [9] (1959), who established that the rate of reduction of pure lead monoxide was proportional to $(p_{H_2})^{1.36}$, i.e. for p_{H_2} = 0.9 atm. the reaction rate is approximately 90% of the reaction rate observed for p_{H_2} = 1.0 atm.

An attempt was also made to estimate the water formed by reaction during the initial period of relatively fast reaction rate. The results were very inaccurate, but the average values obtained from several tests indicated that the overall reaction rate was not markedly affected by the presence of 9% H_2O by volume.

On the basis of the preceding discussion it is therefore considered that the presence of up to 9% water vapour by volume will not affect the measured reaction rates.

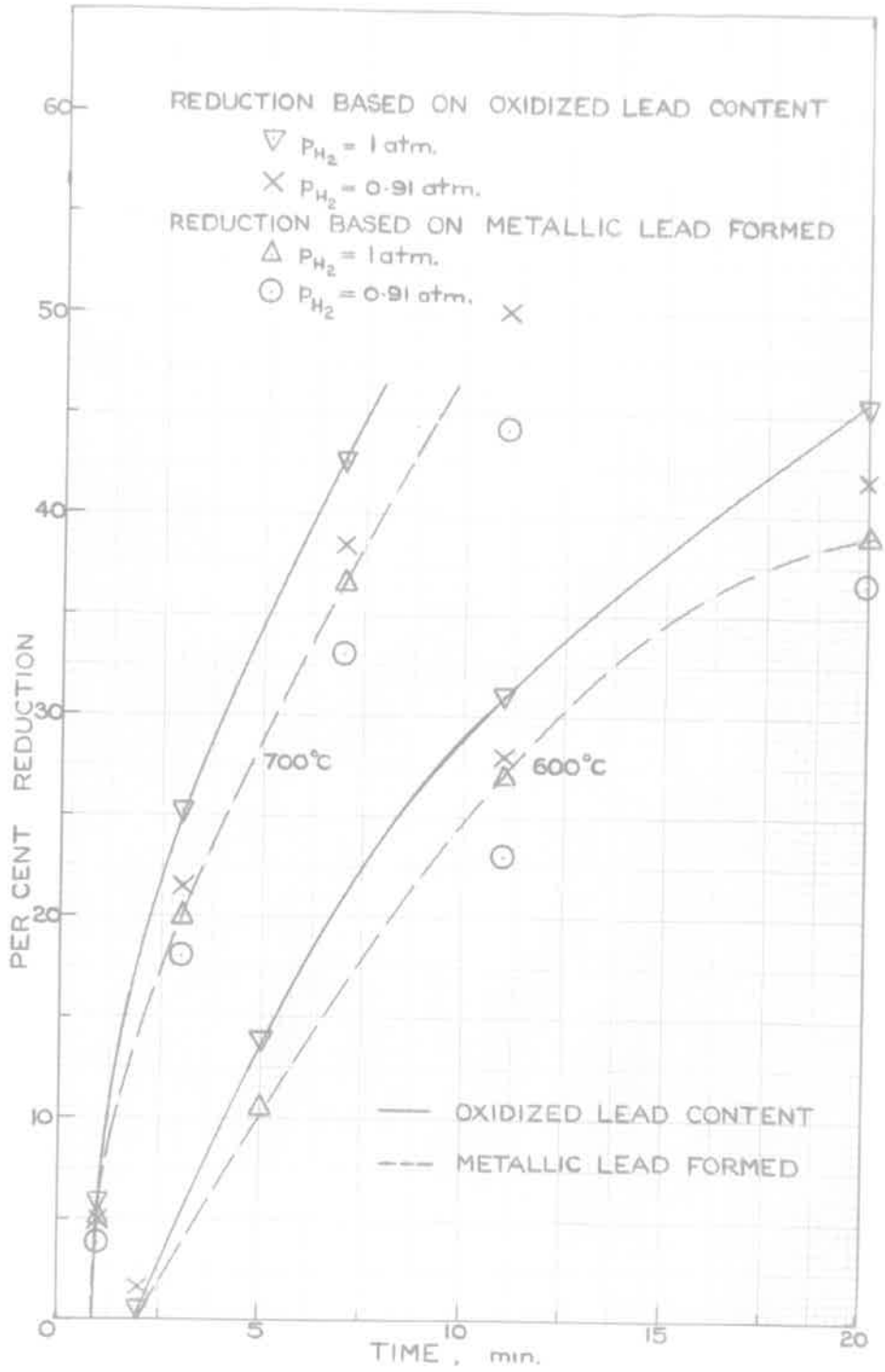

Fig. 13 - The Effect of Water Vapour on the Rate of Reduction of the Lead Compounds, -52 + 72 # (B.S.S.) Particles Reduced at 600°C and 700°C

6.6 Summary and Conclusions

The experimental data lead to the following conclusions

(i) The overall reaction rate may be used to represent the rate of reduction of the lead compounds without serious error. Up to 70 per cent reduction the overall reaction rate, followed by collecting and weighing the water formed, is approximately equal to the rate of reduction of the lead compounds to metallic lead. Beyond this point the overall reduction still indicates the degree of oxygen removal from the lead compounds, but all the oxidized lead is not reduced to metallic lead. In particular, the reduction of compounds such as $PbSO_4$ apparently occurs; these compounds contribute to the overall reaction rate without increasing the amount of metallic lead formed.

(ii) At temperatures up to 700°C the overall reaction rate is not controlled by gas-film diffusion provided the gas flow rate exceeds 10 l. s.t.p./min.; this is equivalent to a superficial gas velocity of 32.8 cm/sec at s.t.p.

(iii) The initial rate of reaction is only slightly affected by the presence of 9% water vapour by volume.

(iv) The reaction rate is increased by decreasing the particle size and increasing the temperature. The time required for a given reduction appears to be directly related to the initial specific surface and the specific surface area increases with decreasing particle size. However, the effect of particle size is obscured at temperatures

of 600°C and above by partial fusion of the particles. It may therefore be anticipated that the reaction rate will be faster in a fluidized bed than in the fixed-bed reactor for comparable system conditions. The temperature dependence of the reaction is quite high; the value of the index "n", which indicates the temperature dependence, is 9.7 at 10% reduction and 15.5 at 80% reduction. This suggests that the reaction mechanism depends on the degree of reduction, i.e., different reactions occur as the reduction proceeds.

(v) Despite the fact that the overall reaction rate is a satisfactory measure of the reduction of the lead compounds to metallic lead, the various reactions appear to occur consecutively rather than simultaneously. The limited experimental data suggest that the reduction sequence involves

(a) iron oxides,

(b) oxidized lead compounds,

(c) zinc compounds, and

(d) lead compounds containing sulphur.

No inferences can be made concerning the reduction of calcium sulphate. The reduction of the oxidized lead compounds does not commence until approximately 10% overall reduction has occurred and the autocatalytic effect observed at 500°C suggests that the initial reaction is the reduction of hematite, Fe_2O_3. From 10%

to 70% reduction the overall per cent reduction, the per cent reduction based on the decrease in oxidized lead content, and the per cent reduction based on the metallic lead formed, are very similar. This indicates that the oxidized lead compounds are reduced to metallic lead during this period. Above 70% reduction the per cent reduction based on the metallic lead formed increases much more slowly than the overall and oxidized lead reductions. Also, the lead sulphide content, which is relatively constant up to 60% reduction, begins to increase above this value. These facts suggest that the reduction of some oxidized lead compounds containing sulphur commences at approximately 60% reduction. Finally, mass balances of the differential reactor show that the major material loss from the sinter, apart from oxygen, is metallic zinc; these losses are not significant until approximately 50% overall reduction has occurred, which suggests that the reduction of the zinc compounds is not significant in the initial stages of the reaction.

7. THE REDUCTION OF LEAD SINTER IN A FLUIDIZED BED REACTOR

The basic aim of this project is to study the reduction of impure lead oxide in fluidized systems and this Section deals with reaction rates in a small fluidized bed reactor. Firstly, the experimental apparatus and technique are described and the fluidization characteristics of beds of crushed and sized lead sinter are discussed. Secondly, the effects of various system variables on the overall reaction rate are discussed, and, finally, the fluidized bed reaction rates are compared with reaction rates measured in the differential, fixed-bed, reactor.

7.1 Selection of Operating Conditions and Experimental Technique

The interpretation of data obtained in the fluidized bed requires a knowledge of the reaction rate in fixed beds; consequently the scope of the experimental work carried out in the fluidizer is limited to the range of system variables covered by the fixed-bed data. Also, pure hydrogen has been chosen as the reducing gas and the effect of diluents, such as water vapour and nitrogen, is not considered.

Theoretically, the rate of reduction of lead sinter by hydrogen should be obtained by following the change in composition of the solids. In the present case it is intended to operate the fluidizer as a batch process and it is not possible to sample the solids during the reaction. However, in Section 6.5.3 it is shown that the rate of water formation is a satisfactory measure of the rate of reduction of the lead compounds in the sinter; consequently, the reaction rate may be measured from the gas phase composition.

The literature review presented in Section 3.2.2 reveals that the rate of reaction in a bed of solids fluidized by a reducing gas may be conveniently followed by

(i) measurement of the change in gas composition from inlet to outlet of the reactor, and

(ii) measurement of the volume of hydrogen consumed by reaction.

The change in composition of the reducing gas may be measured by performing a continuous analysis on the exit gases or by collecting and weighing the water formed by reaction. The first of these possibilities involves the use of special apparatus, such as an infra-red gas analyzer, while the probable high gas flow rates and relatively large quantities of water vapour formed make the second method unattractive. Consequently, the reaction rate will be determined by measuring the rate at which hydrogen is consumed by reaction. In this technique hydrogen is pumped at a constant rate around a closed system which includes the fluidized bed of solids heated to the reaction temperature. The reactor exit gases are cooled and dried and the residual hydrogen is returned to the suction of the circulating pump; the rate at which the additional hydrogen necessary to maintain the constant volume flow enters the apparatus is indicated by a gas-meter, and this rate is proportional to the rate of water formed by reaction. The major difficulty associated with this method is to ensure that the rate at which hydrogen leaks from the apparatus is constant and is small compared with the rate of reaction over the major part of the reduction.

The experimental data consist of a series of time intervals for constant increments of volume; the volume increment is equal to the sum of the hydrogen consumed by reaction and the leakage to atmosphere. In treating the results it is assumed that hydrogen escapes from the system at a constant rate equal to the final steady rate of hydrogen consumption. The apparent amount of hydrogen consumed during a given time interval is converted to the amount actually used to reduce the solid by subtracting the amount of leakage during the interval. These corrected volumes are converted to the equivalent weight of water and divided by the bed weight and the time interval to give the average rate of reaction for the time interval. The average rate calculated in this manner is assumed to occur at the middle of the time interval.

7.2 Experimental Apparatus and Procedure

7.2.1 Preliminary Apparatus and Procedure

The initial apparatus, which was similar in design to the arrangement used by Hamdorf [63] (1956) to measure the rate of reduction of barytes, proved to be satisfactory. A few minor modifications are mentioned in Appendix III, but basically the preliminary apparatus was similar to the final arrangement illustrated in Figure 14. However, the initial series of tests, which were exploratory in nature and were used to develop an operating technique capable of yielding accurate and reproducible rate data, revealed that the preliminary experimental procedure was unsatisfactory; the various modifications made to the experimental technique and the apparatus are described in detail in Appendix III.

7.2.2 Final Experimental Apparatus

A photograph of the fluidizer used in the experimental work is given in Figure 15, and the apparatus is shown diagrammatically in Figure 14.

The apparatus consists essentially of a heat-resistant stainless steel reactor, S, 3 in. internal diameter and 76 in. long, heated by radiant heat transfer from the heating elements of three furnaces, L, M and N, having a total capacity of 11 kW; the overall heated length is 52 in., of which the preheating section, M, occupies 32 in. The reaction mass is supported on a perforated stainless steel plate located at the top of the preheater. A detail drawing of the original reactor-preheater tube is shown in Figure 16, and the final apparatus differs only slightly from this arrangement; instead of forming an integral part of the reactor the grid is welded to the bottom of a stainless steel liner, G, which fits inside the original reactor. This liner is flanged at the top and is supported by the flanges at the top of the reactor section.

Hydrogen, which is circulated by a small centrifugal pump, P, flows through the preheater-reactor tube, S, into a small, high efficiency, cyclone, T, which removes any solids, and then passes through a water-cooled, concentric pipe, condenser, U. The gases leaving the condenser are dried in a bed of silica-gel, V, and are then returned to the suction side of the pump. The main reaction product - water - is removed from the gas stream by the condenser-gas drier arrangement, while caustic soda pellets placed in the bottom of the gas drier absorb any H_2S or SO_4; pure, almost dry, hydrogen is

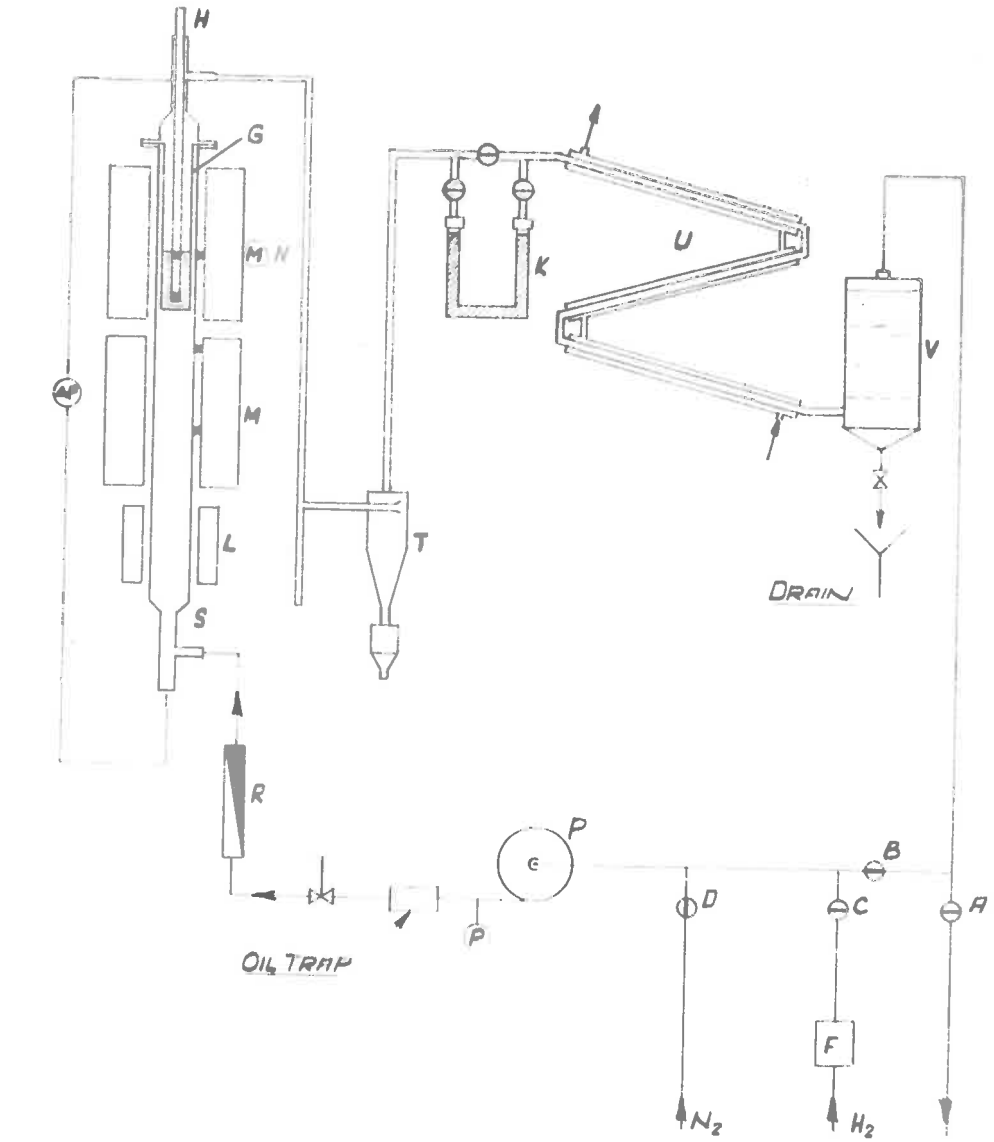

Fig. 14 - Line Diagram of Final Arrangement of Fluidizer

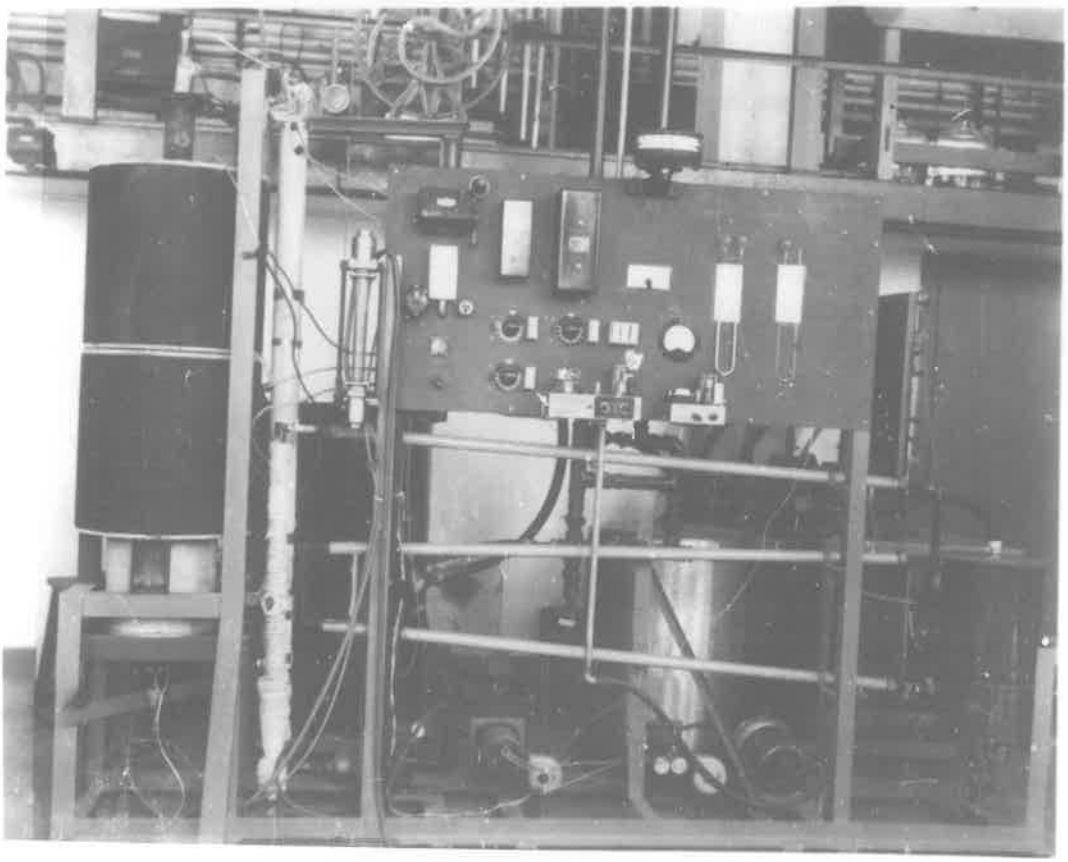

Fig. 15 - Photograph of Fluidizer

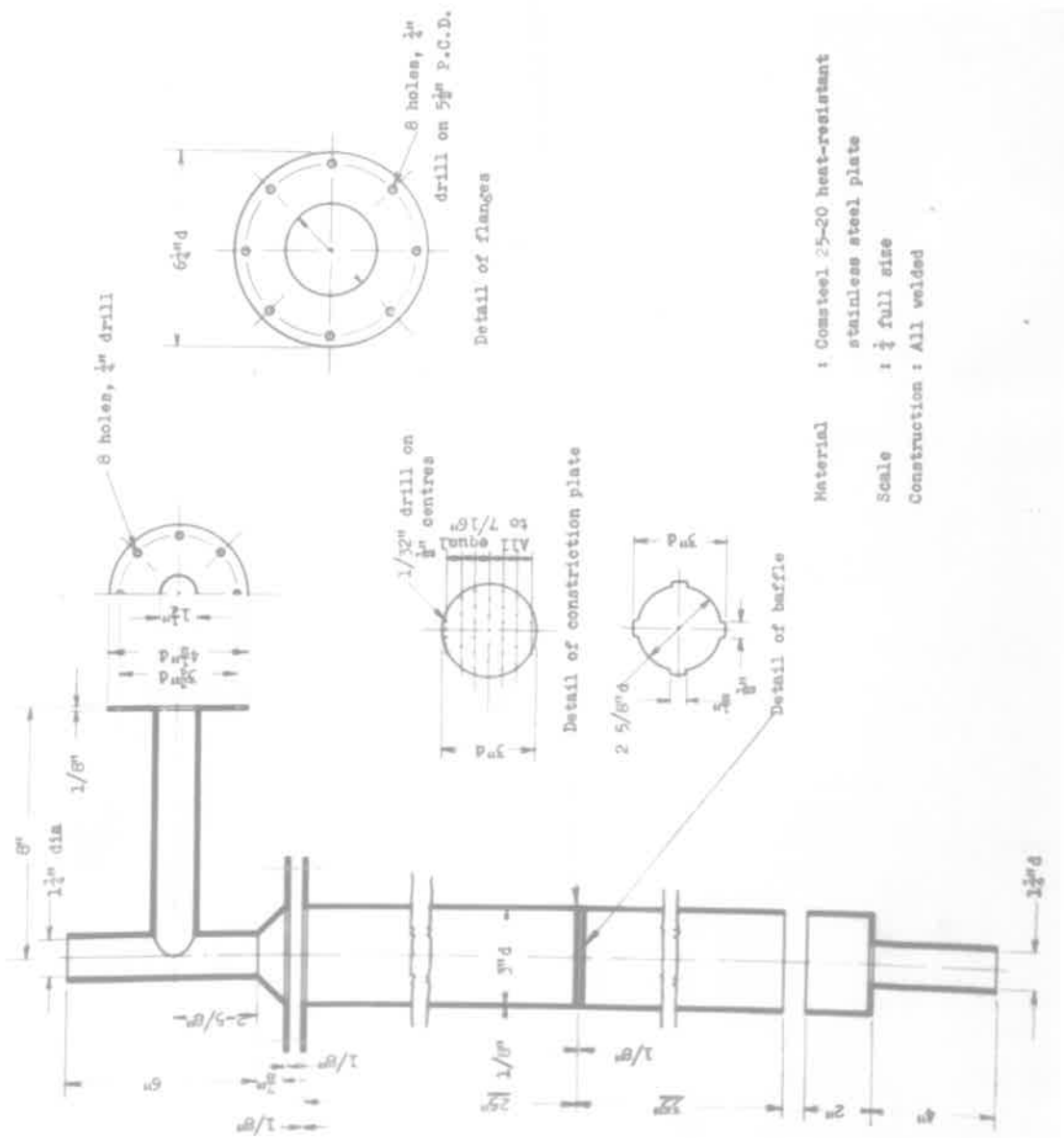

Fig. 16 - Detail Drawing of Original Reactor-Preheater Tube

therefore returned to the pump. Make-up hydrogen to maintain the constant volume flow of circulating gas enters the circuit via a gas-meter from a 50 ft^3 gas holder held at a small positive pressure to prevent air leaking into the system. An arrangement of 1 in. gas taps (see Fig.14) permits either hydrogen or nitrogen, from a pressurised 10 ft^3 gas holder, to be circulated or vented to atmosphere. The gas flow rate, which is measured by a rotameter, R, is controlled by means of a Ward-Leonard variable speed drive on the motor coupled to the circulating pump.

The bed temperature is controlled manually. One kilowatt Sunvic Energy Regulators are used to switch the power input to the furnaces by incorporating them in the hot-wire circuit of hot-wire vacuum switches; with this arrangement the energy regulators are not used to switch loads exceeding their rated capacity of 1 kW.

The temperature of the fluidized bed is measured by two chromel-alumel thermocouples protected from the reducing atmosphere by a silica sheath, H. These couples are standardized against a sub-standard platinum-platimum, 13% rhodium thermocouple having a claimed accuracy of $\pm 5^{\circ}C$ at $1000^{\circ}C$. The bed temperatures are indicated by a Cambridge wall-pattern temperature indicator, which is calibrated with a Cambridge portable potentiometer. Thermocouples are also provided at various points between the reactor and the heating windings (see Fig.14).

The make-up hydrogen necessary to maintain a constant volume flow through the circulating pump is measured with a bellows-type gas-meter, F. This meter, which was supplied by the South Australian

Gas Company, has a guaranteed accuracy of ±2% of the indicated volume, and the scale is graduated in $\frac{1}{2}$ ft^3 intervals.

7.2.3 Final Experimental Technique

The experimental technique used throughout the final series of tests may be described by the following steps:-

(1) The reactor liner is loaded with a known weight of crushed and sized sinter and placed inside the reactor. The flanges, separated by asbestos gaskets, and the water reservoir (see Fig. 37) are then bolted together.

(2) The thermocouple sheath is placed in position and carefully packed with magnesia-impregnated asbestos paper; the bed is fluidized during this operation to decrease the possibility of breaking the silica sheath as it is forced down into the bed.

(3) Tap D is opened and nitrogen, circulated by the pump, is vented to atmosphere by closing tap B and opening tap A (see Fig.14); approximately 10 ft^3 are exhausted to ensure that all air is purged from the system.

(4) With tap B open tap A is closed and the pump speed is adjusted to give the required nitrogen flow through the bed.

(5) The heating furnaces are switched on and the bed of solids, fluidized by the circulating nitrogen, is brought up to the set temperature for the run.

(6) The drying tube is weighed and placed in position, and nitrogen is vented to atmosphere by opening tap A and closing tap B.

(7) The run is commenced by opening tap C and closing tap D; the stopclock is started and approximately 5 ft^3 of hydrogen is exhausted to atmosphere via the drying tube to purge the nitrogen from the system.

(8) Tap B is opened and tap A closed so that pure hydrogen is circulating around the system. The drying tube is isolated from the circuit and the measurement of the rate at which make-up hydrogen enters the system is commenced. The hydrogen flow rate is controlled by altering the pump speed and the pump pressure is adjusted with a screw clip.

(9) At the completion of the reaction the rate at which hydrogen escapes from the system is determined; this value is indicated by a constant rate of make-up hydrogen.

(10) With tap A open and tap B closed, the hydrogen is replaced with nitrogen by opening tap D and shutting tap C. After approximately 10 ft^3 of nitrogen are exhausted to atmosphere tap B is opened and tap A is closed and the reactor is allowed to cool with the bed fluidized by nitrogen.

(11) The reactor liner is removed and the bed of solids is inspected and weighed.

(12) The reaction rate and per cent reduction against time curves are calculated by the method outlined in Section 7.1. The weight of water formed during the

period when the H_2-N_2 mixture is exhausted to atmosphere is obtained from the change in weight of the drying tube.

7.3 The Fluidization of Lead Sinter

A knowledge of the fluidization characteristics of the lead sinter used in this investigation is essential in planning the experimental work and in discussing the measured data.

The fluidization of beds of sinter by nitrogen and hydrogen was studied visually in a perspex replica of the stainless steel reactor, and the characteristics were also investigated in the actual reactor on the basis of the pressure drop across the bed. The results of these tests are discussed in detail in Appendix IV.

The closely sized fractions used in the experimental work do not fluidize well; little circulation is observed until the gas velocity exceeds 2 V_{mf}, and at higher velocities the material tends to slug. At gas flow rates approaching 10 V_{mf} the upper surface of the bed is not clearly defined and "spouts" of solids are seen to leave the bed and then fall back. In this condition the solids are violently agitated, but the quality of fluidization is poor and the system does not constitute a true fluidized bed. However, even at these high velocities there appears to be very little elutriation of solids from the reactor.

The experimental values of the minimum fluidizing velocity, which were obtained for hydrogen and nitrogen at temperatures in the range 20°C to 400°C, agree quite satisfactorily with the values predicted from the equations of VanHeerden et al. [52] (1952) and

Leva [64] (1957). Figure 38 illustrates the agreement between the theoretical and experimental values. In the present case the equation presented by Leva [64] (1957) is easier to apply than the correlation of van Heerden et al.[52] (1952), which was developed specifically for mixtures of particle sizes; consequently, Leva's equation was used to predict the minimum fluidizing velocity for the various temperatures and particle sizes used in the experimental work. The values of V_{mf} calculated from this equation are summarized in Table 14, and a type calculation is presented in Appendix IV.2.

TABLE 14

GAS VELOCITIES AT THE POINT OF INCIPIENT FLUIDIZATION FOR BEDS OF LEAD SINTER FLUIDIZED BY HYDROGEN

Screen fraction (B.S.S.)	Temperature (°C)	Gas flow at minimum fluidization l. s.t.p./min.
-25 +36	600	46.7
-36 +52	600	24.2
-52 +72	600	13.2
-72 +100	600	7.9
-25 +36	700	42.3
-36 +52	700	21.8
-52 +72	700	11.9
-72 +100	700	7.1

7.4 Accuracy of Results

The accuracy of the experimental data obtained on the rate of reduction of lead sinter by hydrogen in a fluid bed is discussed in detail in Appendix VI.2.

The accuracy of the measured reaction rates depends on the magnitude of the rate of reduction; at the beginning of the reduction the reaction rate is fast and the data are accurate to approximately ±15%, while the very slow rates measured towards the end of the reaction are probably only correct to ±50%. On this basis it is claimed that the bulk of the rata data have an accuracy exceeding ±25%.

7.5 Experimental Programme

A summary of the experimental work carried out in the fluidized bed reactor is presented in Table 15, which lists the test conditions for each run. The rata data obtained in these tests are presented in detail in Appendix VIII.2.

Table 15 does not include the initial series of tests - runs A.1 to A.27 - in which the final experimental technique was developed. These tests are discussed in Appendix III.

TABLE 15

EXPERIMENTAL PROGRAMME - FLUIDIZED BED REACTOR

Run No.	Size fraction (B.S.S.)	Temperature (°C)	Bed Weight (g.)	Flow Rate (l. s.t.p./ min.)
B.1	-72 +100	500	500	114
B.2-B.4	-52 +72	600	250	114

TABLE 15 (contd.)

Run No.	Size fraction (B.S.S.)	Temperature (°C)	Bed Weight (g.)	Flow Rate (l. s.t.p./ min.)
B.5	-52 +72	600	500	76
B.6	-52 +72	600	500	92
B.7	-52 +72	600	500	114
B.8	-52 +72	600	500	131
B.9	-52 +72	700	500	114
B.10	-52 +72	600	750	114
B.11	-52 +72	600	1000	114
B.12	-25 +36	600	500	144
B.13	-36 +52	600	500	132
B.14	-72 +100	600	500	92
B.15	-36 +52	700	500	132
B.16	-25 +36	700	500	163

7.6 Discussion of Results

The experimental results obtained in the fluidized bed reactor are reported in detail in Appendix VIII. In this Section the behaviour of fluidized beds of sinter during reduction is considered and the effects of system variables such as fluidizing gas velocity, bed depth, particle size and reaction temperature are discussed from the viewpoint of their influence on the overall reaction rate. The results are also compared with the data obtained in the fixed-bed reactor.

7.6.1 The Fluidization Characteristics of Lead Sinter during Reduction

In Section 7.3 the fluidization of beds of lead sinter by hydrogen and nitrogen is considered at room temperature and at elevated temperatures which are less than the temperature at which reaction takes place. From these results the gas velocities required to fluidize the various size fractions at the temperatures used the experimental work were calculated. However, it may be anticipated that the degree of fluidization will alter during reduction at elevated temperatures. Firstly, during the initial stages of the reaction considerable water vapour is formed in the bed, and at the reduction temperatures the viscosity of water vapour is almost twice that of hydrogen. Consequently, since the minimum fluidizing velocity, V_{mf}, is inversely proportional to the viscosity of the fluidizing gas [52,64] (1952) and (1957) it follows that V_{mf} will vary with the ratio of H_2O:H_2 in the gas stream [31] (1958). Secondly, the density of the particles changes during the reduction and therefore V_{mf} will vary with time. In particular, the metallic lead is formed in the liquid state and this may be removed from the particles.

The pressure drop across a properly fluidized bed is basically constant and independent of the gas velocity. Therefore, any loss of fluidization, channelling, or transport of material out of the reactor, will be indicated by a change in pressure drop across the bed. The variation in pressure drop across the reactor, measured with a water differential manometer (see Fig. 14), was recorded during each test. Normally, this value gradually decreased during the run,

but in some cases there was a sudden increase in the pressure drop across the reactor towards the end of the reaction. The results plotted in Figure 17, which is a graph of per cent reduction against pressure drop, are typical of this behaviour.

From equation (19) the pressure drop across a fluidized bed is given by

$$\triangle P = \frac{\text{weight of material in the bed}}{\text{bed area}}$$

and, for a 500 g. bed in a 3 in. diameter reactor,

$$\triangle P = 4.33 \text{ in. } H_2O$$

The reported values are much higher than this because the pressure drop is measured across the whole reactor rather than across the fluidized bed alone; consequently, the pressure drop for a given bed weight increases with increasing gas velocity as shown in Figure 17. An examination of these curves reveals that the pressure drop at first decreases slowly with increasing per cent reduction and then rises sharply between 50 and 70 per cent reduction. The initial decrease results from the decrease in bed weight due to oxygen removal from the sinter together with some losses due to vapourization and elutriation. Now, examination of beds of reduced sinter for runs in which the pressure drop varied as shown in Figure 17 disclosed that the particles were in the form of a partially fused solid mass containing a series of channels through which the gas obviously flowed. Consequently, it is considered that the sharp rise in pressure drop results from a loss of fluidization which permits the bed to sinter. During the initial tests it was found that the likelihood of sintering occurring was decreased by increasing the fluidizing gas velocity, and for this

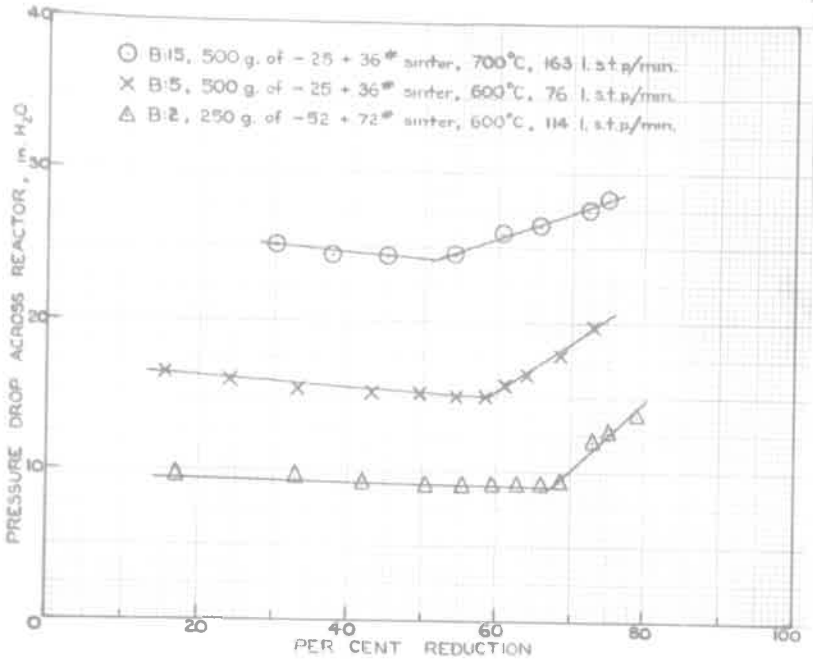

Fig. 17 - Variation in Pressure Drop across a Fluidized Bed as Reduction Proceeds.

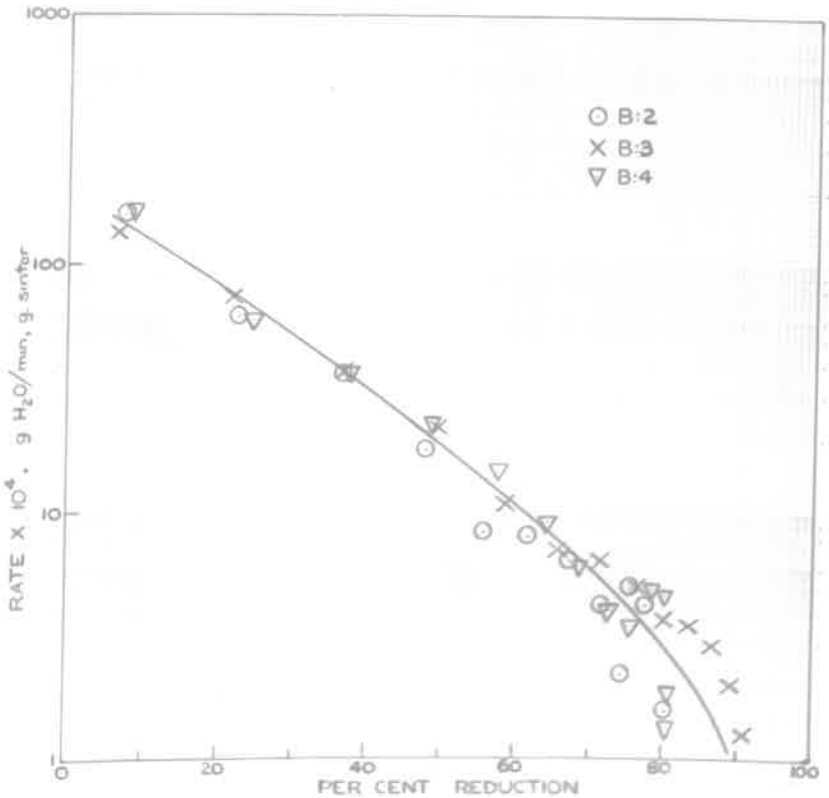

Fig. 18 - Reproducibility of Fluidized Bed Rate Data, 250 g. beds of -52 +72 # (B.S.S.) particles reduced at 600°C

reason high gas flow rates were used in the experimental work. However, in some cases the beds suffered a loss of fluidization with gas flows as high as 10 V_{mf}, and it is thought that the loss of fluidization was caused by liquid metallic lead which escaped from the particles and collected on the gas distribution grid.

In view of the preceding discussion it is considered that, for the runs in which the pressure drop across the reactor showed a sudden increase, the measured reaction rates only represent the rate of reaction between hydrogen and fluidized beds of lead sinter up to the point at which the pressure drop begins to increase; in general, this occurred at about 60% reduction and was more pronounced at 700°C than at 600°C.

7.6.2 Reproducibility of Results

In Appendix VI.2, which deals with the accuracy of the experimental data, it is shown that the measured reaction rates are subject to large errors (±50%) towards the end of the reaction. Further, if this reaction rate is plotted against a derived value, such as per cent reduction, rather than a directly measured variable, such as the reduction time, additional errors are introduced. Consequently, it may be anticipated that a plot of log (reaction rate) against per cent reduction for several identical tests would show a scatter of points rather than a single line and that the scatter would increase as the reaction rate decreases.

In Figure 18 the results of three tests carried out under identical system conditions, viz., 250 g. beds of -52 +72 # (B.S.S.) sinter reduced at 600°C, are shown as a graph of per cent reduction

against $\log_{10}$ (reaction rate). An examination of this plot reveals that the scatter of the data increases as the reaction rate decreases; after about 70 per cent reduction the points represent a band rather than a single line. However, it is considered that this scatter is within the limits of accuracy imposed by the experimental method.

Since the three sets of data are represented by a single line for the major part of the reaction (up to 70 per cent reduction), the line of best fit drawn through the results of a single test is a satisfactory approximation for the true result, which is ideally obtained as the average of several tests; consequently in the remainder of the work the reaction rate was obtained from the results of a single test.

7.6.3 The Effect of System Variables on the Reaction Rate

The overall rate of a solid-gas reaction may be considered to consist of a series of individual steps, any one of which may be so much slower than the others that it substantially determines the overall reaction rate. These steps may be kinetic or diffusional, and, in general, the chemical reaction rate depends markedly on the reaction temperature whereas the mass transfer rates are normally determined by the physical properties of the system. In a fluidized bed reactor the major factors influencing the mass transfer rates are particle size, gas velocity and the quality of the fluidization, and this Section discusses the effect of gas velocity, bed temperature and particle size on the overall reaction rate. The effect of altering the bed weight is also considered.

7.6.3.1 Fluidizing Gas Velocity

In the present system the possible factors controlling the overall rate of reaction which may be altered by changes in the gas velocity are

(i) diffusion of reactants and products through the inert gas film surrounding the particles,

(ii) retardation of the rate of any reaction by water vapour,

(iii) mass transfer from the continuous to the discontinuous phase, and

(iv) attainment of the equilibrium gas phase composition for a particular reaction.

The effect of the fluidizing gas flow rate on the reaction rate was determined at 600°C for 500 g. beds of -52 +72 # sinter reduced at gas flow rates varying from 76 l. s.t.p./min. to 131 l. s.t.p./min.; these gas flows correspond to 5.75 V_{mf} and 10 V_{mf}, respectively. The results of these tests are illustrated in Figure 19, which is a plot of log (reaction rate) against per cent reduction, and an examination of this graph reveals that the influence of the fluidizing gas velocity is not very marked even during the initial stages of the reaction.

This result could have been anticipated since

(i) it is shown in Section 6.5.4.1 that the overall rate of reaction at 600°C is not influenced by the superficial gas velocity for gas flow rates exceeding 5 l. s.t.p./min., and this corresponds

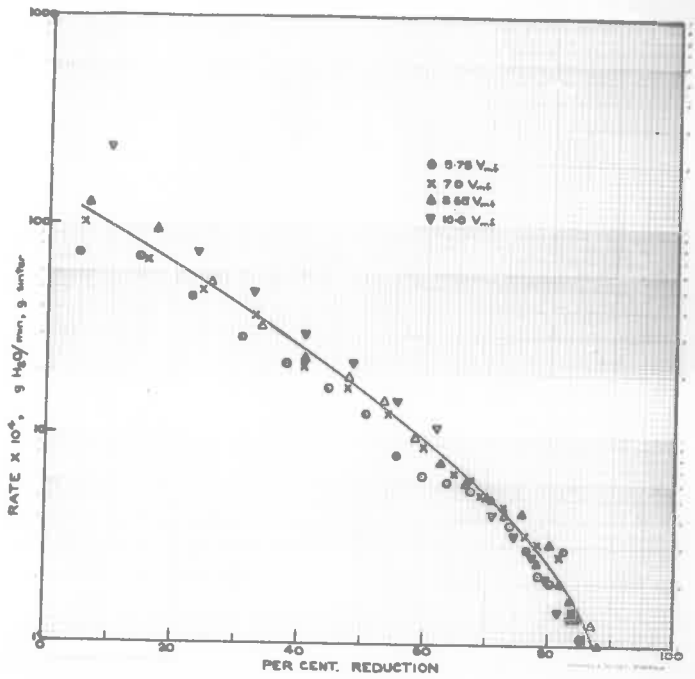

Fig. 19 - The Effect of Fluidizing Gas Velocity on the Reaction Rate for -52 +72 # (B.S.S.) particles reduced at 600°C

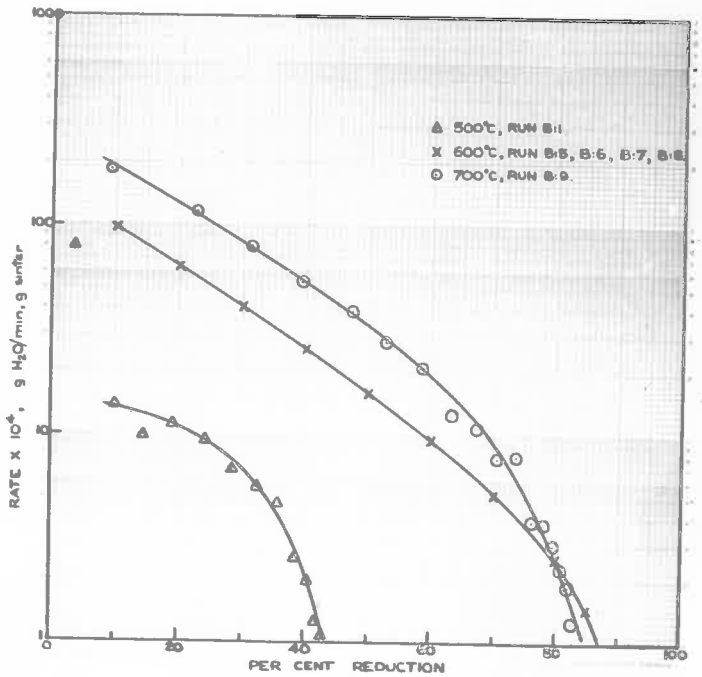

Fig. 23 - The Effect of Temperature on the Rate of Reduction of 500 g. beds of -52 +72 # (B.S.S.) particles

to 45 l. s.t.p./min. in the fluidized bed reactor,

(ii) the overall reaction rate at 600°C is not retarded by H_2O-H_2 mixtures containing up to 9% H_2O by volume, and the maximum H_2O content of the gases leaving the reactor at 10% reduction is approximately 9% by volume, and

(iii) with the high gas flows used to keep the material fluidized the bed is intensely agitated and it is unlikely that the rate of mass transfer between the continuous and discontinuous phases limits the rate of reaction.

7.6.3.2 Temperature

The rate of reaction was measured for 500 g. beds of -52 +72 # (B.S.S.) sinter reduced at 500°C, 600°C and 700°C, and the results are illustrated in Figure 20, which is a plot of log (reaction rate) against per cent reduction. It is apparent that the reaction rate is markedly influenced by the temperature; at 20% reduction an increase in temperature from 500°C to 700°C produces a twelve-fold increase in reaction rate, and the time required to reach 45% overall reduction is decreased from 110 min. at 500°C to 5 min. at 700°C.

The relation between the measured pressure drop across the reactor and the per cent reduction for Run B.9 is similar to the curve obtained for Run B.15 (see Fig.17); consequently, the sharp decrease in rate, which starts at approximately 65% reduction and finally causes the 700°C rate curve to cut the curve obtained at

600°C, is attributed to loss of fluidization and sticking of the bed. Apart from the final section, the shape of the curves is the same at 600°C and 700°C; however, at 500°C the curve tends to show the initial autocatalytic effect which is clearly defined in the data obtained from the fixed-bed reactor.

The temperature dependence of the overall reaction rate was determined by the method described in Section 6.5.4.2 and the results are reported in Table 16. The accuracy of these data is limited by the number of results obtained in the fluidizer; due to practical difficulties it is not possible to measure reaction rates at temperatures above 700°C, and, therefore, the value of the index "n" is obtained from the line of best fit drawn through only three points. Also, after 45% reduction the graph of log T against log (reaction rate) consists of two points only, and the value of "n" has therefore only been reported at 10%, 20% and 40% reduction. Table 16 reveals that the value of the index "n" increases with increasing per cent reduction. This is similar to the results obtained in the fixed-bed, and, although the values of "n" are somewhat higher in the fluidized bed than in the fixed bed, it may be concluded that the mechanism of the overall reaction is essentially the same in both systems.

TABLE 16

EFFECT OF THE DEGREE OF REDUCTION ON THE TEMPERATURE DEPENDENCE OF THE OVERALL REACTION RATE

Size Fraction (B.S.S.)	Value of "n" at different overall per cent reductions		
	10%	20%	40%
-52 +72	10.4	12.1	15.4

7.6.3.3 Bed Depth

The effect of bed depth on the rate of reaction was studied at 600°C for beds containing 250 g., 500 g., 750 g., and 1000 g. of -52 +72 #(B.S.S.) sinter reduced by a hydrogen flow equivalent to 8.6 V_{mf}. The results of these tests are presented in Figure 21 as plots of log (reaction rate) expressed as g. H_2O formed/min., g. sinter against per cent reduction. The data used for the 250 g. and 500 g. beds are taken from the lines of best fit in Figures 18 and 19.

The reaction rate is independent of the bed weight for beds up to 750 g. weight, but increasing the bed weight to 1000 g. causes a marked decrease in reaction rate. Since the gas velocity, the particle size, and the temperature are constant the observed difference in reaction rate should result from

(i) the presence of water vapour, or

(ii) changes in the quality of fluidization.

The approximate H_2O/H_2 ratio in the gas leaving the fluidized bed may be calculated from the experimental results and Figure 22 is a plot of exit gas composition against per cent reduction for the different bed weights. From this Figure it may be deduced that the presence of approximately 10% H_2O by volume does not affect the overall reaction rate in fluidized beds. This conclusion is in agreement with the limited data obtained in the fixed-bed apparatus (see Section 6.5.4.4) which showed that the rate of reaction at 600°C was not significantly retarded by the presence of 9% H_2O by volume in the reducing gas.

The behaviour of the 1000 g. bed is anomalous since the

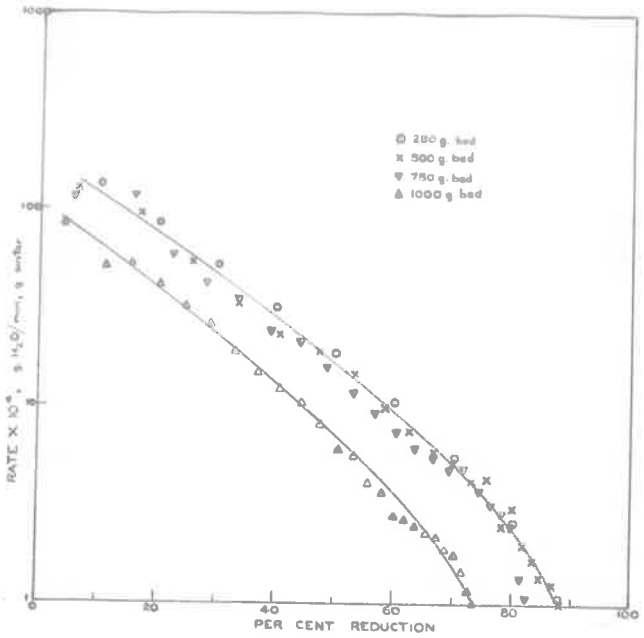

Fig. 21 - The Effect of Bed Depth on the Reaction Rate for -52 +72 # (B.S.S.) particles reduced at 600°C

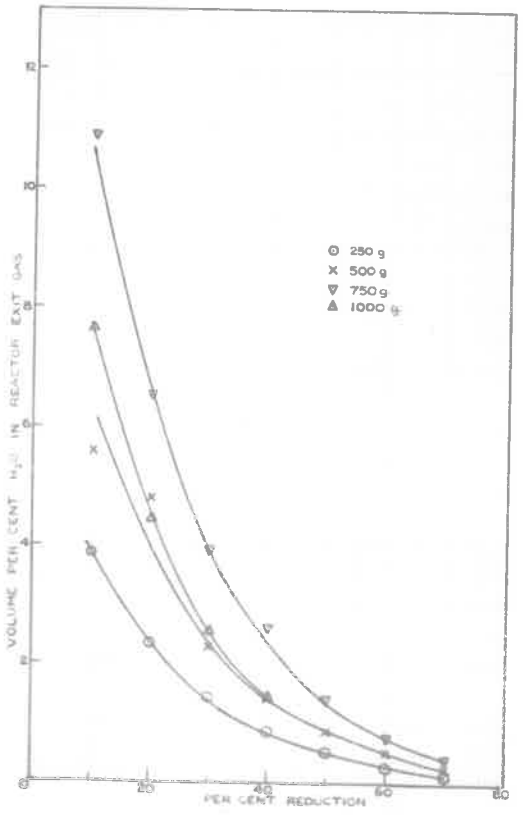

Fig. 22 - The Effect of Bed Depth on the Water Vapour Content of the Reaction Exit Gases for -52 +72 # (B.S.S.) particles reduced at 600°C

curve of H_2O/H_2 ratio against per cent reduction lies below the curve for a 750 g. bed; the slower reaction rate may not therefore be attributed to the presence of water vapour. Slugging, which has a tendency to be more severe with deep, small diameter, beds [44] (1951), decreases the contact between the solids and the fluidizing gas and may therefore decrease the overall reaction rate. Shen and Johnstone [65] (1955), who studied the decomposition of nitrous oxide in a fluidized bed of catalyst particles, have reported behaviour similar to this; however, in the present case, it is unlikely that any change in fluidization pattern resulting from increasing the bed weight from 750 g. to 1000 g. would cause the observed decrease in reaction rate. The pressure drop data obtained during this run indicate that the bed remained fluidized, and therefore the observed effect can not be explained on the basis of the available data.

From the preceding discussion it may be concluded that increasing the bed weight from 250 g. to 750 g. does not alter the reaction rate; consequently, the presence of up to 10% H_2O by volume in the reducing gas does not affect the overall reaction rate at 600°C.

7.6.3.4 Particle Size

The reaction between a solid and a gas may be considered to consist of the series of steps set out in Section 3.5. A consideration of these steps reveals that the effect of particle size on the reaction rate is due to changes in particle thickness and specific surface area; the particle thickness determines the resistance to gaseous diffusion through the solids and the specific surface influences the rate of the chemical reaction.

The rate of reaction for -25 +36 #, -36 +52 #, and -52 +72 # (B.S.S.) particles reduced by hydrogen at 600°C and 700°C is plotted against per cent reduction in Figures 23 and 24. The curve for -72 +100 # (B.S.S.) material reduced at 600°C is also included, although the shape and position of the curve and the pressure drop data indicate that the bed was not fluidized after about 50 per cent reduction.

An examination of these Figures shows that up to 80% reduction the reaction rate at a given per cent reduction increases as the particle size decreases. Above 80% reduction the reaction rate tends to be independent of the initial particle size. Also, the effect of particle size is more marked in the fluidized beds than in the differential reactor; this is due to the intense agitation in the fluidized bed which prevents the particles from sticking together.

Now, if the particle thickness is the rate-determining factor, the reaction rate at a given per cent reduction should be proportional to the particle diameter, i.e., at a given per cent reduction the reaction rate for -52 +72 # (B.S.S.) particles (average particle diameter = 0.01 in.) should be twice as great as for -25 +36 # (B.S.S.) particles (average particle diameter = 0.02 in.). However, a study of the graphs shows that the effect of particle size is less than this. Also, for a reaction controlled by the rate of chemical reaction it might be anticipated that the reaction rate would be directly proportional to the specific surface. In the present case only the initial surface area of the particles was determined and the reaction rates, corresponding to these areas

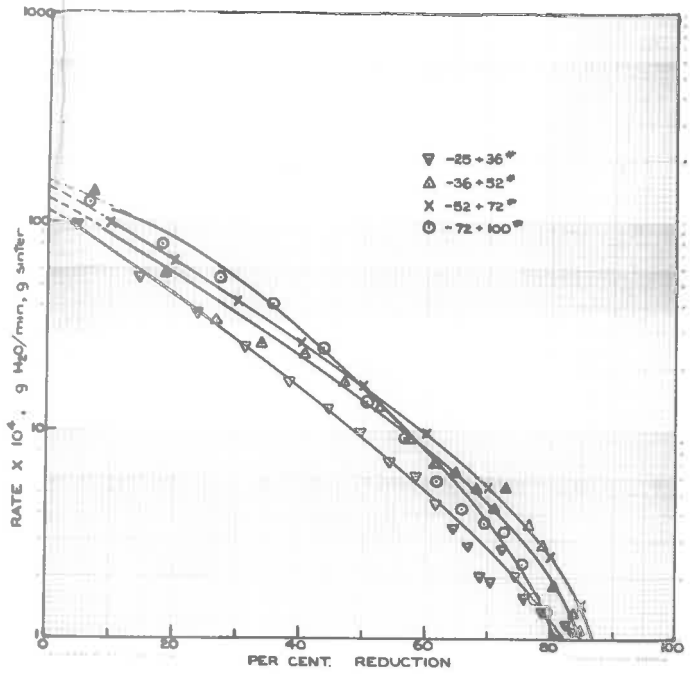

Fig. 23 - The Effect of Particle Size on the Rate of Reduction of 500 g. beds at 600°C

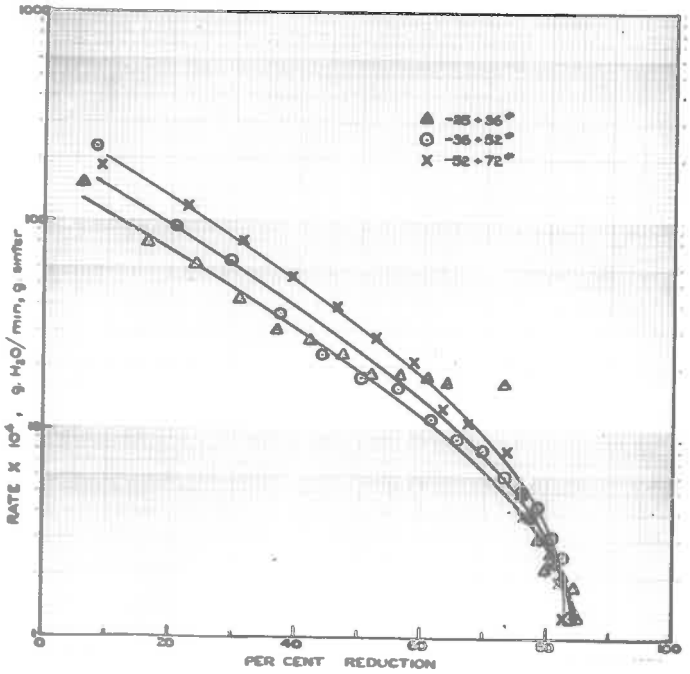

Fig. 24 - The Effect of Particle Size on the Rate of Reduction of 500 g. Beds at 700°C

were estimated by extrapolating the rate curves to 0% reduction. The results are shown in Table 17, and it is apparent that, within the limits of accuracy of the experimental data, the initial reaction rate is determined by the surface area of the particles. Now, although no measurements were made of the surface areas of partially reduced samples, an examination of the curves suggests that the reaction rate is determined by the surface area up to 80% reduction.

TABLE 17

THE EFFECT OF SPECIFIC SURFACE ON THE INITIAL REACTION RATE AT 600° AND 700°C

Size fraction (B.S.S.)	Specific surface, A_o. $cm^2/g.sinter$	Reaction Rate at 0% reduction, R_o. g. H_2O/ min. g. sinter		$R_o/A_o \times 10^5$ g. H_2O/min,cm^2	
		600°C	700°C	600°C	700°C
-25 +36	3250	0.0115	0.0165	3.54	5.08
-36 +52	3900	0.0132	0.0220	3.38	5.64
-52 +72	4600	0.0150	0.030	3.26	5.55
-72 +100	5400	0.0161	-	2.98	-

Beyond 80% reduction the points for each particle size tend to lie on a single line and this may be caused by

(i) cracking and fissuring of the particles which tends to make the surface area independent of the particle size,

(ii) the presence of a film of liquid metallic lead, and

(iii) the difficulty associated with the removal of the last traces of oxygen.

From the preceding discussion it may be concluded that

(a) the effect of particle size is more marked in the fluidized bed than in the fixed bed because the intense gas agitation prevents the particles from sticking and,

(b) decreasing the particle size increases the rate of reaction, and the change in reaction rate is proportional to the surface area up to 80% reduction.

7.7 Comparison of Reaction Rates in Fixed and Fluidized Beds

In Section 3.5 it is shown that any difference between the rate of reaction in thin, fixed, beds and fluidized beds of the same material may result from

(i) changes in the efficiency of gas-solid contacting,

(ii) changes in uniformity of temperature control, and

(iii) the effect of water vapour on the rate of reaction.

The data obtained in the differential bed relating to the effect of the H_2O/H_2 ratio on the overall reaction rate indicate that the presence of up to 9% H_2O by volume does not affect the measured reaction rate at 600°C. This conclusion is confirmed by the data presented in Figure 21, which show the effect of bed depth on the rate of reaction at 600°C for -52 +72 # (B.S.S.) particles; at 10% reduction increasing the bed weight from 250 g. to 750 g. does not affect the overall reaction rate although reference to Figure 22 reveals that the H_2O/H_2 ratio in the exit gas is increased from 4% to 11% by volume. Also, it would be anticipated that retardation of

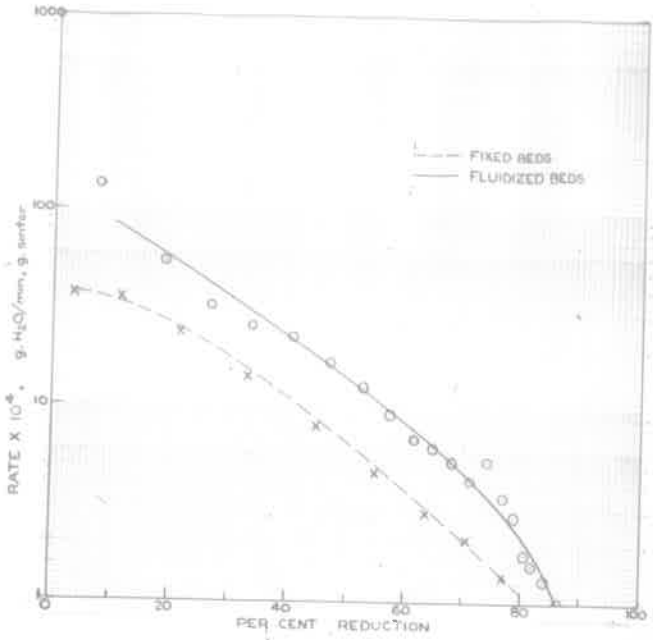

Fig. 25 - Comparison of Fixed and Fluidized Bed Reaction Rates, -36 +52 # (B.S.S.) particles reduced at 600°C

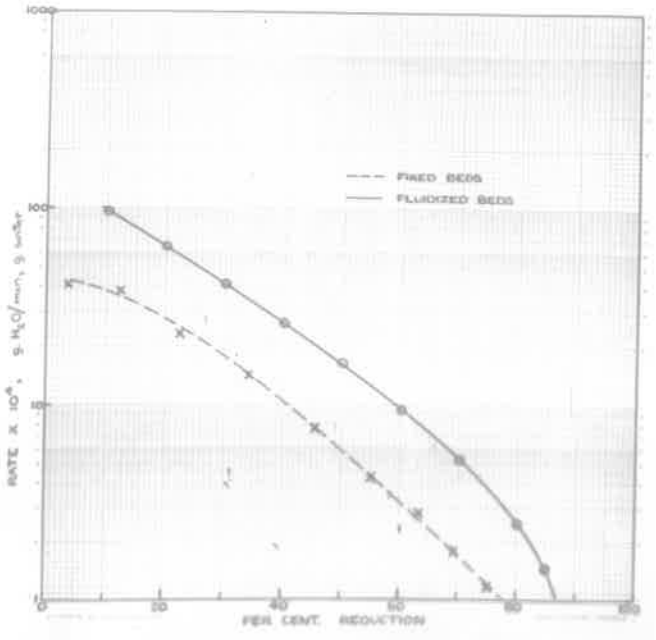

Fig. 26 - Comparison of Fixed and Fluidized Bed Reaction Rates, -52 +72 # (B.S.S.) particles reduced at 600°C

the reaction rate by water vapour would cause the fluid bed rates to be slower than the rates measured in the fixed-bed reactor. Experimentally, the fluidized bed reaction rates at 500°C and 600°C are found to be faster than the rates in the corresponding differential bed. Consequently, it may be concluded that the amount of water vapour encountered during the measurement of reaction rates at 500°C and 600°C does not affect the overall reaction rate.

The temperature of the differential bed should also be very uniform, and therefore any difference between the fluidized bed and fixed-bed reaction rates at 500°C and 600°C may be attributed to differences in the efficiency of contact between the gas and solids in the two systems.

The fixed-bed reaction rates were measured at a standard flow rate of 10 l. s.t.p./min. of hydrogen, and in the 3 in. I.D. fluidized reactor this is equivalent to a flow rate of 90 l. s.t.p./min. In general the flow of fluidizing gas exceeds this value. However, in Section 6.5.4.1 it is shown that the fixed-bed reaction rate for a given temperature and particle size is not increased by increasing the gas flow beyond 10 l. s.t.p./min. Further, it was established experimentally that the gas velocity does not affect the overall rate of reaction of -52 +72 # particles reduced at 600°C for the range of fluidizing gas velocities used in the experimental work. Therefore, despite the difference in superficial gas velocities, the reaction rates measured in the two systems may still be compared.

The rate of reaction in fixed and fluidized beds for the reduction of -36 +52 # and -52 +72 # (B.S.S.) size fractions at 600°C

is plotted against the per cent reduction in Figures 25 and 26. These graphs reveal that the reaction rate is approximately twice as fast in the fluidized bed as in the differential bed and that this difference is maintained throughout the reduction; the time required to reach a given per cent reduction is therefore only half as long in the fluid bed as in the fixed bed. On the basis of the preceding discussion this difference is attributed to the better gas-solid contact which occurs in the fluidized system.

The curves presented in Figures 27 and 28, which refer to -36 +52 # and -52 +72 # (B.S.S.) particles reduced at 700°C in fixed and fluidized beds, show that the difference between the fixed and fluidized bed reaction rates is not as great as at 600°C. Also, the curves for the fluidized bed reactor fall below the fixed-bed curves at approximately 70% reduction. However, the pressure drop-per cent reduction relations for these tests show a sudden increase at about 70% reduction; consequently, the marked decrease in the fluidized bed reaction rate which occurs at 70% reduction is attributed to a loss of fluidization (see Section 7.6.1). Therefore, it is considered that the difference between the fixed and fluidized bed reaction rates would exist throughout the reaction if the thick beds used in the fluidizer were maintained in the fluidized state. The reason for the comparatively small difference between the rate in fixed and fluidized beds at 700°C, compared with 600°C, can not be established from the available data. However, since the H_2O/H_2 ratio in the exit gases is only approximately 6% by volume at 10% reduction, it is unlikely that the fluidized bed reaction rate is retarded by the presence of water

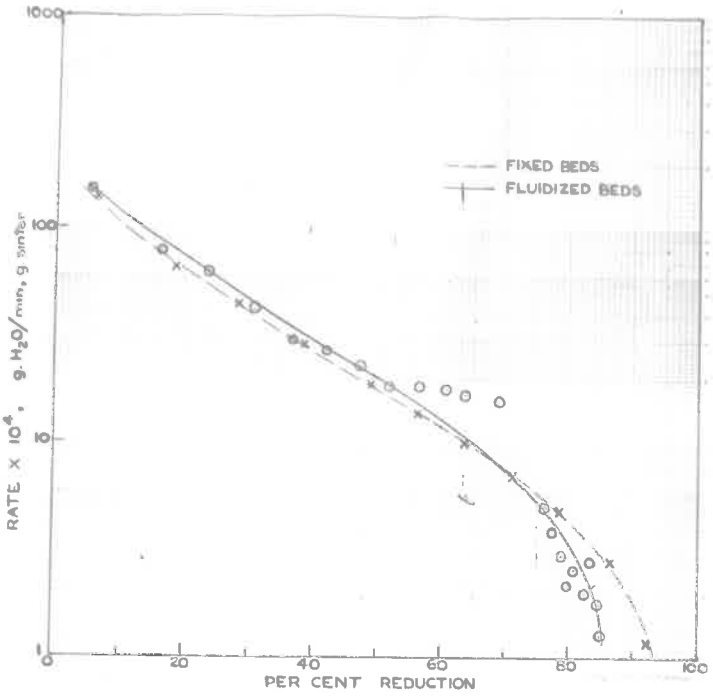

Fig. 27 - Comparison of Fixed and Fluidized Bed Reaction Rates, -36 +52 # (B.S.S.) particles reduced at 700°C

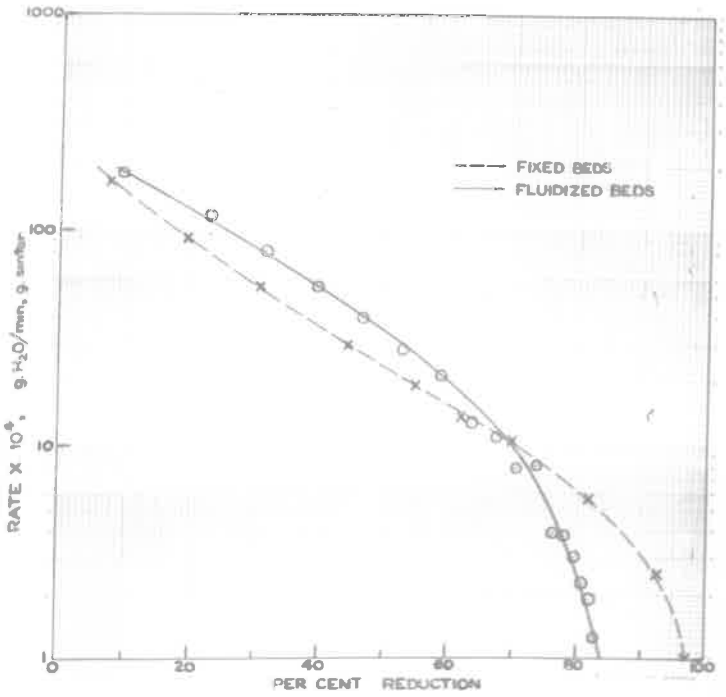

Fig. 28 - Comparison of Fixed and Fluidized Bed Reaction Rates, -52 +72 # (B.S.S.) particles reduced at 700°C

vapour. The effect is more probably due to the influence of gas velocity; however, the effect of this variable on the reaction rate was not determined at 700°C.

The temperature dependence of the reaction is similar in the fixed and fluidized beds. In the fixed bed the reaction rate for -52 +72 # (B.S.S.) particles is proportional to $T^{9.7}$ at 10 per cent reduction and the value of the index increases to 12.3 at 40 per cent reduction. The data obtained in the fluidized bed reactor give the corresponding values of the index as 10.4 and 15.4, respectively. The shapes of the curves of per cent reduction against reaction rate are also similar in the fixed and fluidized beds and it may be concluded that the mechanism of the reaction is essentially the same in both systems.

The effect of particle size on the overall reaction rate is more marked in the fluidizer than in the fixed bed, and again this is attributed to the more efficient gas-solid contact in the fluidized bed; it appears that the reaction rate is determined by the surface area and the tendency for the particles to stick together in the fixed bed decreases the reaction rate by decreasing the contact area between the reducing gas and the solids.

On the basis of the preceding discussion it may be concluded that the differences between the measured rates of reaction in fixed and fluidized beds are essentially due to the more efficient gas-solid contact in the fluidized bed; this results from the intense particle agitation and circulation associated with the high gas velocities used

in the fluid bed which prevents the material from sticking.

7.8 Practical Aspects of the Reduction in Fluidized Beds

The feasibility of the proposed process outlined in Section 1 depends to a large extent on the attainment of extremely fast reaction rates. Now, the data obtained in both the fixed and fluidized beds show that the overall reaction rate, and hence the rate of reduction of the lead compounds, is markedly dependent on the reaction temperature and is also increased by decreasing the particle size.

In the fluidized-bed reactor an increase in temperature from 600°C to 700°C decreases the time required for 80 per cent overall reduction from approximately 100 min. to about 50 min.; accordingly, from a practical viewpoint the temperature range of greatest interest is above 700°C. Also, it is desirable to use very small particle sizes to avoid pretreatment of the roasted flotation concentrates. However, the results obtained in the fluidized bed reactor show that a fluidized bed is unsatisfactory for the high temperature reduction of fine particles of a material such as sinter. The crushed sinter tends to become sticky during reduction at 600°C, and this effect is more noticeable as the bed temperature is increased. It is therefore necessary to use high gas velocities to keep the bed fluidized and this introduces an additional problem - elutriation of particles from the bed. Above 700°C the elutriation losses are serious even with -25 +36# (B.S.S.) particles, and at 700°C this effect precludes the use of material finer than 100 # (B.S.S.). Consequently, it is impossible to attain the conditions conducive to extremely fast reaction rates in a fluidized bed.

Various investigators encountered similar difficulties during the reduction of iron oxides by hydrogen, and Lloyd and Amundson [18] (1961), and Dalla Lana and Amundson [19] (1961) have overcome the tendency for partially reduced iron oxide particles to stick by carrying out the reaction in heated transport lines. Alternatively, Ezz and Wild [59] (1960) make use of a dilute suspension of iron oxide particles in a stream of hydrogen. Both these techniques are inherently suited to the high temperature reduction of fine particles, and, although a full-scale investigation of the reaction between lead oxide and hydrogen in a transport reactor is beyond the scope of this project, it should be possible to assess the feasibility of the process from a limited number of tests. Consequently, it is considered that the present experimental programme should be extended to include a preliminary study of the reduction of small particles of lead sinter transported by hydrogen through a heated vertical reactor.

7.9 Conclusions

(1) The rate of reaction in a fluidized bed is faster than the reaction rate in the equivalent thin, fixed, bed due to the better gas-solid contact in the intensely agitated, highly circulating, fluidized beds.

(2) Crushed and sized fractions of lead sinter are difficult to fluidize. It is sometimes necessary to use gas velocities of the order of 10 V_{mf} to prevent agglomeration and sticking, and under these conditions the bed is not truly fluidized. Also, during reduction liquid metallic lead is removed from the particles and this

collects at the bottom of the bed and prevents uniform distribution of the fluidizing gas; for this reason some beds which are satisfactorily fluidized at the start of the reduction suffer a loss of fluidization towards the end of the reaction.

(3) The reaction rate is increased by increasing the temperature and decreasing the particle size, and the effects of these variables are more marked in the fluidized bed than in the fixed bed.

(4) The overall reaction rate at 600°C is not influenced by the presence of up to 10% water vapour by volume. This conclusion follows from the fact that increasing the bed weight from 250 g. to 750 g., and increasing the gas velocity from 5.75 V_{mf} to 10 V_{mf}, does not alter the rate of reduction of -52 +72 # (B.S.S.) particles at 600°C.

(5) The correlation presented by Leva [64] (1957) adequately predicts the minimum fluidizing velocity for the nitrogen and hydrogen fluidization of beds of crushed and sized lead sinter at room temperatures and at elevated temperatures.

(6) The reduction of lead sinter by hydrogen in a fluidized bed is unsatisfactory from a practical viewpoint, and it is desirable to study the reaction in a transport system so that smaller particle sizes and higher temperatures may be used.

8. REDUCTION OF LEAD SINTER BY HYDROGEN IN A VERTICAL FLOW REACTOR

In Section 7.8 it is concluded that a fluidized bed reactor is unsatisfactory for the high temperature reduction of small particles of a material such as sinter which tends to become sticky during reduction. However, it is considered that the relatively high particle velocities and short residence times which exist in a vertical flow reactor of the type recently used by Lloyd and Amundson [18] (1961), and Dalla Lana and Amundson [19] (1961), to study the reduction of iron oxides by hydrogen make an apparatus of this nature inherently suitable for the present investigation. Consequently, it is felt that further investigational work on the reduction of lead oxide by hydrogen should be carried out in a vertical transport apparatus, and this Section describes the results of a preliminary investigation of the reduction of impure lead oxide in a transport reactor. In particular, it deals primarily with the design and operation of the small transport apparatus built for this purpose.

Firstly, the literature relating to the transport of solids through pipes is reviewed, then the design of the apparatus is discussed, and, finally, the preliminary experimental results are considered.

8.1 Literature Review

This survey is limited to those aspects of pneumatic conveying which are relevant to the design and operation of a vertical transport line suitable for studying the reaction between finely divided lead sinter and hydrogen; consequently, in general, most of the data relating to horizontal transport are omitted.

The review deals firstly with the various aspects of the

design of transport systems which have a theoretical basis; these include the minimum gas velocity necessary to entrain a solid particle and the pressure drop due to the flow of solid-gas mixtures. Secondly, those features of the design, e.g., feeding devices, which are necessarily based on practical experience are discussed, and, finally, the conclusions reached on the basis of the available literature are given.

8.1.1 Properties of solid-gas Transport Systems

If the velocity of a gas stream passing up through a bed of closely sized material contained in a pipe exceeds the terminal velocity of the particles, the material suspends in the gas and the resultant solid-gas mixture flows through the pipe in a manner similar to a true fluid. However, the equations developed for calculating the pressure drop for the flow of fluids in pipes are not directly applicable to the flow of solid-gas mixtures because of the additional energy losses caused by the friction between the solids and the tube walls and the static head of the suspended solids. Consequently, two of the basic factors which must be estimated in designing a transport line are

(i) the minimum gas velocity which will entrain the solid particles, and

(ii) the pressure drop to be overcome in transporting the solid through the pipe.

This Section deals with the methods available for the calculation of the minimum transporting velocity for solid particles, and the procedures reported in the literature for estimating the pressure drop in the flow of solid-gas mixtures through pipes.

8.1.1.1 Calculation of the minimum gas velocity necessary to entrain a Solid Particle

Although a body falling in a viscous fluid is accelerated by the force of gravity, the resistance offered by the fluid also increases with increasing particle velocity. Eventually, these two forces become equal and the body continues to fall at a constant velocity. This final steady velocity is called the terminal velocity, and the minimum gas velocity necessary to entrain a given particle size must at least be equal to the terminal velocity of the particles. Consequently, an estimate of the gas flow necessary to carry a particle through a transport line may be obtained by calculating the terminal velocity of the particle.

By equating the frictional resistance of the fluid to the gravitational acceleration caused by the buoyant weight of the solid it can be shown [66] (1950) that the terminal velocity, v_t, is given by

$$v_t = [2g_c \cdot m_p \cdot (\rho_s - \rho_g)/A_p \cdot C \cdot \rho_s \cdot \rho_g]^{\frac{1}{2}} \qquad (24)$$

In the general case of turbulent flow the solution of this equation involves a trial and error calculation since the drag coefficient, C, depends on the terminal velocity. However, several methods of obtaining a direct solution have been proposed. Korn [67] (1951) gives a plot of the group $4(\rho_s - \rho_g)\,\rho_g \cdot d^3/3\, g_c \cdot \mu_g^2$ against the Reynolds number for a particle moving at its terminal velocity; calculation of the value of this group then enables the terminal velocity to be estimated directly from the Reynolds number taken from the graph. Alternative methods have been reported by Perry [66] (1950) and

Brown [68] (1950).

The experimental data of several investigators describing the steady-state velocity reached by free-falling particles in fluids have been summarised by Lapple and Shepherd [69] (1940) and presented as curves of drag coefficient against Reynolds number for various regular particle shapes. Data for irregular particles are rather scarce, but the drag coefficient curve for spheres holds fairly well [66] (1950) for irregular particles for Reynolds numbers less than 50, where the diameter measured by screening, elutriation, etc., is taken as the diameter of an equivalent sphere. For Reynolds numbers greater than 50 the drag coefficient rapidly reaches a constant value showing approximately two-fold variations from an average of about 1.2.

The above considerations apply only to the case of free settling where the concentration of solids is low enough (less than 0.044 lb/ft^3) to prevent interaction between the particles. Steinour, in a series of articles [70,71,72] (1944), has considered the case of the hindered settling of spheres and non-uniform particles in still fluids, and has derived equations which enable the terminal velocity to be calculated for conditions of hindered settling.

From the preceding discussion it appears that in general the terminal velocity of a solid particle can be calculated from the properties of the solid and the transporting gas. However, from the viewpoint of designing a transport line this terminal velocity is not entirely satisfactory. Although, theoretically, the difference between the gas velocity and the velocity of the solids - designated the "slip velocity" - is equal to the particle terminal velocity, in

practice, the presence of external retarding forces, such as friction between the flowing solids and the wall, means that the slip velocity is generally higher than the terminal velocity. Consequently, the slip velocity is the factor which actually determines the magnitude of the gas flow necessary to transport a given solid, and it is essential to relate the slip velocity to the terminal velocity. Unfortunately, the limited data available on the transport of solids through tubes by gases do not clearly indicate the relative magnitudes of these two velocities. Hariu and Molstad [73] (1949), who determined the velocity of the solids in their system by direct measurement, have shown that the slip velocity depends on the gas velocity, the particle size, and the tube diameter. In particular, they state that the slip velocity decreases and approaches the terminal velocity as the pressure drop due to the flowing gas and the pressure drop due to friction between the solids and the walls become smaller. However, they do not give any quantitative relation between these factors and the slip velocity, and an examination of the experimental results discloses that the slip velocity can be twice the terminal velocity. Belden and Kassel [74] (1949), on the other hand, suggest that the slip velocity in the turbulent range can be calculated from the equation

$$v_{slip} = 1.32\left[g_c \cdot d_p \cdot (\rho_s - \rho_g)/\mu_g\right]^{\frac{1}{2}} \qquad \text{(25)}$$

This equation is essentially similar to the relation between the terminal velocity and the particle properties given earlier, and they have, in fact, assumed that the particle velocity is the difference between the gas velocity and the terminal velocity of the particle. Consequently, it seems unlikely that this equation will

hold when applied to systems other than that investigated by the authors.

In view of the doubt concerning the correct value to assign to the slip velocity in a given system it seems reasonable to assume for the purposes of design that the minimum velocity required to transport a particle is twice the terminal velocity of the particle. Consequently, since the particle terminal velocity can be calculated from the properties of the solid and the system conditions by means of equation (24), the minimum gas velocity necessary to transport a given particle size can be estimated.

8.1.1.2 Estimation of the Pressure Drop in the Flow of Solid-gas Mixtures

In large commercial applications, e.g., the addition and removal of catalyst to catalytic cracking units by pneumatic conveying through large diameter ducts, the total pressure drop is almost entirely due to the static head of the suspended solids. However, in smaller equipment the friction between the solids and the container walls is an unknown, and possibly large, part of the total pressure drop. Consequently, it is desirable to discuss the methods available for calculating the value of the total pressure drop. This can be achieved

(i) by estimating the value of each component of the total pressure drop separately, or

(ii) by using the general correlation developed by Korn [67] (1951).

(a) Calculation of the Values of the Components of the Total Pressure Drop

In general the total pressure drop due to the flow of a

solid-gas mixture through a pipe can be considered to consist of

(i) the pressure drop due to the gas flow alone, ΔP_g,

(ii) the pressure drop due to the static head of the suspended solids, ΔP_x, and

(iii) the pressure drop due to friction between the solids and the container walls, ΔP_s.

This can be expressed as

$$\Delta P = \Delta P_g + \Delta P_x + \Delta P_s \qquad \text{(26)}$$

For horizontal transport $\Delta P_x = 0$, and the equation reduces to

$$\Delta P = \Delta P_g + \Delta P_s \qquad \text{(27)}$$

(i) Pressure drop due to the flowing gas stream, ΔP_g.

For the flow of solid-gas mixtures through tubes it is generally agreed [73,74,75] (1949), (1949) and (1948), that the suspended solids have little or no effect on the flow characteristic of the gas stream; consequently, it is satisfactory to calculate the pressure drop due to the flowing gas from the Fanning equation, viz.,

$$\Delta P_g/\rho_g = f.L.v_g^2/2g_c.D \qquad \text{(28)}$$

The results of Clarke et al. [76] (1952), who studied the horizontal flow of various materials, suggest that this method is not applicable to high feed rates at low gas velocities; however, under these extreme conditions the solids are not continuously suspended in the gas stream but move, as described by Korn [67] (1951), in a series of "jumps". Therefore, it seems probable that this condition is peculiar to horizontal transport lines, and it is considered that

the portion of the total pressure drop due to the flowing gas may be adequately predicted in the present case of vertical transport by the Fanning equation.

(ii) Pressure drop due to the static head of suspended solids, ΔP_x.

The pressure drop in the carrier gas required to support the weight of suspended solids is calculated as a solids static head from the density of the solids in the transport line, ρ_{ds}. However, because of the effect of "slippage", the true dispersed solids density in the line is higher than the flow density expressed as total weight flow per hour/total volume flow per hour. Consequently, ρ_{ds} cannot be estimated without a knowledge of the velocity of the solids, i.e., a knowledge of the slip velocity. In the present case it is proposed to calculate the pressure drop due to the suspended solids on the assumption that the slip velocity is equal to twice the terminal velocity, and ΔP_x may be calculated on this basis.

(iii) Pressure drop due to the presence of the flowing solids, ΔP_s.

Cramp and Priestley [77] (1924), studying the transport of wheat, derived the following equation for the pressure drop due to the presence of the flowing solids,

$$\Delta P_s = G'_s \left[(v_{sf}/g_c) + (\beta . L/c . v_{sf}) \right] \qquad (29)$$

where

G'_s = weight rate of flow of solid $[lb/(ft^2),(sec)]$,

v_{sf} = final velocity of material (ft/sec),

g_c = gravitational constant (ft/sec^2),

β = $(w + w')/w$, where w is the weight of an individual particle, and w' is the equivalent frictional force acting on the material,

c = ratio of average grain velocity to final grain velocity, and

L = length of pipe (ft).

They assumed that the friction factor, w', was proportional to the square of the particle velocity and inversely proportional to the rate of flow of solids, i.e.,

$$w' = c'.v_s^2/(G_s')^{\frac{1}{2}} \qquad \text{---------- (30)}$$

and, by measuring the additional pressure drop due to the presence of the solids for different air velocities and material loadings, a value for the constant, c, was deduced. The energy losses due to friction between the solids and the walls, which were small in relation to the other losses, were then determined as the difference between the total pressure drop and the sum of the pressure drop due to the flowing gas alone and the static head of solids in the line. This procedure results in relatively high percentage errors in the values obtained for the friction losses, and equation (29) must therefore be used with caution .

Hariu and Molstad [73] (1949) investigated the total pressure drop and the static pressure drop in the transport of closely sized solids through glass tubes. By assuming that the Fanning friction equation applied to the energy losses caused by the impacts between the flowing particles and the container walls, and the collisions between particles, they derived the equation

$$(\Delta P_x + \Delta P_s)/L.G_s = 0.1925\left[1/v_s + (2f/g_c.D)v_s\right] \qquad \text{---- (31)}$$

where

ΔP_x = pressure drop due to the static head of suspended solids (lb/ft^2),

ΔP_s = pressure drop due to friction between the solids and the container walls (lb/ft^2),

L = length of transport line (ft),

G_s = mass flow rate of solids $[lb/(ft^2),(sec)]$,

v_s = particle velocity (ft/sec),

f = friction factor (dimensionless),

g_c = gravitational constant $ft/(sec)^2$, and

D = diameter of transport line (ft).

The experimental data for the total pressure drop, ΔP, plotted against the solids flow rate for each carrier gas velocity gave straight lines which cut the pressure drop axis at the experimental value of the friction loss due to the flowing gas alone. The slope of these lines is a measure of the value of $(\Delta P_x + \Delta P_s)/L.G_s$, and, since the solids static head component could also be calculated from the measurements of the solids density in the transport line, a value for the pressure drop due to solids friction was obtained. However, because the test section was close to the solids feed point, the friction loss included the initial acceleration effects, and the validity of assuming that the Fanning friction equation applied to the flow of solids could not be tested. Despite this the authors recommend that the friction loss component be estimated using the linear velocity of the solids and the dispersed solids density in the Fanning equation.

Belden and Kassel [74] (1949), who studied the total pressure drop in the vertical transport of spherical catalyst material by air

and carbon dioxide, calculated the energy loss due to the static head of suspended solids from the material density in the transport line. Then, by ignoring the effect of gas friction, the energy loss due to solids friction was obtained as the difference between the measured total pressure drop and the calculated static head of solids. Using the pressure drop due to the flowing solids obtained in this manner they calculated the friction factor in the following generalisation of the Fanning equation

$$\Delta P_s/L = 2f(G_g + G_s)v_g/g_c.D \qquad \text{---------- (32)}$$

where

ΔP_s = pressure drop due to flowing solids (lb/ft^2),

L = length of transport line (ft),

f = friction factor (dimensionless),

G_g = gas mass velocity $[lb/(ft^2),(sec)]$,

G_s = particle mass velocity $[lb/(ft^2),(sec)]$,

v_g = gas velocity (ft/sec),

g_c = gravitational constant $ft/(sec)^2$, and

D = diameter of transport line (ft).

The greater part of the experimental data were represented by

$$f(Re)^{0.2} = 0.049 + 0.22\, G_g.G_s/(G_g + G_s)^2 \qquad \text{---------- (33)}$$

where the symbols have the same meaning as above, and, consequently, equations (32) and (33) can be combined to give an expression for the pressure drop due to friction between the flowing solids and the walls of the transport line.

In view of the preceding discussion it appears that the normal form of the Fanning friction equation may be used to estimate

the pressure drop due to the friction between the flowing solids and the walls of the transport line. In using this equation the value of the friction factor can be obtained from the general friction factor against Reynolds number curve. Alternatively, equation (33) can be used to provide an estimate of the friction factor.

(b) General correlation of the Total Pressure Drop

Korn [67] (1951) suggested that the specific pressure drop - defined as the total pressure drop divided by the velocity head of the flowing fluid - be correlated with the specific loading (mass rate of flow of solid/mass rate of flow of fluid) by the following equation

$$k/h = f + br^n \qquad \text{---------- (34)}$$

where

k = specific pressure drop (dimensionless),

h = velocity head of the flowing fluid using the superficial gas velocity (lb/ft^2),

f = friction factor (dimensionless),

b = factor (dimensionless),

r = specific loading (dimensionless), and

n = exponent (dimensionless).

Two more dimensionless groups - h/t, the ratio of the fluid velocity head using the superficial gas velocity to the fluid velocity head using the terminal velocity of the particles, and $\rho_g.D/h$, which includes the effect of pipe diameter - were also defined. The results of previous investigators were examined from the viewpoint of equation (34), and the data obtained relate the dimensionless groups h/t and $\rho_g.D/h$ to the values of "b" and "n". Therefore, approximate

values of "b" and "n" may be estimated for any system, and, in combination with the gas velocity and the pipe friction factor, these values may be used to calculate the head loss due to the flow of a solid-gas mixture in a pipe.

8.1.2 General Design Information

Very little recent information is available in published literature concerning the design of gas-solid transport systems; however, the design of fluidized-bed reactors, which involves problems similar to those encountered in transport systems, has received considerable attention. This Section, therefore, deals with information relevant to the design of transport systems, together with a summary of the published design data relating to the flow of solid-gas mixtures.

8.1.2.1 Solids Feeding

The design of the solids feeding system is important from the viewpoint of the stability of flow and the maintenance of steady-state conditions in the system. The fundamental problem is to feed the solid at a controlled rate from a relatively low pressure zone (a hopper or standpipe) into the relatively high pressure zone of the flowing gas stream. The feeders in general use are shown in Figure 29 [after Sittig [78] (1953)], but, as Gregory [79] (1952) emphasises, neither the star feeder, the slide valve, nor the screw conveyor can operate against a pressure differential, and the effective head of the solid in the standpipe must be used to overcome any pressure drop across the feeder. For applications where the pressure in the reactor or the flowing fluid can only be overcome by an excessive head

of solids it is claimed [78] (1953) that the solids pump - a centrifugal pump operating on powdered solid material - may be used for pressure differentials between 10 and 100 lb/in.^{2} gauge without serious erosion of the pump components. For higher pr ssures the solids may be stored under a higher pressure than exists in the reactor and fed through a valve [80] (1949). For free-flowing powders the star feeder and the slide valve can be replaced by the non-mechanical I.C.I. valve which utilizes the natural angle of repose of the non-fluidized solid to half flow. Aeration at the point indicated by the arrow (Figure 29) disturbs the angle of repose and causes the flow of solids to resume.

Both Sittig [78] (1953) and Farbar [81] (1949) stress that the design of the mixing nozzle at the point of introduction of the solids into the fluid stream is very important; dropping the solids directly into the gas stream gives operating difficulties at all solids and gas flow rates. Gregory [79] (1952) lists the factors necessary for the design of a satisfactory suspension mixer as

(i) provison of sufficient momentum in the gas stream,

(ii) transfer of the required momentum to the suspended solid particles in a reasonably short time,

(iii) no possibility of build-up of suspended solids, and

(iv) ease of maintenance.

Two commercial designs used in catalytic cracking plants are of interest from this viewpoint. In the first the mixer tube is horizontal and the high velocity is given to the gas by a venturi throat; the solid is introduced immediately after the throat by a pipe bent to give

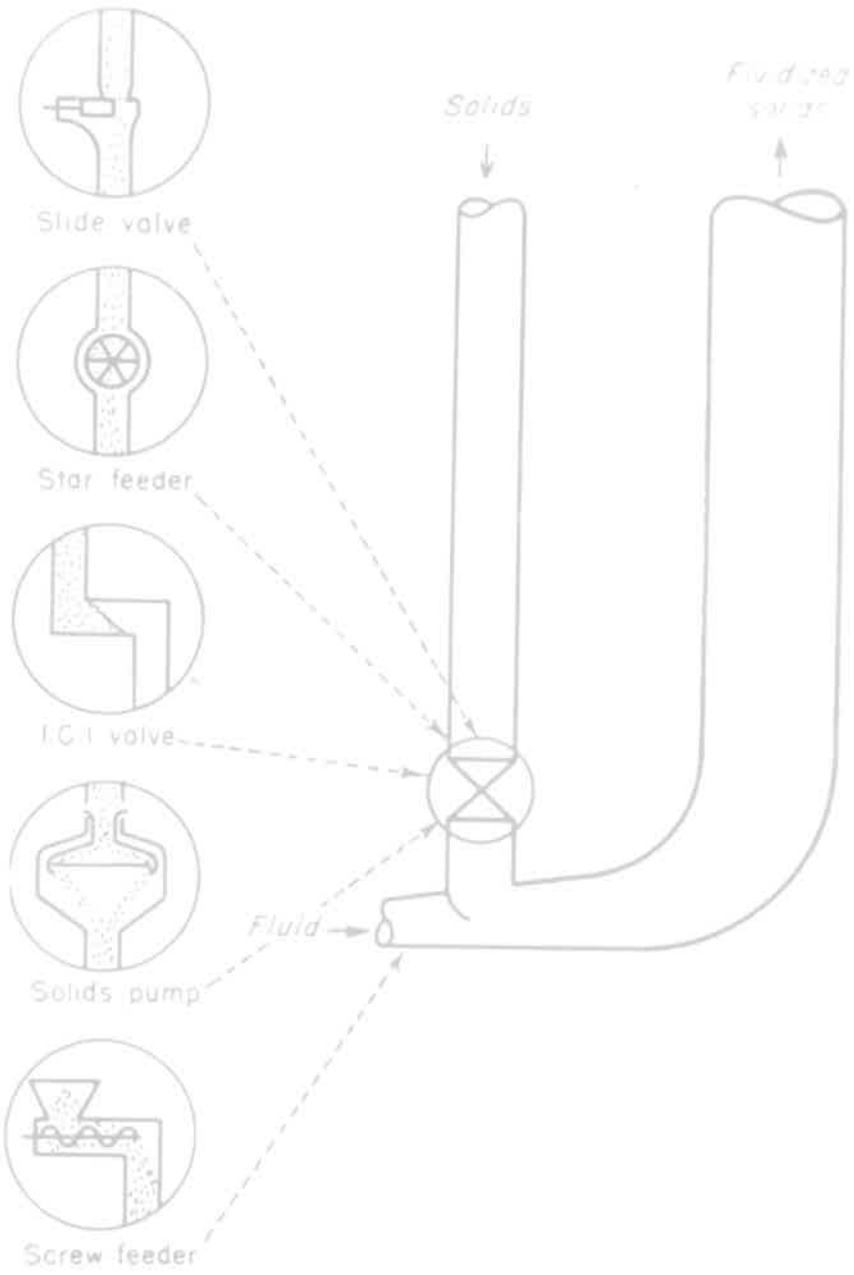

Fig. 29 - Methods of Feeding Solids into Transport Lines [78] (1953)

horizontal motion to the solids. The second design employs a vertical tube with a pheripheral feed [82] (1951).

The few published papers concerning the transport of solids by gases describe a variety of methods of feeding the solids into the gas stream. Farbar [81] (1949), investigating material with a wide size range, used gravity flow through a slide valve to a carefully designed glass nozzle extending into the horizontal gas stream. In this system the fluctuations in feed rate due to bridging and agglomerating of the solids above the slide valve were overcome by heating and fluidizing the solids in the feed hopper. With the inclusion of this procedure the slide valve provided an adequate means of controlling the flow of solids into the gas stream when the downstream conditions were favourable; these conditions were profoundly influenced by the design of the mixing nozzle. However, although several nozzle designs were investigated, the solids were fed into the pipe in a direction normal to the gas flow. The failure to provide the solids with a velocity in the same direction as the gas therefore appears to be one of the major causes of the difficulties. Belden and Kassel [74] (1949), on the other hand, used an orifice equipped with a gas by-pass to feed closely sized solids directly into the gas stream. They state that this arrangement delivered solids to the transport line at a rate determined solely by the material characteristics and the orifice dimensions; it can, however, only be used for free-flowing materials. Hariu and Holsted [73] (1949) made use of a slide valve constructed from a gate valve to control the rate at which solids from the fluidized bed in the storage pipe entered the gas stream.

They reported no operating difficulties despite the absence of any provision for gas-solid mixing at the feed point. Pinkus [83] (1952), who studied the horizontal transport of closely sized sands, experienced considerable difficulty with solids feeding. His feeding mechanism was a screw conveyor which transported the solid from a hopper to the transport line. Initially the back pressure of the gas prevented operation, but this was overcome by passing the gas stream through a nozzle to reduce the pressure at the feeding point. Another source of difficulty was the jamming of the screw by particles caught in the clearance space between the screw and the enclosing conduit. A clearance of about twice the particle diameter was found to be satisfactory.

From the preceding discussion it is apparent that there are several methods suitable for feeding a controlled flow of solids into a transport line, and, in general, the pressure differential between the storage space and the gas stream may be overcome either by increasing the head of solids in the storage or by reducing the pressure of the flowing gas at the feed point with a construction. It is also desirable to introduce the solid into the gas stream with a velocity in the same direction as the flow of gas. This minimises any difficulties experienced in mixing the gas and the solids.

8.1.2.2 Solids Separation from the Effluent Gas Stream

Sittig [78] (1953) and Gregory [79] (1952) have reviewed the methods available for the removal of solids from the effluent gases leaving fluidized-bed reactors. They recommend porous ceramic filters, or a combination of cyclones and bag filters, for pilot plant

installations. The design of filters and cyclones is reviewed by Lapple [84] (1951), and Stairmand [85] (1951) presents design data and test results for a small laboratory cyclone.

8.1.2.3 Materials of Construction

Evans and Kepper [86] (1952), who considered some of the commercial applications of fluidization techniques, conclude that the abrasive effect of the suspended particles is usually insignificant. It appears that the individual particles are protected from particle to particle attrition by a thin film of the fluidizing gas, while near the sides of the reactor the particles generally move parallel to the walls and are separated from them by the adhering gas film. On the other hand, Sittig [78] (1953) considers that erosion is an important problem in the design of fluidized-solids systems. Specifically, he mentions the design of the dust collection equipment and recommends a silicon-killed carbon steel for the construction of these components as this material has more resistance to erosion than stainless alloys.

The published data on the flow of gas-solid mixtures contain little reference to erosion. Hariu and Molstad [73] (1949), who studied the vertical transport of sands and cracking catalysts in glass tubes, found no change in the roughness of the tube walls with time. However, Farbar [81] (1949), who investigated both horizontal and vertical transport in glass tubes, suggests that it is necessary to include baffle plates wherever the direction of flow is changed; it appears that the solids accumulate in a dense phase at the outer wall, and, although this does not affect the flow characteristics, it causes a marked increase in the rate of erosion.

The above discussion indicates that attrition between the flowing solids and the pipe walls is not significant except where the direction of flow is altered. This effect can be minimised by the addition of baffle plates to oppose the effect of centrifugal force, and, with this modification, it appears that stainless steel is a satisfactory material for the construction of a transport line.

8.1.3 Solid-Gas reactions in Vertical Flow Reactors

The most recent data concerning solid-gas reactions carried out in heated transport lines relate to the reduction of iron oxides by hydrogen.

The reduction of powdered ferric oxide by hydrogen was studied by Lloyd and Amundson [18] (1961) in a vertical flow reactor. Powdered oxide, entrained in a stream of reducing gas by elutriation from a small fluidized bed, was carried through a heated 1 in. I.D. transport line, approximately 6 ft. long, and the amount of reduction was measured by chemical analysis of the solids leaving the reactor. Extremely fine (0.3 microns) particles were used and it is claimed that this eliminated the necessity to consider particle velocities in the calculation of residence times; the dispersed solids-gas mixture was assumed to have the characteristics of a single phase. There was no evidence of the sticking and sintering which occurs in fluidized beds. It is considered that sintering, like reduction, is a rate process, which is influenced by temperature, and may be avoided in a flow reactor because of the short system residence times.

Dalla Lana and Amundson [19] (1961) extended the data of Lloyd and Amundson [18] (1961) by investigating the reduction of

coarser iron oxide particles (2 to 22 microns) in a 16 ft. long reactor. The solids, which were fed into a cold, vertical, section of the transport line by a variable speed screw feeder, were entrained by part of the reducing gas and mixed with the remainder of the hydrogen, which is preheated, in a venturi mixer; the amount of preheating was adjusted to make the temperature of the mixture leaving the venturi mixer equal to the desired reaction temperature. The solids leaving the reactor were cooled and separated from the gas stream by a small cyclone. The amount of reduction was calculated from the chemical analysis of the solids collected in the cyclone, and residence times were estimated from the assumption that the particle slip velocity was equal to the terminal velocity for the particle settling in stagnant hydrogen at the reaction conditions. The calculated residence times varied from 2 to 13 seconds, and approximately 95 per cent reduction was obtained in 4 seconds at 600°C.

Ezz and Wild [59] (1960) also studied the reduction of iron oxide particles, but in this investigation the tendency for the particles to stick was overcome by reducing particles suspended as a dispersed cloud in the reducing gas. However, this system did not constitute a flow reactor since the particles were not removed from the reactor. The reaction rate was measured by collecting and weighing the water in the gases leaving the reactor.

8.1.4 Conclusions

(1) In the design of a transport line the minimum gas velocity necessary to entrain a bed of closely sized solids may be taken as twice the terminal velocity of the particles; methods for

calculating the terminal velocity of both regularly and irregularly shaped particles for conditions of free and hindered settling are available in the literature.

(2) The total pressure drop due to the flow of a gas-solid mixture may be estimated from the equation due to Korn [67] (1951). Alternatively, the magnitudes of the individual components of the total pressure drop may be estimated; the pressure drop due to the flowing gas stream alone may be predicted by the Fanning equation, the pressure drop due to the static head of solids (zero in the case of horizontal flow) is equal to the density of the solids in the transport line, and the pressure drop due to friction between the flowing solids and the container walls may be estimated by several methods, the most common being to assume that the Fanning friction equation applies to the case of solids flowing through pipes.

(3) There are several methods available for feeding a controlled flow of solids into a transport line, but, in general, the pressure differential between the storage space and the flowing gas stream is overcome either by the head of solids in the storage or by reducing the pressure at the solids feed point. It is also desirable to introduce the solids into the gas stream with a velocity in the same direction as the flow of gas to prevent difficulties in mixing the gas and the solids.

(4) Attrition between the flowing solids and the pipe walls is not significant except where the direction of flow is altered. This effect may be minimised by the addition of baffle plates to oppose the centrifugal force, but, in any case, it appears

that stainless steel is a satisfactory material of construction.

8.2 Design of the Transport Apparatus

The present investigation is exploratory in nature and is only intended to provide a limited experimental basis for future study of the reduction of lead oxide in vertical flow reactors; consequently, the design of the apparatus was made as simple as possible. The general considerations behind the selected design are outlined in this Section, and a detailed description of the various items of equipment is given in Appendix V.2.

8.2.1 General Arrangement of Apparatus

The primary function of the apparatus is to measure the amount of reaction which occurs when crushed and sized lead sinter is carried through a heated transport line by hydrogen at a fixed elevated temperature. Consequently, the solids, which will enter the system immediately before the section in which reaction takes place, must be entrained by hydrogen previously preheated to the required reaction temperature. Then, after removing the solids from the gas stream, it is proposed to conserve hydrogen by recycling the unreacted hydrogen content of the reactor exit gases; this necessitates the inclusion of a condenser in the circuit to remove the steam from the reactor effluent gases. Also, before returning the cold hydrogen leaving the condenser to the circuit, the heat load on the preheater will be reduced by using the hot gases leaving the cyclone to heat the cold gas leaving the condenser. The water vapour content of the return hydrogen will be minimized by including a gas drier in the system, and make-up hydrogen will enter the system between the drier and the pump. The pump will be located between the drier and the heat

exchanger and will operate on cold, dry, hydrogen.

On the basis of these considerations the schematic flowsheet shown in Figure 30 has been adopted.

8.2.2 Dimensions of Transport Line

The length of the vertical section of the transport line is limited to a maximum height of 12 feet by the head room available in the laboratory; consequently, the length of the heated section of the transport line was selected as 11 feet.

The limited data available on the transport of solid-gas mixtures through pipes generally relate to tubes of 1 in. diameter or smaller, and 1 in. O.D. heat resistant stainless steel tube was chosen for the present apparatus.

8.2.3 Selection of Operating Conditions:

The initial reaction rates measured in the fluidized bed reactor show that the reaction rate is too slow below 700°C to allow significant reduction to occur in the limited gas-solid contact time available in the transport apparatus; the equipment must therefore be suitable for studying the reaction at temperatures of 700°C and above. The upper limit of the temperature range is fixed by the properties of the materials of construction; the best heat-resistant stainless steel available has a maximum safe working temperature of 1100°C, and this limits the maximum temperature attainable in the apparatus to approximately 950°C.

The smallest particle size used in the fluidized bed reactor was -72 +100 # (B.S.S.), but the bulk of the data relate to -52 +72 # (B.S.S.) particles; consequently, the -52 +72 # (B.S.S.) size fraction was chosen as the maximum particle size to be used in the

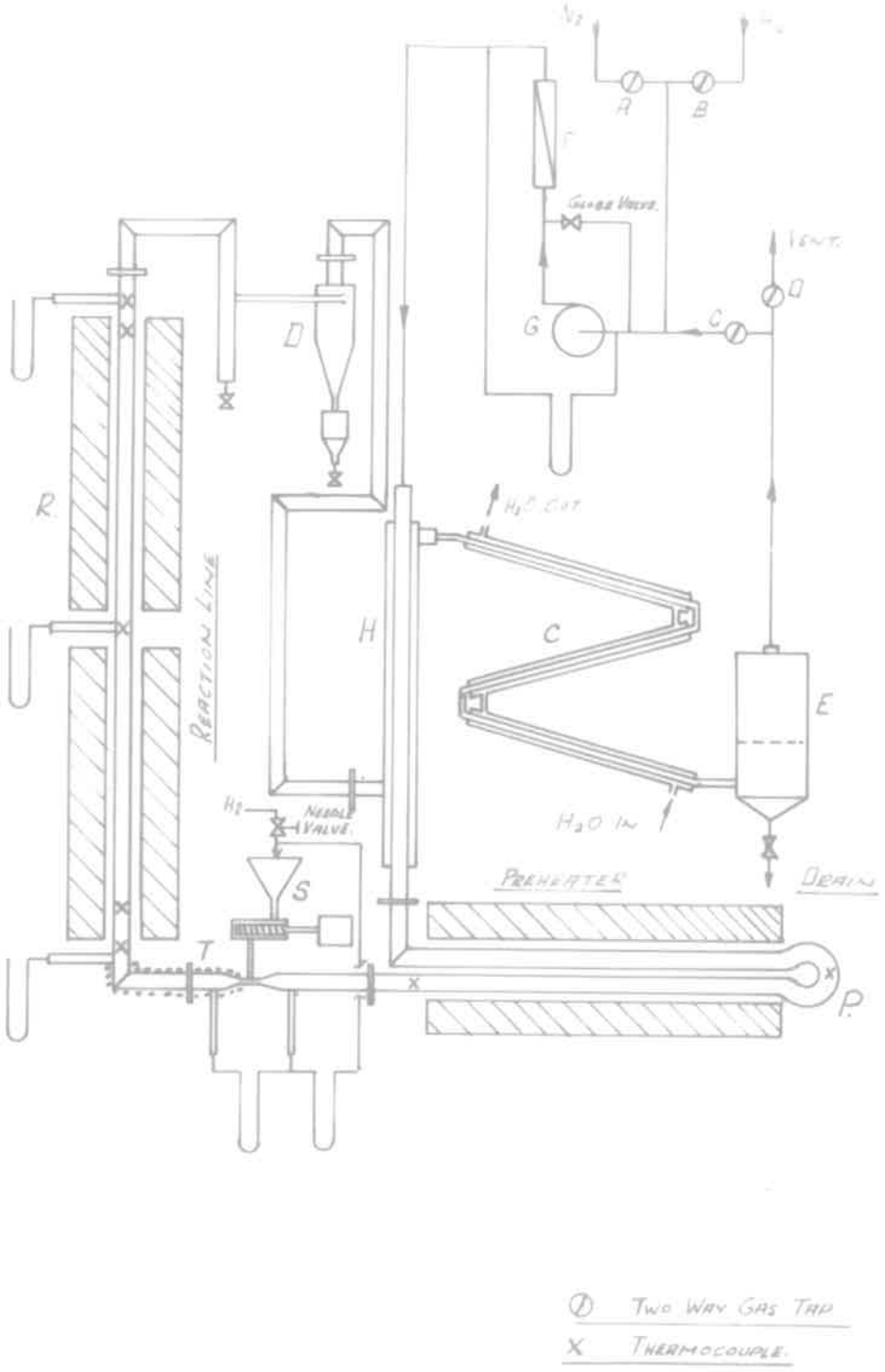

Fig. 30 - Line Diagram of Transport Apparatus

transport apparatus.

8.2.4 Measurement of Amount of Reduction

The various techniques available for measuring the rate of a solid-gas reaction in a dynamic system are discussed in Sections 6.1 and 7.1, and some of these methods are applicable to the present case, e.g. measurement of the amount of hydrogen consumed by reaction. However, the most direct and generally used method is to determine the per cent reduction of the solids leaving the reactor by chemical analysis; a curve of per cent reduction against time is constructed by varying the particle residence times and the rate curve may then be obtained by differentiation.

In the present case the solids contain several compounds which are reducible by hydrogen, and the per cent reduction calculated from the reduced and unreduced lead content of partially reduced solids should be corrected for the weight loss during reduction. The situation is also complicated by vapourization losses, and liquation of metallic lead from highly reduced particles. However, in view of the preliminary nature of this investigation the degree of reduction may be calculated directly from the chemical composition of the solids collected in the cyclone and dust trap without introducing serious errors; the short residence times inherent in a transport apparatus should prevent significant losses due to vapourization and liquation of metallic lead from the particles.

8.2.5 Summary of Design Methods

In general, the design is based on methods presented by Perry [87] (1950), and the heat transfer data are obtained from

Stoever [88] (1941) and McAdams [89] (1954). However, the dimensions of the high efficiency cyclone were selected in accordance with the values reported by Stairmand [85] (1951). Also, the design of the cooler-condenser is separated into two sections; a cooling section in which the H_2-H_2O mixture leaving the cyclone is cooled to 100°C, and a condensing section in which the steam is condensed and the non-condensibles are cooled to 30°C. The design of the partial condenser is based on the method proposed by Colburn [90] (1951).

In addition it is assumed that

(i) the minimum entrainment velocity for a given particle size is twice the particle terminal velocity at the selected temperature,

(ii) the gases entering the preheater are heated to 200°C in the heat exchanger,

(iii) the maximum solids feed rate is 7.5 lb/hr, and

(iv) the minimum ambient temperature is 12°C, and the maximum cooling water temperature is 25°C.

8.3 Experimental Apparatus and Procedure

8.3.1 Initial Experimental Apparatus

A diagram of the layout visualized at the completion of the design is given in Figure 30, and Figure 31 is a photograph of the initial arrangement. However, it was necessary to modify this original apparatus on the basis of the operating experience gained in a preliminary series of tests. These alterations are discussed in Appendix V.1.

8.3.2 Final Experimental Apparatus

The final apparatus, which is essentially similar to the initial apparatus shown in Figures 30 and 31, is described in detail in Appendix V.2. In the main it is constructed from 1 in. O.D. Comsteel 25-20 heat-resistant stainless steel; however, several sections, including the condenser and the heat exchanger, which are not subjected to high temperatures, are fabricated from ordinary 18-8 stainless steel. The reaction zone consists of 11 feet of vertical pipe heated by two tube furnaces each capable of dissipating 1 kW, and the reducing gas is preheated to the required temperature by a double pass through a tube furnace of 3 kW rated capacity.

Hydrogen is circulated around the system by an oil-lubricated vane pump and the flow is measured by a rotameter which was calibrated against a wet-test meter. Coarse control of the gas flow is achieved with a mechanical variable-speed drive located between the motor and the pump, and precise flow control is obtained from a small gate valve situated in a by-pass line.

A controlled, variable, flow of solids into the reaction line is obtained by means of a screw feeder. A photograph of this device is given in Figure 33, and Figure 34 is a detail drawing showing the dimensions and layout of the feeder components. A horizontal screw, which carries material from the hopper, discharges into a short duct leading to the throat of a venturi placed in the gas line; the screw speed is adjusted by the two banks of pulleys shown in Figure 33.

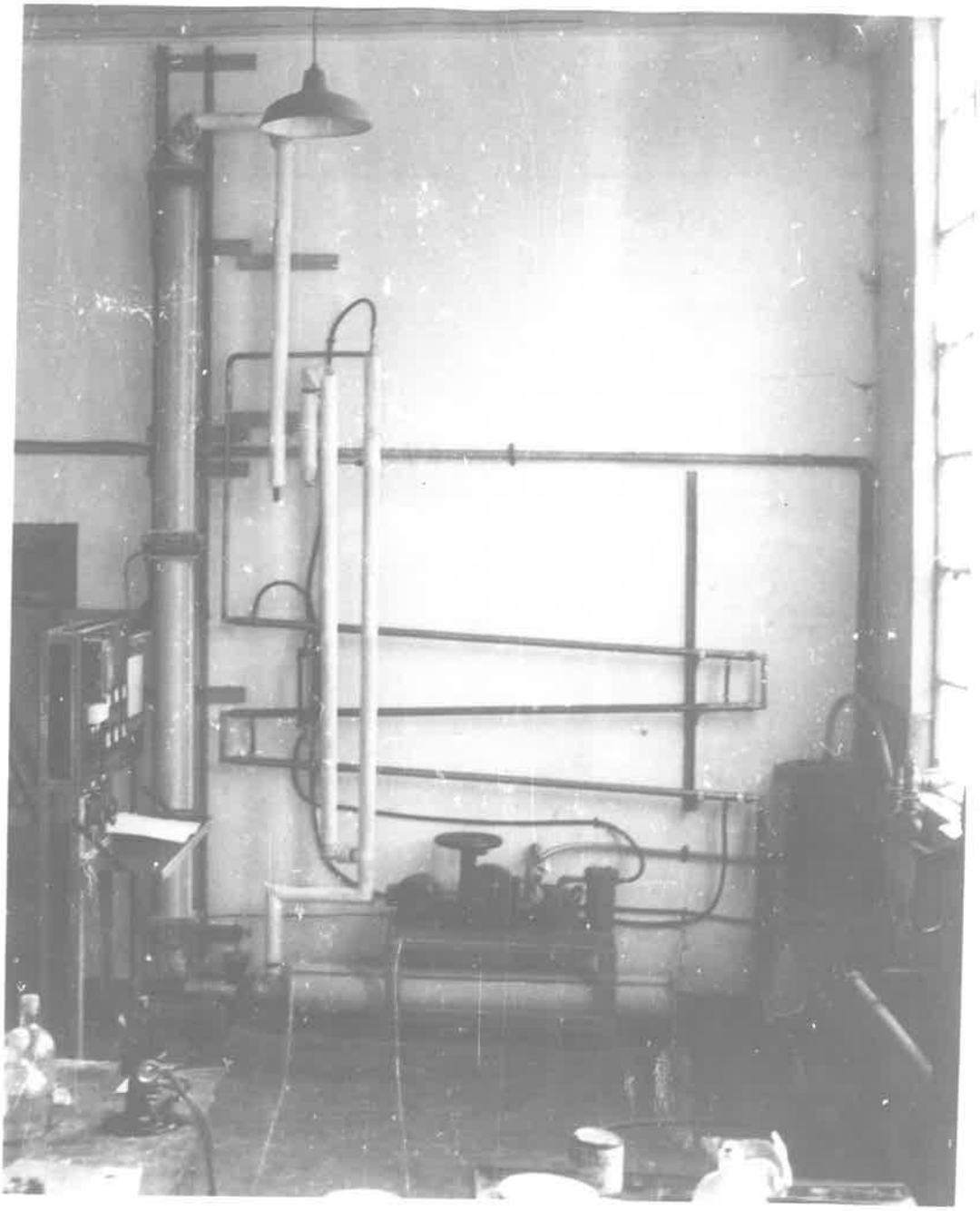

Fig. 31 - Photograph of Transport Apparatus

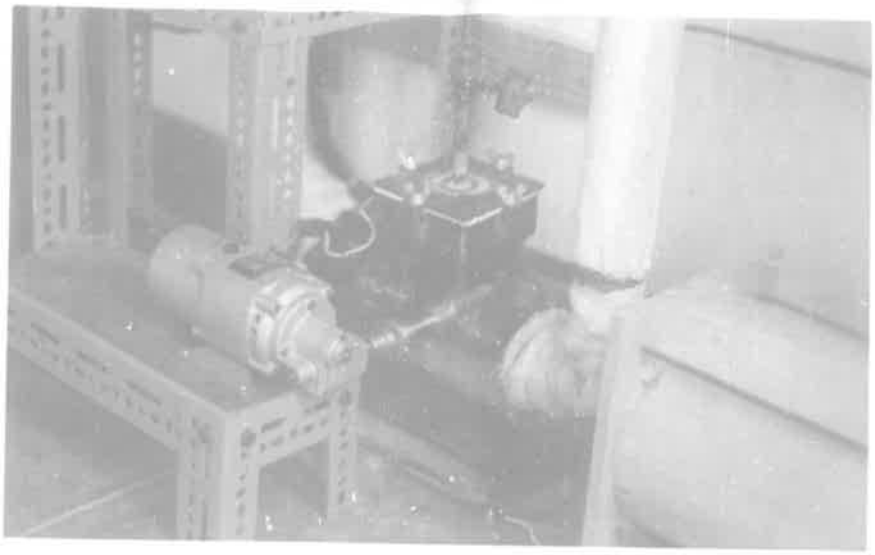

Fig. 32 - Photograph of Initial Screw Feeder

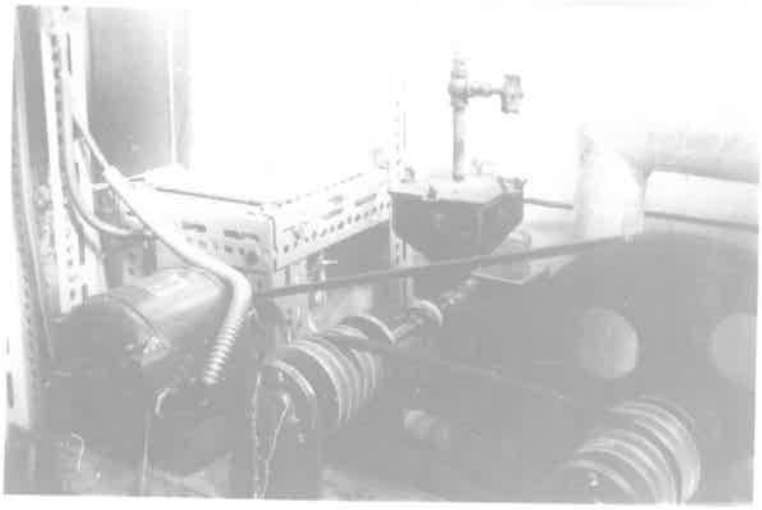

Fig. 33 - Photograph of Final Screw Feeder

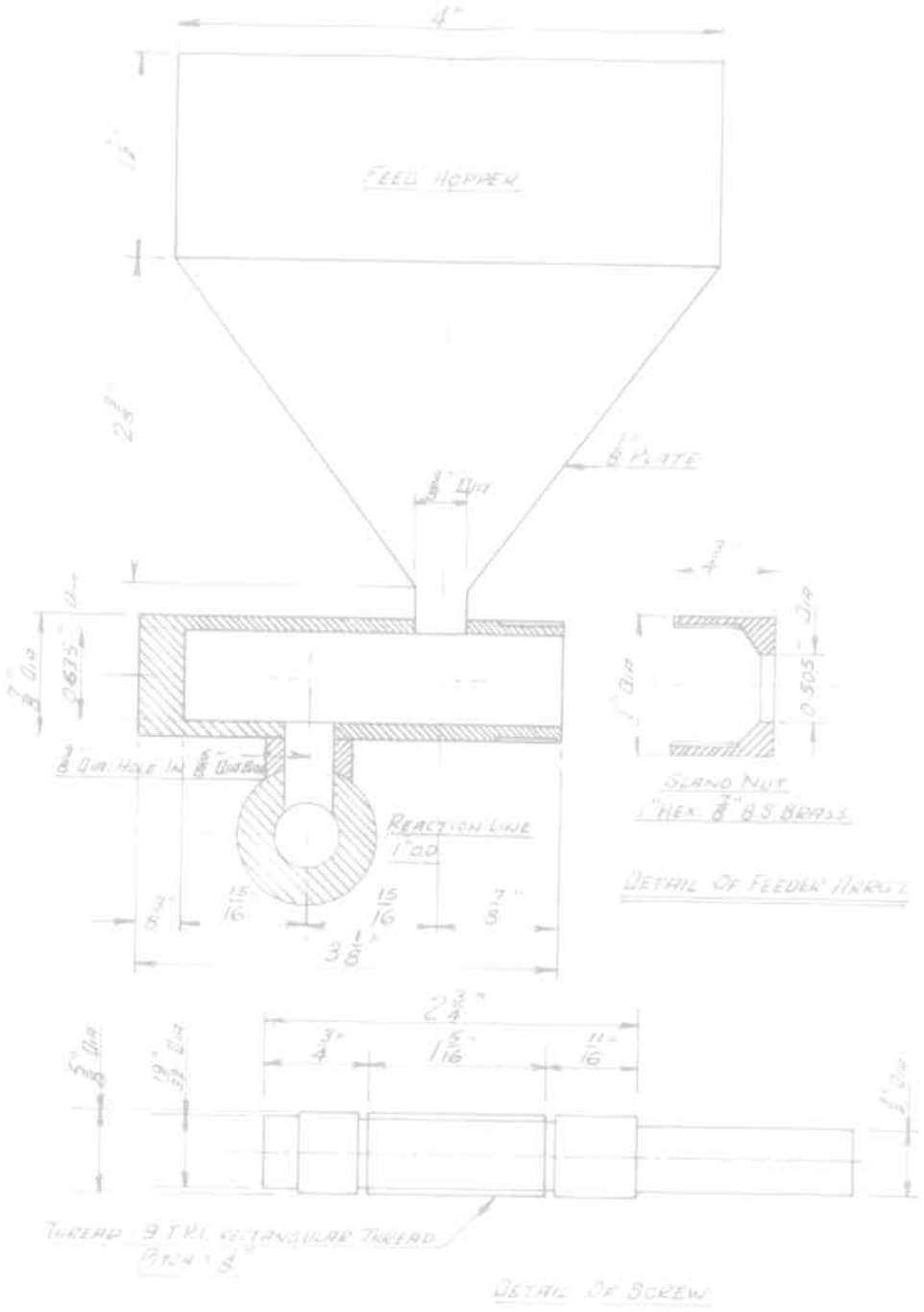

Fig. 34 - Dimensions of Screw Feeder

The reacted solids leaving the apparatus are collected in a dust trap-cyclone arrangement and the hot gases, which consist mainly of hydrogen, pass through the shell side of a concentric pipe heat exchanger to heat the gas entering the preheater. The hydrogen-rich gases leaving the exchanger are purified in the condenser-gas drier arrangement shown in Figure 30. The main reaction product - steam - is removed in the condenser and the residual water vapour is reduced to a very small value by the bed of silica gel in the gas drier. Pellets of caustic soda are also placed in the bottom of the gas drier to remove any H_2S and SO_2 present. The almost pure, dry, hydrogen leaving the gas drier is returned to the suction side of the pump.

Make-up hydrogen enters the system from a 50 ft^3 gas holder held at a small positive pressure to prevent air leaking into the system, and an arrangement of 1 in. gas taps (see Fig.30) enables either hydrogen or nitrogen, from a 10 ft^3 gas holder, to be circulated or vented to atmosphere.

All temperatures are manually controlled; 2 kW "Variac" autotransformers are used to regulate the power input to the preheater windings, and Sunvic Energy Regulators provide the means of varying the input to the furnaces heating the vertical section of the transport line. The temperature of the solid-gas mixture is measured at the top and bottom of the vertical reaction line by chromel-alumel thermocouples protected from the reducing atmosphere by small diameter, thin walled (0.01 in.), thermocouple wells projecting about 10 in. into the transport line. Temperature

points are also provided at the various positions shown in Figure 30, but these couples are located in short stainless steel wells and errors due to conduction of heat away from the measuring point are introduced; the temperatures indicated by these couples are therefore only used as a guide to assist in the operation of the apparatus. All thermocouples were previously standardized against a sub-standard platinum/platinum-13% rhodium couple, and the indicators are tested by comparing the measured e.m.f. - provided by a Cambridge Workshop potentiometer - required for a given deflection with the standard e.m.f. obtained from Tables. With this arrangement it is considered that the temperatures indicated by the two thermocouples in the vertical reaction line are correct to within $\pm 10^{\circ}C$.

In addition to the pressures measured at the points indicated in Figure 30, the pressure differential between the feed hopper and the flowing gas is also measured. This pressure drop is controlled by means of a needle valve in a line from the hopper to a gas cylinder fitted with a reducing valve.

8.3.3. Experimental Procedure

The experimental procedure is described by the following series of steps:

(i) The hopper above the screw feeder is filled with a sample of the particle size fraction under investigation, and the dust trap and cyclone are carefully cleaned out.

(ii) The furnaces are switched on and the circulating pump is started. With tap A open and tap B closed (see Fig. 30), taps C and D are arranged to vent the gas

leaving the drier to atmosphere; the air is purged from the system by about 8 ft^3 of nitrogen and then tap C is opened and tap D closed to allow nitrogen to circulate around the system.

(iii) When the temperature of the reaction line reaches the set point for the test, tap A is closed and tap B is opened to admit hydrogen to the system. Tap D is opened and, with tap C closed, the nitrogen is purged from the system by venting approximately 10 ft^3 of hydrogen to atmosphere. Tap C is then opened and tap D is closed to allow hydrogen to circulate around the system.

(iv) The temperature of the vertical section of the transport line is stabilized at the required set point for the run. The additional heating winding on the line between the preheater and the reactor is also switched on and the temperature of the hydrogen flow is adjusted to the set point for the run. During this period of temperature stabilization the feed hopper is pressurized with hydrogen from a cylinder to prevent contact between the solids and the hot hydrogen flowing in the system.

(v) The pressure drop across the solids feeder is adjusted to a small positive value - generally about 1 in. of water - and the run is commenced by starting the solids feeder. A stopclock is started at the same time.

(vi) The flow of solids through the reactor is continued for two to three minutes. During this period the pressure drop across the solids feeder is manually controlled at a constant value to ensure that the solids flow rate is constant.

(vii) The solids feeder and the stopclock are switched off, and the hydrogen is purged from the system by nitrogen. The furnaces and heating windings are switched off and the system is allowed to cool in an atmosphere of nitrogen.

(viii) When the temperature has fallen to about 400°C the circulating pump is stopped and the reduced sample is removed from the dust trap and cyclone. This material is stored in a nitrogen atmosphere and weighed when it reaches room temperature. The system may then be heated up for the next run.

(ix) The reduced material is carefully sampled and a 1 g. sample is analysed for acetate-soluble lead, metallic lead, and total lead contents by the methods described in Appendix I.2.

(x) The per cent reduction of the sample is estimated from the chemical composition of the reduced sample. The initial compositions of the material used in the experimental work are reported in Table 5, Section 5.2.3, and the per cent reduction is calculated from these data by the method set out in Section 6.5.2;

however, the loss in weight of the particles is not considered in this calculation.

8.4 Results

The results obtained in the transport reactor are presented in Table 18, which shows the degree of reduction which occurs when particle size fractions varying from -52 +72 # to -200 +325 # (B.S.S.) are transported through a heated reaction zone by hydrogen. The reduction temperatures investigated were 700°C, 800°C and 900°C. The per cent reductions were calculated from the oxidized lead content of the solids by the method described in Section 6.5.2, and the initial compositions of the various size fractions are listed in Table 5, Section 5.2.3.

In the present case the loss in weight of the particles is not readily measured, and the calculated per cent reductions are inaccurate due to

(i) removal of oxygen,

(ii) liquation of metallic lead from the particles, and

(iii) vapourization losses.

However, the particle residence time in the heated section is short and it is considered that vapourization losses and loss of metallic lead from the particles will not be very significant; consequently, it is claimed that the per cent reductions reported in Table 18 are sufficiently accurate to permit generalized conclusions to be drawn.

TABLE 18

SUMMARY OF THE EXPERIMENTAL DATA OBTAINED IN THE TRANSPORT REACTOR

Size fraction (B.S.S.)	Reduction temperature (°C)	Hydrogen flow rate (l. s.t.p./ min.)	Solids flow rate (g./min.)	Per Cent reduction (Oxidized lead)
-100 +150		87	20.0	18.1
-100 +150		130	30.5	14.3
-100 +150	700 ± 15	130	31.5	25.0
-100 +150		130	35.0	11.6
-100 +150		163	29.0	13.5
-100 +150		130	17.3	48.0
-100 +150		130	18.0	46.7
-100 +150		130	21.5	38.3
-100 +150	800 ± 15	163	18.0	42.2
-52 +72		175	22.5	28.2
-72 +100		175	23.3	48.0
-200 +325		130	3.5	82.3
-100 +150	900 ± 20	153	20.0	83.6
-200 +325		130	2.0	91.5

8.5 Discussion of Results

8.5.1 Experimental Data

The limited data obtained in the transport reactor are only intended to provide a basis for assessing the feasibility of

reducing lead sinter in a vertical flow reactor. Consequently, the per cent reduction is measured by the simple, but inaccurate, method of chemical analysis of the reduced material, and the results presented in Table 18 are only discussed in general terms.

At 700°C, the average per cent reduction of -100 +150# (B.S.S.) material is 16.5 for a range of gas and solids flow rates. However, at 800°C the average reduction of the same material is 43.8 per cent, and the single result at 900°C indicates approximately 80 per cent reduction. Also, at 700°C the measured per cent reduction per pass is increased from 28.2 to 82.3 per cent by decreasing the particle size from -52 +72# to -200 +325# (B.S.S.). Therefore, the degree of reduction per pass, or reaction rate, is markedly influenced by temperature and particle size. A similar conclusion applies to the fixed and fluidized bed data. However, the results summarized in Table 18 are not comparable with fixed and fluidized bed data for the following reasons:

(i) the magnitude of the gas velocity relative to the solids is unknown,

(ii) the average particle residence time is altered by system conditions such as gas flow, solids flow, particle size, and degree of reduction, and

(iii) the flow of gas and solids is co-current, and the reaction may be retarded by the presence of water vapour.

Nevertheless, it is apparent that the reaction rate is faster in the transport reactor than in the other systems. In fact, the process is

very attractive kinetically for certain system conditions, e.g., -200 +325 # (B.S.S.) particles reduced at 800°C.

8.5.2 General Operation of the Transport Reactor

Technologically, the tendency for the sinter particles to adhere to the reactor walls is the most significant feature of the operation of the transport line. This effect is aggravated by temperature and the degree of reduction, and the reactor eventually blocks.

Now, iron oxides are observed to become "sticky" during reduction [17] (1960), and lead oxide and lead silicate, which have relatively low melting points, soften at approximately 600°C. The tendency for particles containing lead oxide and iron oxides to stick to the reactor walls is therefore difficult to avoid. However, the build-up of material in the transport line may be prevented by the use of small particles of pure lead oxide; these particles would still stick to the walls but continued reaction would convert any particles adhering to the reactor walls entirely to liquid metallic lead, which would then collect at the bottom of the reactor.

The general design of the transport system is satisfactory, but the operation of the apparatus may be improved by

(i) altering the position of the screw feeder so that the solids are dropped into the bottom of the vertical transport line,

(ii) including an expansion loop at the top of the reactor, and

(iii) providing a better method of reactor temperature control.

8.6 Conclusions

(1) Kinetically, the transport reactor is suitable for the reduction of finely divided lead sinter to metallic lead; at 800°C the oxidized lead content of -200 +325 # (B.S.S.) sinter is approximately 80 per cent reduced in a single pass through the apparatus.

(2) Practically, the reduction of a "sticky" material such as lead sinter presents operating difficulties; the particles build up on the reactor walls and eventually block the line. However, the apparatus may be suitable for the reduction of pure lead oxide.

9. SUMMARY AND CONCLUSIONS

As mentioned in Section 1 this thesis deals with one aspect of an investigation into the possibility of producing metallic lead by the reduction of lead oxide in fluidized systems. This reduction constitutes the second step in a proposed two-stage process in which finely divided galena flotation concentrates are first oxidized to lead oxide and then reduced to metallic lead. In the present case the reaction chosen for study was the hydrogen reduction of a typical lead sinter containing 41.7 mass per cent lead.

A literature survey revealed that there was no published information relating to the reduction of lead sinters by hydrogen although several of the possible reactions, notably the reduction of various iron oxides, have recently been subjected to intensive investigation.

Lead sinter is a heterogeneous substance with a complex physical and chemical structure, and the equilibrium conditions for the reactions which occur during reduction by hydrogen can not be definitely specified. However, a thermodynamic analysis of a suggested sequence of reactions, based on the available information relating to the composition of lead sinters, indicates that the reduction of most of the probable oxidized compounds present, viz., lead oxide, lead silicate, calcium sulphate, ferric oxide and zinc oxide, can proceed almost to completion even at high water vapour pressures. Consequently, although the reduction of Fe_3O_4 and FeO may only occur at relatively low H_2O/H_2 ratios, it is considered that the various reactions will not be influenced by equilibrium considerations under normal conditions.

An analytical technique was developed which enabled the total lead content of a sample to be separated into the constituent lead compounds. The lead present as lead oxide, lead sulphate, and lead silicate, is determined by an ammonium acetate extraction, the residual solids are treated with silver nitrate to extract the metallic lead, and, finally, the lead sulphide is determined by extraction with a ferric chloride-sodium chloride solution.

The overall reaction rate may be used to represent the rate of reduction of the lead compounds without serious error. Up to 70 per cent reduction the overall reaction rate is approximately equal to the rate of reduction of the oxidized lead compounds to metallic lead. Beyond this point the overall reduction still indicates the degree of oxygen removal from the lead compounds but the reduction of compounds such as $PbSO_4$ contribute to the overall reaction rate without increasing the amount of metallic lead formed.

The rate of reduction of a lead sinter by hydrogen was studied in a differential fixed bed, in a fluidized bed, and in a small transport line. Size fractions varying from -25 +36 # to -200 +325 # (B.S.S.) were reduced at temperatures in the range 500°C to 900°C and the following conclusions were reached.

(1) For equivalent system conditions the overall reaction rate is faster in a fluidized bed than in a fixed bed. This difference is essentially due to the more efficient gas-solid contact in the fluidized bed and results from the intense particle agitation and circulation associated with the high gas velocities used in the fluid bed; these high gas velocities also tend to prevent sticking

of the sinter.

(2) The reaction rate is increased by increasing the temperature and decreasing the particle size. The temperature dependence of the reaction rate is similar in the fixed and fluidized beds, e.g., at 40 per cent reduction the reaction rate is proportional to $T^{12.3}$ in a fixed bed and to $T^{15.4}$ in a fluidized bed. Also, the effect of particle size is more marked in the fluidized beds than in the fixed beds.

(3) The reaction rate is faster in fluidized beds than in fixed beds, but the nature of the material limits the usefulness of the fluidization technique. Lead sinter, which contains lead oxide, lead silicates, and iron oxides, becomes sticky during reduction at temperatures of 600°C and above. Therefore, high velocities are required to keep the bed fluidized and elutriation of particles from the bed precludes the use of material finer than 100# (B.S.S.) at temperatures above 600°C. In addition, liquation of metallic lead from the particles tends to restrict the flow of fluidizing air. Because of these limitations the reaction rates obtained in the fluidizer are not sufficiently fast to be of practical interest.

(4) The limited experimental data obtained in a small transport apparatus indicate that extremely fast reaction rates may be obtained with small particle sizes; at 800°C the oxidized lead content of -200 +325# (B.S.S.) sinter was approximately 80 per cent reduced in a single pass through a 1 in. dia. tube, 11 ft. long. However, the particles still tended to stick to the reactor walls and eventually blocked the apparatus. Therefore, although this effect

may be less serious in a larger apparatus, the utility of this technique and the feasibility of the proposed process appear to depend on

(a) the possibility that the "sticking" problems will not be serious with almost pure lead oxide which is reduced to metallic lead, and

(b) the use of an additive to overcome the tendency for the particles to stick to each other and to the walls of the reactor.

APPENDIX I

Analytical Methods

APPENDIX I

I.1 Development of the Analytical Technique for the Determination of Individual Lead Compounds

The review of the various methods used to determine specific lead compounds in materials containing lead oxide, lead silicate, lead sulphate, lead sulphide and metallic lead (see Section 3.3) reveals that the most serious divergence of opinion between the various investigators relates to the solubility of metallic lead and lead silicate in ammonium acetate.

A series of tests using this reagent as a solvent were performed on samples of lead oxide, lead sulphate, lead sulphide and metallic lead. These compounds were attacked individually and in mixtures of known composition. An artificial lead silicate was not included since it was considered very unlikely that a compound prepared by the fusion of silica and lead oxide would simulate the behaviour of the complex silicates present in a lead sinter. The results obtained from these tests showed that ammonium acetate was a specific solvent for lead oxide and lead sulphate in the presence of lead sulphide and metallic lead. This conclusion applied to pure compounds only, and, in addition, the solubility of lead silicate in ammonium acetate remained debatable.

The normal method used to estimate the lead sulphide, viz., the use of ferric chloride dissolved in a saturated solution of sodium chloride as a specific solvent, is accepted by both Read [36] and Oldright and Miller [34] (1929) as satisfactory; consequently, the selectivity of this solvent was not investigated. The method

employed by Collee [32] (1956) to estimate the lead sulphide involved oxidation with hydrogen peroxide followed by extraction of the resulting lead sulphate with ammonium acetate. The doubtful issue in the use of this reaction is the effect of the peroxide on the metallic lead present. The contention that the metal is completely and rapidly oxidized to the peroxide, which is then inert to ammonium acetate, was not confirmed experimentally; the white solid resulting from the oxidation of metallic lead by hydrogen peroxide was found to contain a considerable quantity of acetate-soluble lead.

The remaining reaction of interest to the present investigation is the estimation of the metallic lead by solution in silver nitrate. Experimental results obtained by McIntosh [37] (1927) indicate that the amount of lead sulphide dissolved is relatively small ($< 5\%$ of the total lead sulphide) provided the contact time is no longer than two hours. In the present case this solubility is insignificant since the lead present as sulphide is small.

A consideration of the above data suggests that an assay method which meets the requirements of the present investigation may be based on the following sequence of operations

(i) extraction with hot ammonium acetate to give the lead present as oxide, silicate and sulphate,

(ii) extraction with silver nitrate to obtain the lead present as metallic lead, and

(iii) an attack on the residual solids with chloride reagent to dissolve the lead present as lead sulphide.

However, this procedure is based on tests carried out using pure

materials and the selectivity of the various reagents may be altered by the presence of other compounds as well as by impurities in the lead compounds. Further, the solubility of lead silicate in ammonium acetate was not established experimentally.

In an attempt to clarify these points the suggested procedure was used to analyse samples of lead sinter varying in composition from unreduced material containing approximately 37% lead as lead oxide, lead silicate and lead sulphate to almost completely reduced samples containing 35% lead as metallic lead. These samples were prepared in an apparatus essentially similar to that used by Ward [91] (1960) to measure the reducibility of various lead sinters. A weighed amount of sinter held in silica boats is reduced by hydrogen at various, controlled, temperatures and the approximate degree of reduction is measured by collecting the water formed. After the desired reduction the sample is cooled in a stream of nitrogen and removed from the reactor. The weight change is measured and then the sample is analysed by the method set out above. The results of these tests, which were carried out on -25 +36 # material, are reported in Table 19 as mass percentages of the various lead compounds.

TABLE 19

COMPOSITION OF SAMPLES OF LEAD SINTER

Temperature (°C)	Reduction time (min.)	Acetate-soluble lead	$AgNO_3$ soluble lead	$FeCl_3$-NaCl soluble lead	Total
500	10	36.0	1.9	2.9	40.8
	70	26.9	9.3	3.1	39.3
	120	23.3	13.9	3.4	40.6
	210	21.9	16.5	3.0	41.4
600	5	32.9	5.0	3.0	40.9
	30	22.1	15.3	3.0	40.4
	90	16.5	20.8	3.5	40.8
	240	8.6	28.8	3.4	40.8
	330	5.5	32.6	3.0	41.1
700	2	31.5	4.4	4.3	40.2
	10	18.7	17.3	5.6	41.6
	25	12.1	25.5	3.5	41.1
	80	4.5	31.2	5.3	41.0
	330	1.9	35.9	3.1	40.9
800	5	22.6	13.7	3.9	40.2
	15	6.0	29.4	4.9	40.3
	90	3.1	35.0	2.7	40.8

A consideration of the values given in Table 19 suggests that the analytical procedure is satisfactory; the amount of acetate-soluble lead in the samples decreases as the reduction time increases and the metallic lead content shows a corresponding increase. In particular, in the highly reduced samples which contain a large amount of metallic lead, the acetate-soluble lead reported in only of the order of 2 per cent despite prolonged attack with boiling ammonium acetate. Consequently, it may be concluded that metallic lead is almost insoluble in ammonium acetate.

The other contentious point in the suggested procedure relates to the solubility of lead silicate in ammonium acetate. The assay figures for the unreduced samples, which are reported in Table 5, Section 5.2.3, show that approximately 90% of the total lead content is soluble in ammonium acetate. Also, the total of the lead reported as acetate-soluble lead, silver nitrate soluble lead, and chloride-soluble lead, is almost the same as the total lead determined by direct analysis. Therefore, either the lead silicate content of the sinter is small or this compound is almost completely soluble in ammonium acetate. Consequently, it is claimed that any lead silicate in the sinter may be considered as soluble in ammonium acetate.

The procedure outlined above is therefore considered a satisfactory method to use in the present investigation and the final experimental technique is described in detail in the next Section.

I.2 The Method of Chemical Analysis

I.2.1 Sample Preparation

In order to obtain an accurate value for the chemical composition of a sample of partially reduced sinter it is essential to ensure that a representative sample is selected. With relatively large particle sizes this means that the sample must be ground, preferably to -100# B.S.S. However, this is difficult with samples containing both lead oxide and metallic lead; the metallic lead tends to smear and spread over the particles and this may prevent extraction from the interior of the particle during the ammonium acetate leaching. Also, the analysis of various size fractions used in this investigation (see Table 5) reveals that after crushing the lead content of the material varies from size fraction to size fraction. Consequently, it is not desirable to screen the sample after crushing. Therefore, in general, a large sample weight (approximately 1 g.) is used. This is crushed in an agate pestle and mortar and all the crushed material is reweighed and subjected to chemical analysis. The crushing operation is performed under a nitrogen atmosphere in a dry box to minimise the oxidation of metallic lead during grinding.

I.2.2 Reagents

(a) Ammonium acetate

1000 ml. of glacial acetic acid are just neutralized with a strong solution of ammonia, using litmus as the indicator, and the resulting solution is diluted with 500 ml. of distilled water to give an approximately 50% by weight solution of ammonium acetate.

(b) Silver nitrate

100 g. of A.R. grade silver nitrate are dissolved in 900 ml.

of distilled water to give a 10% by weight solution of silver nitrate.

(c) Ferric chloride-sodium chloride

100 ml. of distilled water are saturated with A.R. grade sodium chloride and 60 g. of A.R. grade ferric chloride is added to give an approximately 6% solution of ferric chloride in sodium chloride.

(d) Ammonium molybdate

4.3 g. of ammonium molybdate are dissolved in 1000 ml. of distilled water. The solution is standardized against a known weight of pure lead foil. 0.2 g. of pure lead are dissolved in 10 ml. of concentrated sulphuric acid in a 250 ml. flask. The solution of lead sulphate is then cooled and diluted to 200 ml. with distilled water to precipitate the lead sulphate. After this the procedure described in I.2.6 is followed.

(e) Tannin indicator

0.1 g. of tannic acid is dissolved in 20 ml. of distilled water; this solution is freshly prepared before each batch of titrations.

I.2.3 Assay Method for Individual Lead Compounds

Step (a)

A 1 g. sample of ground material is placed in a 500 ml. flat-bottomed flask together with 150 ml. of ammonium acetate solution and boiled for four hours; the vapour leaving the flask is condensed with a Liebig condenser and returned to the flask. After four hours boiling the beaker is removed from the hot plate and the solution

immediately filtered. The residual solids are washed with hot distilled water, returned to the flask, and subjected to a further attack by ammonium acetate; this procedure is repeated until the filtrate contains no traces of lead. In general, boiling for six hours is sufficient to remove all the acetate-soluble lead. The filtrates are combined and evaporated almost to dryness and allowed to cool. The volume is made up to 200 ml. with distilled water and the lead present in this solution is precipitated with 20 ml. of concentrated sulphuric acid. The lead content is then determined gravimetrically if the acetate-soluble lead content is less than 10% of the original sample; if it is greater than 10% the volumetric molybdate method may be used. These methods are described in Appendices I.2.5 and I.2.6. The acetate-soluble lead is reported as lead present as lead oxide, lead silicate, and lead sulphate.

Step (b)

The residue from the acetate extraction is shaken with 30 ml. of 10% silver nitrate solution and allowed to stand, with intermittent shaking, for two hours. The resulting solution is filtered and the residual solids are carefully washed with hot distilled water. The filtrate is fumed with 20 ml. of concentrated sulphuric acid, and, after cooling to room temperature, the resulting liquid is diluted to 250 ml. with distilled water. This solution is boiled to aid the precipitation of lead sulphate and then filtered. The precipitate is washed with hot 2% sulphuric acid followed by boiling distilled water until the wash water contains no silver sulphate. The lead content is then determined gravimetrically or volumetrically, and

the silver nitrate-soluble lead is reported as metallic lead.

Step (c)

The residue from the silver nitrate extraction is shaken with 50 ml. of chloride reagent and allowed to stand overnight. The solution is filtered and the residual solids are carefully washed with hot water and then discarded. The filtrate is fumed with 20 ml. of sulphuric acid and then cooled to room temperature. The cold solution is diluted to 250 ml. with distilled water and boiled to dissolve the soluble sulphates. The lead sulphate is separated by filtration and the precipitate is washed with hot 2% sulphuric acid and hot distilled water. The lead content is then determined gravimetrically and reported as lead sulphide.

I.2.4 Analysis for Total Lead

The total lead content of a sample is determined in the normal way by dissolving a 1 g. sample in aqua regia, and fuming the resulting solution with sulphuric acid. The solution is cooled and then diluted with distilled water and the lead sulphate separated by filtration after boiling to dissolve the soluble sulphates. The precipitate is carefully washed with 2% sulphuric acid and hot distilled water, and then dissolved in hot ammonium acetate. The lead content of this solution is determined volumetrically as set out in Appendix I.2.6, and is reported as the total lead content of the sample.

I.2.5 Gravimetric Analysis for Lead

The hot solution containing the precipitated lead sulphate is filtered through a weighed sintered glass crucible. The precipitate

is washed, first with hot water containing 10% of sulphuric acid by volume and then with a 50% ethyl alcohol solution. The crucible is dried for 2 hours at 550°C and weighed. The increase in weight gives the amount of lead sulphate precipitated and the lead content of the sample may be calculated from this value.

I.2.6 Volumetric Analysis for Lead

The hot solution containing the precipitated lead sulphate is filtered through a No.42 Whatman filter and washed with 5% sulphuric acid. The precipitate and the filter paper are placed in a 400 ml. conical flask with 30 g. of A.R. grade ammonium acetate and 350 ml. of distilled water. The filter is disintegrated and the solution is boiled gently for 15 minutes. The solution is acidified with 5 ml. of glacial acetic acid and titrated hot with a standard ammonium molybdate solution. Tannic acid is used as an external indicator, the indicator on a spot tile turning yellow on contact with a drop of solution containing ammonium molybdate. A standard colour and intensity must be chosen to give a fixed end point. The lead content of the solution may be calculated from the titre and the equivalent value of the standardized ammonium molybdate in terms of g. of lead per ml. of reagent.

APPENDIX II

Description of the Fixed-Bed Apparatus

APPENDIX II

A line diagram of the apparatus used for studying the reaction in a differential, fixed, bed is shown in Figure 1. The components of this apparatus are as follows:-

V_1, V_2 Two Edwards, high vacuum, needle valves controlling the nitrogen and hydrogen flow rates respectively.

O_1, O_2 Two beds of copper turnings, held at 500°C, to remove the oxygen from the inlet gases. In the nitrogen de-oxidizing furnace, O_1, the oxygen is fixed as copper oxide and the bed is regenerated with hydrogen at regular intervals. The hydrogen de-oxidizing furnace, O_2, converts the oxygen to water vapour and does not require regeneration. The bed of copper turnings in the nitrogen line is contained in a silica tube, 1¼ in. internal diameter x 12 in. long, and a length of bare silica tubing, 6 in. long x ¼ in. internal diameter, is attached to each end so that the de-oxidizing reactor may be connected to the rest of the apparatus by plastic tubing. The de-oxidizing bed of copper turnings in the hydrogen flow is contained in a copper tube, 1¼ in. internal diameter x 12 in. long, and the inlet and outlet copper tubes are water cooled. On the inlet side towns water passes through two turns of ¼ in. internal diameter copper tube soldered to the hydrogen line, and on the outlet side the gas stream is cooled by a spiral condenser. The beds of copper turnings are heated by tubular furnaces with a rated

capacity of 1 kW, and the heat input is controlled with 1 kW Sunvic Energy Regulators. The furnace temperatures are measured by chromel-alumel thermocouples connected to millivoltmeters calibrated in degrees Centigrade.

S_1 Two drying towers, 3 in. dia. x 13 in. high, in series containing indicating silica gel.

D_1 A single drying tower, 3 in. dia. x 13 in. high, containing magnesium perchlorate dispersed on glass wool.

S_2 Two drying towers, 3 in. dia. x 13 in. high, in parallel containing indicating silica gel.

M A copper tube, $2\frac{1}{2}$ in. internal diameter x 20 in. long, packed with "molecular sieves" to remove water vapour from the hydrogen.

D_2 Two drying towers, 3 in. dia. x 13 in. high, in parallel containing magnesium perchlorate dispersed on glass wool.

t A mercury-in-glass thermometer measuring the temperature of the hydrogen stream entering the flowrator.

F_1, F_2 Two rotameters measuring the hydrogen and nitrogen flows, respectively. Each flowrator was calibrated with a bucket-type wet test meter.

P A silica preheater, 12 in. long x 20 m.m. internal diameter, packed with silica chips to give good mixing and heat transfer. The gas temperature at the top of the preheater is indicated by a chromel-alumel thermocouple situated in a silica well, and the e.m.f. generated by this couple is measured with a Cambridge Workshop Potentiometer. The

preheater furnace is of the normal tubular construction. The heating element consists of a silica tube, 18 in. long x 1½ in. internal diameter, wound with 26 gauge (B. and S.) nichrome wire encased in alundum cement. This element is supported in a length of 6 in. diameter asbestos tubing packed with vermiculite insulation to give a furnace rated at 1200 watts. The furnace temperature is controlled by a Honeywell-Brown "Pyrovane" temperature controller actuated by a chromel-alumel thermocouple located between the preheater and the furnace wall. The circuit diagram for this control system is shown in Figure 35.

H An auxiliary winding on the silica tubing connecting the preheater and the reactor. The winding consists of a length of nichrome wire, insulated with small ⅛ in. dia. porcelain beads, wrapped around the silica tube, and covered with asbestos string. The temperature of this winding is measured by a chromel-alumel thermocouple connected to a Cambridge temperature indicator and is controlled by a Variac autotransformer.

r A 0.5 cm. construction which prevents hydrogen from diffusing into the reactor during the temperature stabilization period.

R A silica reactor containing a thermal alumina liner 2.5 cm. internal diameter x 6.5 cm. long. The reactor and the preheater are connected by a B19 ground silica joint, the cone being attached to the preheater section but protruding into the reactor furnace. A B19 silica cone and a Pyrex

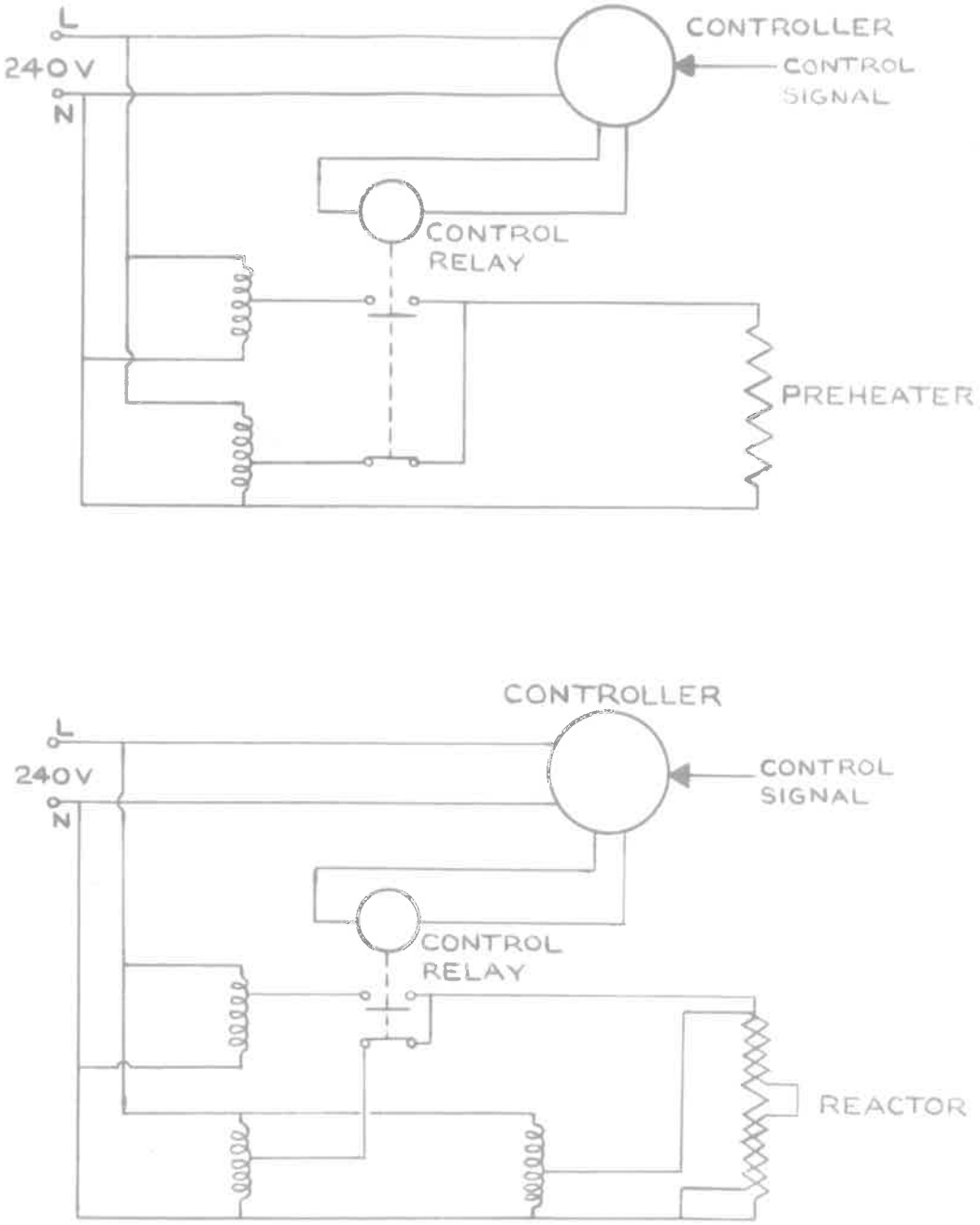

Fig. 35 - Circuit Diagram for Temperature Control of Fixed Bed Apparatus

socket connect the reactor to the distributor Q via another ground glass joint.

The bed temperature is measured by a chromel-alumel thermocouple situated in a silica well, which projects into the body of the reactor, and the e.m.f. generated by this couple is measured with a Cambridge Workshop Potentiometer. Both the preheater and the reactor thermocouples are standardized against a sub-standard Pt : Pt-Rh thermocouple. The reactor furnace contains a 2 in. internal diameter x 12 in. long silica tube around which two windings are wrapped: firstly, a main winding evenly wound along the entire length of the silica tube, and, secondly, a subsidiary winding wrapped for 2 in. along each end of the silica tube. In each case the winding consists of 22 gauge (B. and S.) nichrome wire at a spacing of 8 turns/in., and the subsidiary winding is insulated from the main winding by mica sheet. The input to the main winding is controlled by a Honeywell-Brown "Pyrovane" temperature controller actuated by a chromel-alumel thermocouple located between the reactor and the reactor furnace wall, at the centre of the furnace. The circuit diagram for this control system is shown in Figure 35. The controller actuates a "New-Air" single pole, double throw, switch, which switches the voltage applied to the centre winding from one Variac to another. These Variacs have different settings; the Variac controlling the heating cycle is adjusted to a voltage which slowly raises the

temperature and the setting of the other Variac allows the temperature to fall very slowly. The input to the subsidiary winding is controlled by a Variac autotransformer, and the setting was not altered during the run.

Q A gas distributor constructed from Pyrex glass which enables the reactor exit gas to pass through any one of three outlets via B12 cone and socket joints into the drying tubes B. This distributor is lagged with two heating tapes controlled by a Variac autotransformer to prevent condensation of water vapour.

B Cylindrical drying tubes, $1\frac{3}{8}$ in. internal diameter x 6 in. long, packed with magnesium perchlorate dispersed on glass wool. The tubes are attached to the distributor Q by B12 ground glass joints. The two openings in the tubes are plugged with rubber bungs to prevent water vapour entering the tubes from the atmosphere.

APPENDIX III

Development of the Experimental Technique for the Fluidized Bed Reactor

APPENDIX III

Hamdorf [63] (1956), who used the present system to study the reduction of barytes by hydrogen, points out that the initial control of the bed temperature is very difficult in a system where nitrogen circulated during the heating-up period is replaced by hydrogen at the start of a test. Further, a small, constant, leak rate is essential for accurate measurement of the reaction rate; the rate of hydrogen consumption by reaction is the difference between the measured rate of hydrogen make-up and the rate at which hydrogen escapes from the closed system. Consequently, a preliminary series of runs were carried out to test the apparatus and to develop an operating technique capable of yielding accurate and reproducible rate data; in these tests particular emphasis was placed on the control of the bed temperature and the magnitude and constancy of the leak rate.

None of these data obtained from these initial tests (runs A.1 to A.27) satisfactorily represent the rate of reaction; therefore the actual results are not reported. However, at the completion of these tests it was considered that a satisfactory experimental technique had been developed, and the main experimental work was commenced.

This Appendix describes the development of the final operating procedure; firstly, the methods used to control the bed temperature are considered, secondly, the elimination of variations in the hydrogen leak rate are discussed, and, finally, a method of calibrating the gasmeter is presented.

III.1 Control of the Bed Temperature

The difficulty experienced in controlling the bed temperature results from the design of the fluidizing apparatus in which the preheater and reactor are combined; consequently, the temperature of the preheater can not be stabilized at the chosen set point with hydrogen flowing through it.

The initial procedure adopted at the start of a test was as follows: prior to beginning a run the bed temperature was controlled at the set point for the experiment with nitrogen circulating in the system; the test was then started by replacing the nitrogen with hydrogen. Experience showed that this procedure resulted in a sudden initial rise in bed temperature followed by an equally rapid decrease which continued until the temperature reached equilibrium below the original set point; both these effects were of the order of 20°C, and increasing the heat input had little immediate effect on the final downward trend. These fluctuations were of a transient nature - the upward surge lasting for about two minutes - and manual control of the bed temperature proved very efficient after the heat transfer rates reached equilibrium. Nevertheless, since the initial results suggested that approximately 50 per cent of the total reduction occurred during the first ten minutes, it was essential to have close control of the bed temperature during the initial period.

Before attempting to decrease the magnitude of the bed temperature fluctuations it was desirable to understand the causes underlying these variations, and the following hypothesis may explain the observed behaviour: because of the superior heat transfer properties of hydrogen the rate of heat transfer from the reactor

walls is potentially greater for hydrogen than for nitrogen. However, the amount of heat transferred is limited by the availability of heat at the wall surface. Calculations based on the assumption of a constant rate of heat transfer to the reactor walls show that a quantity of heat sufficient to cause the hydrogen temperature at the top of the preheater to be 20°C higher than the steady value for nitrogen flow may be extracted from the reactor walls. Immediately this heat reservoir is depleted the gas temperature falls because the effect of the decrease in mass flow is outweighed - in determining the gas temperature at the top of the preheater - by the relatively high heat capacity of hydrogen compared to nitrogen. The result of these two facts is that the bed temperature, after an initial upward surge, falls rapidly to a constant value considerably below the set point for the run.

On the basis of this hypothesis a technique was devised and perfected during the initial tests which enabled the bed temperature to be controlled within ± 5°C of the desired set point. Before admitting hydrogen to the system the heat input to the furnaces was switched off for a short period so that heat was transferred away from the reactor walls; then, immediately before replacing the nitrogen with hydrogen, the energy input was raised beyond the original value to a setting dictated by experience and depending on the gas flow rate. Using this procedure the temperature fluctuations were consistently limited to ± 5°C, and this was considered satisfactory for a pilot-scale apparatus of this nature.

III.2 Elimination of Variations in the Hydrogen Leak Rate

Although runs A.1 to A.12 were primarily concerned with the bed temperature control, an examination of the limited rate data obtained from these tests revealed that the rate measurements were grossly inaccurate; the calculated amount of water formed at the completion of the reaction was only 60 per cent of the value obtained from the fixed-bed tests. This discrepancy could have resulted from

(i) errors in the measurement of the water formed during the initial exhaust period, and

(ii) an increase in the rate at which hydrogen escapes from the system during the reaction.

The second possibility appears more likely since reproducible results are obtained for the weight of water formed during the exhaust period.

The initial construction of the apparatus in which the gas distribution plate was an integral part of the reactor made it very difficult to clean the perforated plate between runs. In later runs the grid was welded to the bottom of a removable liner, which was flanged at the top; the reaction mass was, in effect, supported in a basket hanging in the reactor and the grid was readily accessible for cleaning. This modification improved the design of the apparatus but did not improve the accuracy of the results. However, during runs A.13 to A.16 it was observed that both the pump pressure and the pressure drop across the bed increased during the reaction. Accordingly, the leak rate was measured at varying pump pressures with hydrogen circulating through the empty reactor under normal test conditions. These tests revealed that the magnitude of the leak rate was influenced by the pump pressure. Runs A.17 to A.25, which were carried out with

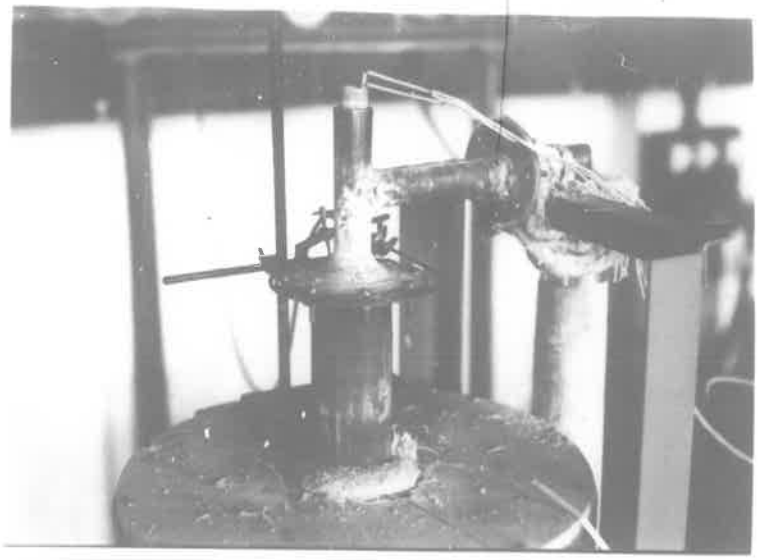

Fig. 36 - Photograph of Initial Method of Cooling the Gasket at the Top of the Fluid Bed Reactor

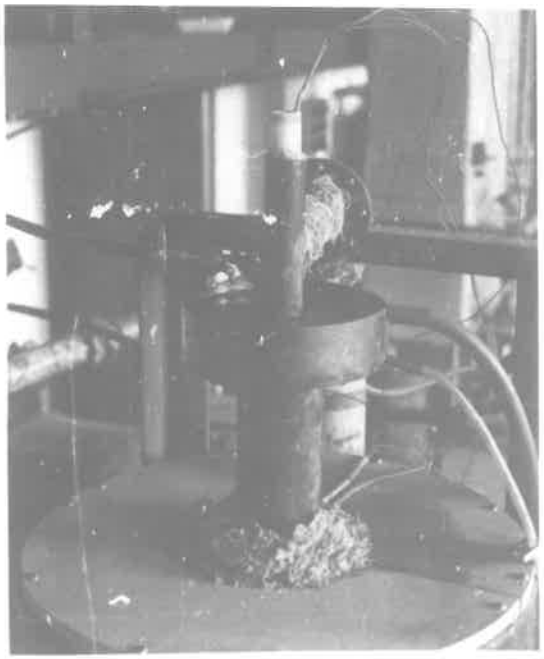

Fig. 37 - Photograph of Final Method of Cooling the Gasket at the Top of the Fluid Bed Reactor

the pump pressure controlled at a constant value by means of a needle valve placed in the inlet gas line to the reactor, showed a slight increase in accuracy; however, the calculated amount of water formed was still considerably less than the value obtained in the fixed-bed apparatus. Also, the pressure drop across the bed still increased as the reaction proceeded. There was some evidence of resintering in the reduced beds, but it was concluded that the increase in pressure drop was due to the accumulation of metallic lead on the baffle plate located $\frac{1}{4}$ in. below the gas distribution grid. The removal of this plate resulted in a remarkable increase in the accuracy of the data; for runs A.27 and A.28 the calculated water formed was very close to the maximum water formed in the fixed-bed tests. The rate at which hydrogen escaped from the system was also much slower, and it was apparent that the main cause of the earlier experimental errors had been eliminated.

Hamdorf [63] (1956) has also shown that the asbestos gasket in the flanged joint at the top of the reactor breaks down on heating, and this causes the rate of hydrogen leakage from this flange to vary during the test. In an attempt to minimise this effect the gasket was cooled with the water spray shown in Figure 36. This arrangement was not very satisfactory and it was replaced by the set-up shown in Figure 37.

III.3 Elimination of Errors in the Measurement of the Rate of Hydrogen Consumption

The experimental technique developed during tests A.1 to A.28 enabled the bed temperature to be controlled within $\pm$ 5°C, and

in the final tests the calculated amount of water formed agreed with the amount obtained in the fixed-bed apparatus. However, an examination of these results revealed that there were marked deviations from the smooth rate v. time curve drawn through the majority of the points; these deviations were systematically related to the position of the gas-meter pointer, and the effect was particularly noticeable during the measurement of the final steady rate of hydrogen consumption. Consequently, it was necessary to calibrate the gas-meter on the basis of the pointer position and this was carried out as follows: the reduced sinters from runs A.27 and A.28 were fluidized with hydrogen at 450°C and the time for the gas-meter pointer to traverse each volume increment was noted. For each test the true leak rate was taken as the average of at least sixteen individual determinations, i.e., two complete revolutions of the pointer, and the deviations from this mean rate were obtained for each volume increment. The gas-meter calibration given in Table 20 was then prepared by averaging the per cent deviation (deviation from the average leak rate/average leak rate) for a number of tests; these corrections were applied to all subsequent results.

TABLE 20

CALIBRATION OF GAS-METER

Scale reading	1	¼	½	¾	2	¼	½	¾	1
Per cent correction	-5.35	+0.6	-	+1.64	+0.4	-2.1	+4.2	+0.35	

APPENDIX IV

The Fluidization Characteristics of Crushed Lead Sinter

APPENDIX IV

IV.1 Experimental Results

The minimum gas flow required to initiate fluidization, V_{mf}, in beds of crushed lead sinter was determined by the method proposed by Leva [64] (1957) and van Heerden et al. [52] (1952). In this approach V_{mf} is defined arbitrarily as the gas flow at which the pressure drop across the bed - measured at maximum bed porosity - is equal to the weight of the bed per unit cross-sectional area. Pressure drops at maximum bed porosity are obtained by starting with a fluidized bed and gradually decreasing the gas flow through the point of minimum fluidization. The value for the pressure drop across the bed was taken as the difference between the pressure drop across the loaded reactor and the pressure drop through the empty reactor. Using this procedure, values of V_{mf} were obtained for varying particle sizes using both nitrogen and hydrogen as the fluidizing gas. The results of these tests are summarized in Table 21, where the experimental values are compared with the theoretical values calculated from the equations suggested by van Heerden et al.[52] (1952) and Leva [64] (1957). Each correlation was derived from data obtained at room temperature, and, consequently, V_{mf} was determined for several samples at 200°C and 400°C to check the validity of the equations at elevated temperatures.

In Figure 38 the experimental data showing the variation in V_{mf} with change in particle size are compared with the predicted values. An examination of this Figure shows that the theoretical values obtained from both equations agree quite satisfactorily with

the experimentally determined values of V_{mf}. However, the equation derived by Leva [64] (1957) is simpler than the correlation suggested by van Heerden et al. [52] (1952), which was developed specifically for mixtures of particle sizes; consequently, the equation presented by Leva was used to calculate the minimum fluidizing velocity for the various conditions encountered during the experimental work.

The fluidization of beds of crushed sinter by hydrogen and nitrogen was studied visually in a perspex model of the stainless steel reactor. The relatively closely sized particles used in the experimental work fluidized very poorly. Little circulation was observed until the gas flow exceeded 2 V_{mf}, and at 3 V_{mf} there was a tendency for slugging to occur; this effect became more severe as the flow rate was increased. At gas flow rates approaching 10 V_{mf} the bed was not clearly defined and "spouts" of solids continually left the upper surface of the bed and then fell back into the main bulk of the solids. At this stage the solids were very violently agitated and circulation was good; however, the quality of fluidization was poor and the bed was not fluidized in the true sense. At these high velocities there appeared to be very little elutriation of small particles from the bed of solids.

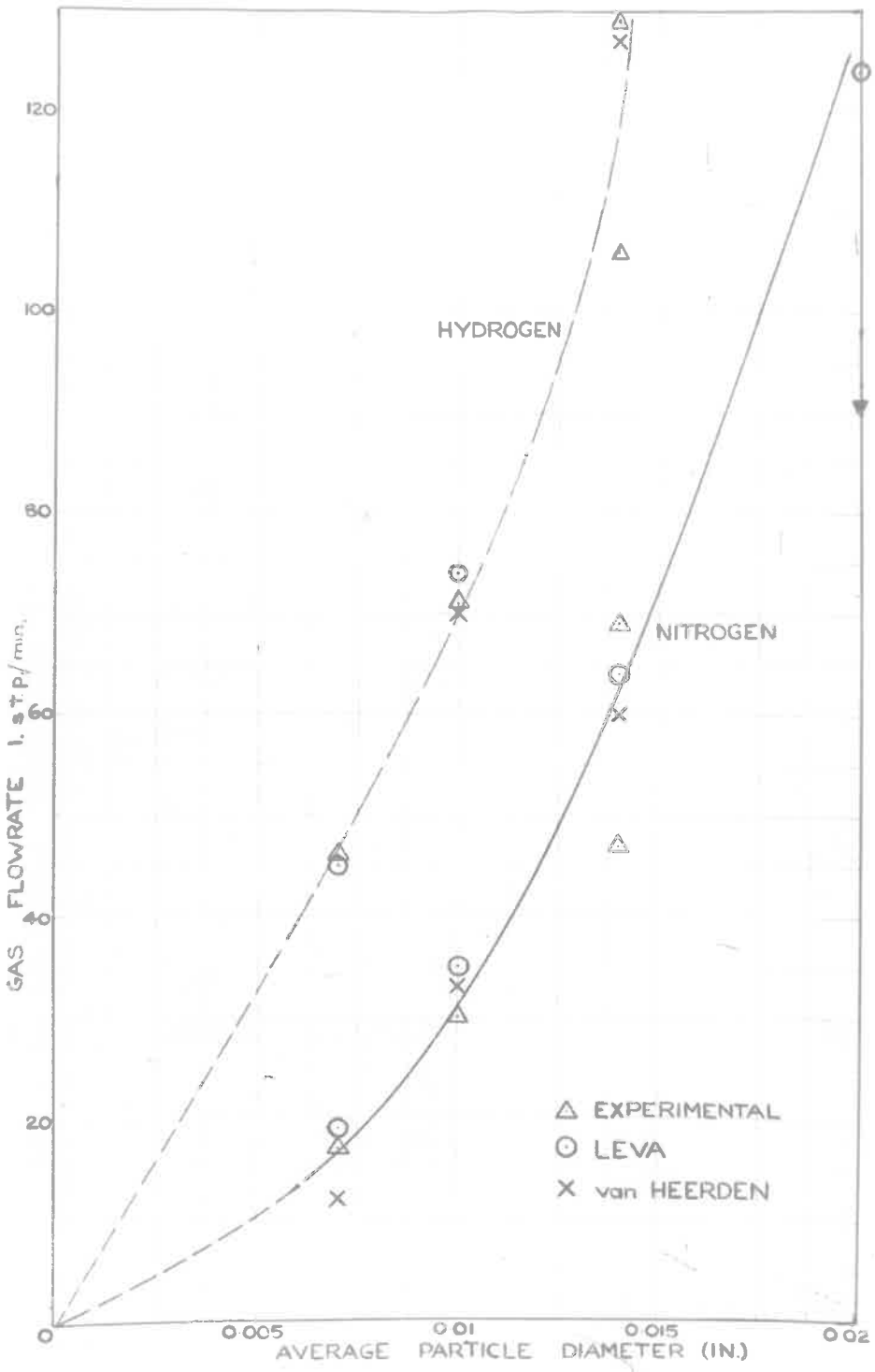

Fig. 38 - Comparison of experimental and predicted values of the Minimum Fluidizing Velocity for various particle sizes.

TABLE 21

EXPERIMENTAL AND THEORETICAL VALUES OF THE GAS FLOW AT INCIPIENT FLUIDIZATION FOR BEDS OF CRUSHED LEAD SINTER

Size fraction (B.S.S.)	Average diameter (in.)	Gas flow at minimum fluidization l. s.t.p./min.			Conditions
		Experimental	Van Heerden	Leva	
-25 +36	0.02	-	131.0	124.0	
-36 +52	0.014	47.0	60.0	64.0	
		69.5			Nitrogen at
-52 +72	0.01	30.0	33.0	34.8	20°C
		34.0			
-72 +100	0.007	20.0	25.4	19.5	
		17.0			
-25 +36	0.02	-	290.0	264.0	
-36 +52	0.014	106.0	127.0	136.0	
		87.0			Hydrogen at
		129.0			20°C
-52 +72	0.01	71.0	70.5	74.0	
-72 +100	0.007	45.0	50.5	44.4	
-36 +52	0.014	28.0	24.0	34.0	N_2 at 200°C
		19.0	13.0	16.7	N_2 at 400°C
		54.0	53.5	65.2	H_2 at 200°C

IV.2 Type Calculations of the Estimation of the Minimum Fluidizing Velocity

(a) The method of van Heerden et al.[52] (1952)

The equation suggested by these workers is

$$G_{mf} = 0.00123 \cdot \rho_g \cdot \rho_{bm} \cdot g_c \cdot d_e^2 / \mu_g \cdot Be. \quad \text{----------(35)}$$

where

G_{mf} = mass velocity at point of minimum fluidization [kg/(m^2)(sec)]

ρ_g = gas density (kg/m^3),

ρ_{bm} = bed density at maximum porosity (kg/m^3),

g_c = gravitational constant (m/sec^2),

d_e = effective particle diameter (m),

u_g = gas viscosity [kg/(m),(sec)], and

Be = shape factor (dimensionless).

The bulk density at maximum porosity, ρ_{bm}, is determined experimentally by measuring the volume occupied by a known weight of solid which has been gradually brought to rest from the fluidized state. In this case the average of three determinations of ρ_{bm} for -72 +100# (B.S.S.) particles is 2400 kg/m^3.

The effective particle diameter, d_e, is defined as "the diameter of the sphere giving the same number of particles per unit volume of packed bed, both counted at maximum porosity". The value of d_e is calculated as follows: assume that the maximum porosity of a bed of spheres is 0.406 [52,92] (1952) and (1949), then the volume of the spheres is 0.594 per unit bed volume. If the bed is assumed

to contain $(n_m)_s$ spheres of diameter d_e, then it follows that

$$\text{volume of spheres in the bed} = \frac{4}{3}\pi (d_{e/2})^3 . (n_m)_s$$

and

$$(n_m)_s = 1.134/d_e^3$$

Now, by definition,

$$(n_m)_s = (n_m)$$

where

(n_m) = number of particles per unit volume of bed at maximum porosity.

Hence it follows that

$$d_e = 1.043/(n_m)^{\frac{1}{3}}$$

Experimentally it is found that 0.0626 g. of -72 +100 # (B.S.S.) sinter contain 1087 particles.

Therefore,

$$n_m = 2400 \cdot 1087/0.0626 \text{ particles/g.}$$
$$= 4.16 \times 10^{10} \text{ particles/kg}$$

and

$$d_e = 1.043/(41.6 \times 10^9)^{\frac{1}{3}}$$
$$= 3 \times 10^{-4} \text{ m.}$$

In the present case the particles are irregular and tend to be flat; the material therefore deviates markedly from a spherical shape and the shape factor has been taken as 1.6 (see Section 3.4.4.2).

For nitrogen flow at 20°C

$g_c = 9.8 \text{ m/sec}^2$,

$\mu_g = 1.75 \times 10^{-5}$ kg/(m), (sec), and

$\rho_g = 1.25 \text{ kg/m}^3$

Substituting these values in equation (35) gives

$$G_{mf} = 0.0116 \text{ kg/(m}^2\text{),(sec).}$$

Hence, in a 3 in. diameter tube

$$V_{mf} = 25.3 \text{ l. s.t.p./min.}$$

(b) The method of Leva [64] (1957)

Leva suggests the use of the following equation

$$G_{mf} = 688(D_p)^{1.82}[\rho_g(\rho_s - \rho_g)]^{0.94}/(\mu_g)^{0.88} \qquad \text{(36)}$$

where

G_{mf} = mass velocity at minimum fluidization [lb/(ft^2)(hr)],

D_p = particle diameter (in.),

ρ_g = gas density (lb/ft^3),

ρ_s = solids density (lb/ft^3), and

μ_g = gas viscosity (cp).

For -72 +100 # (B.S.S.) particles fluidized by nitrogen at 20°C

D_p = 0.007 in.,

ρ_g = 0.0727 lb/ft^3,

ρ_s = 350 lb/ft^3, and

μ_g = 0.0175 cp.

Substituting these values in equation (36) gives

$$G_{mf} = 65.6 \text{ lb/(ft}^2\text{),(hr).}$$

and this value must be corrected if N_{Re} exceeds 10.

Now, $N_{Re} = D_p.G_{mf}/\mu_g$

$= 0.90$

and no correction is necessary.

Therefore, $V_{mf} = 19.5$ l. s.t.p./min.

APPENDIX V

Description of Transport Reactor

APPENDIX V

V.1 Modifications Made to the Original Transport Apparatus

In the initial stages of the experimental programme it became apparent that several modifications to the original apparatus were necessary. These alterations involved

(a) the arrangement of the solids feeder,

(b) the prevention of the effects of thermal expansion, and

(c) the provision of an auxiliary heating winding between the preheater and the reaction line.

V.1.1 Arrangement of Solids Feeder

A preliminary series of tests were carried out on the solids feeder to determine the conditions, i.e., thread dimensions and screw speeds, which would provide a suitable range of solids flow rates. On the basis of these tests the arrangement shown in Figures 32 and 34 was considered satisfactory. However, when the transport line was pressurized by the flowing gas, it was necessary to maintain a positive pressure differential across the feeder to initiate the flow of solids; under these conditions the 1/50 h.p. variable speed motor did not develop sufficient torque to rotate the screw.

The original system was therefore replaced by the $\frac{1}{4}$ h.p. motor and series of pulley banks shown in Figure 33, and this arrangement, although providing a more limited range of screw speeds, operated satisfactorily. The other alteration made to the solids feeding device resulted from the effect of temperature on the flow characteristics of crushed sinter. The feed hopper was originally located immediately above the transport line, and, as the

temperature increased, the particles in the feed hopper tended to bridge across the inlet to the screw feeder thus limiting the flow of solids into the line. This effect was eliminated by increasing the length of the duct leading from the feeder to the venturi. In this way the hopper was separated from the heated line by a length of air-cooled tube which prevented any significant heat flow from the hot zone to the feed hopper. With this alteration, the sinter particles falling through the duct attained a higher velocity and higher gas velocities were required in the venturi throat to ensure that the solids were completely entrained.

V.1.2 Prevention of the Effects of Thermal Expansion

In the original design it was considered that the flexibility of the piping leading to the cyclone and heat exchanger would allow for a reasonable amount of expansion of the transport line. However, in an initial test at 700°C the transport line buckled and shifted the feeder in a horizontal direction thus destroying the alignment of the coupling between the screw feeder and the variable speed drive. This horizontal movement was prevented by clamping the solids feeder to a ½" steel plate bolted to the floor, and, although the consequent vertical expansion caused considerable bending in the downpipe leading to the cyclone, the apparatus operated satisfactorily. However, when the temperature exceeded 700°C the leakage of hydrogen from the flanged joints was sufficient to cause minor explosions and fires. This hydrogen leakage was most noticeable at the flanges at each end of the vertical transport line, and a rigid bearing surface was placed beneath the bottom flange to limit the bending moments developed at

this point. This modification reduced the hydrogen leakage to a negligible value.

V.1.3 Provision of an Auxiliary Heating Winding between the Preheater and the Heated Section of the Transport Line

Initially, the temperature drop across the unheated section of the line between the preheater and the vertical transport line was significantly large, and this temperature gradient was not markedly decreased by increasing the thickness of the lagging. Consequently, the unheated section was wound with 28 ft of carefully insulated 22 gauge nichrome wire to provide an additional heat input of 2 kW rated capacity, and, by using a 2 kW "Variac" autotransformer to control the temperature of this winding, the temperature of the solid-gas mixture was maintained at a constant value.

V.2 Description of Transport Apparatus

A line diagram of the apparatus is shown in Figure 30, and the details of the various components are as follows:-

G A Beecox A.10.J. rotary blower with a rated capacity of 5 ft^3 s.t.p./min. of air at 1440 r.p.m. Coarse control of the gas flow rate is obtained with a mechanical, variable speed, drive and precise control is achieved with the Saunders valve, V, in the by-pass line.

F A Fischer and Porter rotameter, which is calibrated against a wet-test meter.

H A concentric pipe heat exchanger, 8½ ft long, constructed from 1 in. and ¼ in. O.D. heat-resistant stainless steel. The hot gases leaving the reactor flow through the shell side and heat the cold, dry, hydrogen delivered by the

pump. The construction is all welded, and the exchanger is connected to the rest of the apparatus by flanged joints.

P A gas preheater, 7/8 in. internal diameter x 16 ft long, fabricated from Comsteel 25-20 heat-resistant stainless steel. The gas stream temperature is measured by chromel-alumel thermocouples located in stainless steel wells, one 8 ft from the end and the other at the end of the preheater. The temperatures corresponding to the e.m.f. generated by these couples are indicated by millivoltmeters calibrated in ^{o}C. The preheater furnace is of the normal tubular design. Nichrome wire is wound on a silica tube, 3.5 in. internal diameter x 8.5 ft long, covered with alundum cement, and this heating element is encased in a length of 8 in. diameter asbestos tube packed with 85% magnesia insulation. The heating windings are

(i) a primary winding of 20 gauge (B. and S.) nichrome wire with a resistance of 57.5 ohms consisting of 3 turns/in., and

(ii) a second winding of 16 gauge (B. and S.) nichrome wire with a resistance of 28.8 ohms and 2 turns/in.

The rated capacity of this furnace is 3 kW, and the heat input is manually controlled with "Variac" autotransformers.

S A solids feeder, which consists essentially of a feed hopper and a horizontal screw driven by a $\frac{1}{4}$ h.p. motor. A detailed drawing of this feeder is displayed in Figure 33. The solids enter the transport system via a $\frac{3}{8}$ in. duct which leads to the throat of a venturi mixer. This venturi

is machined from 1 in. dia. Comsteel 25-20 heat-resistant stainless steel rod in accordance with the dimensions suggested by Perry [87] (1950).

R A reaction line, 12 ft long x 7/8 in. internal diameter, constructed from Comsteel 25-20 heat-resistant stainless steel. Pressure tappings and thermocouple wells are provided at the bottom, middle and top of this line. The temperature of the solid-gas stream is measured with chromel-alumel couples and indicated by "Paton" millivoltmeters calibrated in ^{o}C. The differential pressures are indicated by U-tube manometers containing water. The heated section of the reaction line is 11 ft long, and is heated by two identical tube furnaces, each 5½ ft long. The heating elements for these furnaces have a resistance of 57.6 ohms and consist of 2 turns/in. of 20 gauge (B. and S.) nichrome wire wound on a silica former, 2.5 in. external diameter x 5.25 ft long, and encased in alundum cement. These elements are placed in a 6 in. asbestos tube packed with 85% magnesia insulation. The rated capacity of each furnace is 1 kW, and the heat input is controlled by Sunvic Energy Regulators.

T An auxiliary heating winding consisting of 28 ft of 22 gauge (B. and S.) nichrome wire, insulated with ¼ in. dia. porcelain beads, wrapped around the transport line. This winding provides an additional heat input of 2 kW rated capacity, and the energy input is controlled with a 2 kW "Variac" autotransformer.

D A solids collection system consisting of a dust trap and a small, high efficiency, cyclone. The dust trap is an inertial separator and consists of a piece of 25-20 Comsteel heat-resistant stainless steel tube, 12 in. long x 7/8 in. internal diameter, situated below a sharp change in direction of flow. The solids may be removed from the bottom of this trap. The dimensions of the cyclone, which is fabricated from 16 gauge, 25-20 heat-resistant stainless steel, are in accordance with the values reported by Stairmand [85] (1951) for a small, high efficiency, cyclone. The solids are removed from the bottom of this cyclone via a small valve.

C A cooler-condenser in the form of four concentric pipe heat exchangers in series. Each exchanger is constructed from 18-8 stainless steel pipe, 9 ft long x 7/8 in. internal diameter, surrounded by a 1.5 in. internal diameter water jacket. The exchangers are joined together with silver solder on the tube side and flexible hose on the shell side. The flow is countercurrent and the exchangers are sloped for condensate removal. The cooling water is towns water.

E A gas drier, constructed from 18 gauge copper sheet, containing a bed of 20% indicating silica gel, 12 in. dia. x 12 in. deep, supported on a perforated plate. Condensate from the cooler-condenser is removed from the bottom of the drier and pellets of caustic soda are placed at the bottom of the silica-gel bed to remove any H_2S and SO_2 from the

gas stream. The gas drier is connected to the cooler-condenser with a flexible hose and the exit gas connection is joined to the gas manifold shown in Figure 30 by another flexible hose connection.

APPENDIX VI

Experimental Accuracy

APPENDIX VI

In this Appendix the overall accuracy of the experimental measurement of reaction rates in fixed and fluidized systems is discussed; the assessment of the overall accuracy is made on the basis of the accuracy of the individual measurements.

VI.1 Fixed-Bed Data

VI.1.1 Pure Hydrogen as the Reducing Gas

The measurements which directly influence the accuracy of the rate data are

(i) the change in weight of the drying tubes, and

(ii) the time interval associated with the weight change.

The measured rate of reaction is also indirectly affected by the temperature control, the gas flow rate, and the magnitude of the water carryover value.

VI.1.1.1 Weighing Accuracy

The weight of water formed is obtained from the difference in weight of a drying tube placed in the exit gas line from the reactor. The weight measurements are made on an Oertling single-pan, direct reading, balance with a claimed accuracy of 0.001 g., and the weight increment is therefore correct to within $\pm$ 0.002 g.

VI.1.1.2 Time Measurement

The measurement of time is a direct determination and it is considered that the recorded times are correct to within $\pm$ 1.5% of the true values.

VI.1.1.3 Flow Measurement

The rotameter used to measure the flow of reducing gas

was calibrated against a bucket-type wet-test meter. The accuracy of the calibration is difficult to ascertain but it is thought that the flow rate indicated by the rotameter is within ± 3% of the actual value.

VI.1.1.4 Temperature Measurement

The chromel-alumel couples used to measure the temperature were calibrated against a sub-standard Pt : Pt - 13% Rh thermocouple which has a claimed accuracy of ± 4°C. Consequently, the corrected, measured, bed temperature should not deviate from the true bed temperature by more than ± 5°C.

The indicated bed temperature is controlled to within ± 5°C of the set point during the major part of a run. Therefore, it is possible that the true bed temperature may differ from the intended set point temperature by as much as ± 10°C.

VI.1.1.5 Measurement of Carryover Water Rate

The change in weight of a drying tube during a given time interval is equal to the sum of the water formed by reaction and the carryover water. The carryover water results from incomplete removal of oxygen from the inlet hydrogen and inefficient drying of the gas stream; throughout each run this value is considered to remain constant and the magnitude is determined at the completion of the run. The size of the carryover rate depends on the gas velocity, but it is of the order of 0.0003 g. H_2O/min. for the basic flow rate used during the tests, viz., 10 l. s.t.p./min. The accuracy of the value assigned to the carryover rate is indeterminate but it is considered that the error does not exceed ± 10%.

VI.1.1.6 Overall Accuracy of Rate Measurements

The accuracy of the measured reaction rate decreases as the reaction proceeds. During the initial stages the water formed by reaction is large in comparison to both the weighing error and the carryover water, whereas as the reaction rate decreases the errors associated with the weight difference and the subtraction of the amount of carryover water become more significant.

An examination of the rate data presented in Appendix VII reveals that the initial weight increments are of the order of 0.2 g. in 5 minutes, and the carryover rate is approximately 0.0003 g. H_2O/min. The weight of water formed by reaction, W, is given by

$$W = (0.2 \pm 0.002) - (5 \pm 1.5\%)\,(0.0003 \pm 10\%)$$

$$= (0.2 \pm 0.002) - (0.0015 \pm 11.5\%)$$

$$= (0.2 \pm 0.002) - (0.0015 \pm 0.0017)$$

$$= 0.1985 \pm 1.1\%$$

Hence, the calculated reaction rate, which is given by W/T, is equal to

$$R = \frac{0.1985 \pm 1.1\%}{5 \pm 1.5\%}$$

$$= 0.0379 \pm 2.6\%$$

Therefore, it may be concluded that the accuracy of the rate determination exceeds ± 5% provided the weight increment is comparatively large (>0.1 g.). In general, the time interval was selected to give weight changes of the order of 0.1 g. or larger, and the accuracy of the data is considered to be ± 5% until at least 70% of the reduction has taken place.

Towards the end of the reaction the weight increment is

often as low as 0.02 g. for a time interval of 30 minutes. In this case,

$$W = (0.02 \pm 0.002) - (30 \pm 1.5\%)\ (0.0003 \pm 10\%)$$
$$= 0.011 \pm 27\%$$

and it follows that the calculated reaction rate, R, is given by

$$R = \frac{0.011 \pm 27\%}{30 \pm 1.5\%}$$
$$= 0.00037 \pm 28.5\%$$

Therefore, it is apparent that the slow reaction rates measured near the completion of the reaction are subject to errors of the order of $\pm$ 30%.

The previous discussion omits any reference to the inaccuracies present in the measurement and control of the temperature and gas flow rate. Now, small variations in the gas flow rate are unlikely to affect the reaction rate (see Section 6.5.4.1), but the magnitude of the temperature effect cannot be estimated. However, it is claimed that the accuracy of the reported reaction rates exceed $\pm$ 10% for the major part of the reaction.

VI.1.2 Accuracy of Calculation of Chemical Per Cent Reduction

The technique used to obtain the per cent reduction against time curve for H_2-H_2O mixtures is based on chemical analysis of samples reduced for various known times. The accuracy of the method therefore depends on the accuracy of the chemical analysis and the correctness of the sampling procedure.

It is considered that the true per cent lead present as lead oxide or metallic lead in a given sample can be determined within $\pm$ 0.5 mass per cent. Now, the maximum change in either of

these variables is approximately 38 ± 0.5. Therefore, if the sample is almost completely reduced the fractional reduction based on the change in lead oxide content, X_A, may be given by

$$X_A = \frac{(38 \pm 0.5) - (1 \pm 0.5)}{38 \pm 0.5}$$

$$= 0.974 \pm 4\%$$

$$= 0.974 \pm 0.039$$

Hence, the possible error in the per cent reduction is ± 3.9 per cent reduction. For samples which are only slightly reduced the fractional reduction based on the change in lead oxide content, X_A, may be given by

$$X_A = \frac{(38 \pm 0.5) - (37 \pm 0.5)}{(38 \pm 0.5)}$$

$$= 0.0264 \pm 101.3\%$$

$$= 0.0264 \pm 0.027$$

and the possible error in the calculated per cent reduction is ± 2.7 per cent reduction.

In view of sampling difficulties, possible reoxidation of the sample, and the relative complexity of the assay technique, it is therefore claimed that the per cent reduction calculated from chemical analysis is only correct to within ± 5 per cent reduction.

VI.1.3 Accuracy of Calculation of Overall Per Cent Reduction

The overall per cent reduction is calculated from the amount of water formed, and in the C series of tests the water formed is obtained as the difference in weight of a single drying tube less the amount of carryover water. Now, the weight increment is considered to be correct to within ± 0.002 g., and in Section VI.1.1.5 the value

assigned to the normal carryover rate is 0.0003 ± 10% g. H_2O/min. Therefore, for a sample reduced for two hours from which approximately 1.0 g. of water is formed, the water formed by reaction is (1.0 ± 0.002) - (120 ± 1.5%) (0.0003 ± 10%), i.e., 0.964 ± 0.6%. The value assigned to the water formed by complete reduction is 1.70 g. H_2O/15 g. sinter, and assuming that this value, which is obtained from several tests, has an error of ± 0.05 g. H_2O, the overall calculated per cent reduction, X_t, is given by

$$X_t = \frac{0.964 \pm 0.6\%}{1.70 \pm 3\%}$$

$$= 0.566 \pm 3.6\%$$

and the error in the per cent reduction is ± 0.2%. It is therefore claimed that the overall per cent reduction calculated for the C series of runs is correct to within ± 0.5 per cent reduction.

In the A series of runs the weight of water formed by reaction is subject to a cumulative weighing error, and it is considered that the overall per cent reduction calculated from data obtained in the A series of tests is only correct to ± 2 per cent reduction.

VI.2 Fluidized Bed Data

The fluidized bed reaction rate is measured by measuring the rate of hydrogen make-up to a constant volume system from which the reaction product - water vapour - is continually removed. The rate at which hydrogen leaks out of the system is measured at the end of the reaction and it is assumed that this value remains constant throughout the test. The experimental technique consists

of measuring the time intervals required for a known volume of hydrogen to enter the system; when reaction is completed the time interval attains a constant value which is a measure of the rate of hydrogen leakage. The accuracy of the rate measurements is therefore directly influenced by

(i) the measurement of the time interval,

(ii) the magnitude and constancy of the leak rate, and

(iii) the accuracy of the volume measurement.

In addition the data are also affected by the accuracy of the bed temperature control and measurement.

VI.2.1 Volume Measurement

The gas-meter was calibrated against a bucket-type wet-test meter and the two methods of measurement were found to agree within ± 2%. It is therefore considered that the indicated volume is correct to within ± 2%.

VI.2.2 Time Measurement

The movement of the pointer on the gas-meter is very slow towards the end of the reaction, and, although the stopclocks used were accurate, it is considered that the accuracy of the time interval measurement is of the order of ± 5%.

VI.2.3 Measurement of Rate of Hydrogen Leakage

The leak rate is determined at the end of the reaction when the gas-meter pointer movement is very slow. Also, the accuracy of this measurement is influenced by both the time and volume measurements. Consequently, the accuracy should theoretically be only ± 10%. However, the leak rate is calculated as the arithmetic mean of at least four

measurements and it is claimed that the accuracy of this measurement is ± 5%.

VI.2.4 Temperature Measurement

The thermocouples used to measure the bed temperature were calibrated in the same way as the couples used in the fixed-bed tests, and the fluctuations in the bed temperature were of the same order as those experienced in the differential reactor. Consequently, referring to Section VI.1.1.4, the bed temperature may vary from the intended set point temperature by as much as ± 10°C.

VI.2.5 Flow Measurement

The rotameter used to measure the gas flow was calibrated against a wet-test meter. This calibration agreed with the calibration supplied with the flowmeter, and it is therefore felt that the flow indicated by the rotameter is within ± 3% of the actual value.

VI.2.6 Estimation of Overall Accuracy

The accuracy of the reaction rate data decreases as reaction proceeds. The hydrogen consumed by reaction in a given time interval is the difference between the amount of make-up hydrogen and the amount of hydrogen leakage; in the initial stages of reaction the difference between the make-up hydrogen and the hydrogen consumed by reaction is small, but as the reaction proceeds the difference increases and finally equals the constant rate of hydrogen leakage.

It is impossible to assign a single value to the accuracy of the results as a whole, but, since the final slow part of the reaction is not particularly important, the accuracy may be estimated for the initial stages of the reaction. In a typical test the leak

rate is 0.02 ft^3/min. and at 70 per cent reduction the time required for 0.25 ft^2 of make-up hydrogen to enter the apparatus is 7 minutes. The hydrogen consumed by reaction, V_R, is therefore given by

$$V_R = (0.25 \pm 0.005) - (7 \pm 5\%)\ (0.02 \pm 5\%)$$

$$= (0.25 \pm 0.005) - (0.14 \pm 10\%)$$

$$= 0.11 \pm 17\%\ ft^3$$

It is therefore claimed that the accuracy of the reported reaction rates, which are calculated by converting V_R to the equivalent weight of water and dividing by the time interval, exceeds ± 25% for the bulk of the measurements. Towards the end of the reaction this accuracy may be as low as ± 50%, and at the beginning it may be better than ± 10%.

APPENDIX VII

Results - Fixed-Bed Reactor

APPENDIX VII

VII.1 General Conditions and Notation

The chemical and physical properties of the various size fractions used in the experimental work are set out in Section 5.2, and the methods used to calculate the various per cent reductions are detailed in Section 6.5.2. The range of temperature variation specified for each run represents the maximum variation in the reactor bed temperature through the run.

"t" is the time in minutes at which the drying tube was removed at the end of each interval of measurement. The term "Wt. gain" is used to denote the weight in grams gained by the particular drying tube during the measuring interval, and "W" is the cumulative weight of water formed at time "t". The term "Rate" is an abbreviated form for the reaction rate, the units being g.H_2O/min.g. sinter. "x_{mid}" is the overall per cent reduction of the sample at the mid-point of the interval of measurement, and "x_{end}" is the overall per cent reduction at time "t" minutes.

The sample compositions are reported as mass percentages based on the original sample weight; the actual composition of a reduced sample is corrected for the weight lost during reaction. The term "weight loss" represents the loss in weight in grams of the sinter due to oxygen removal and the vapourisation of various other materials, and is equal to the total loss in weight of the reactor less the water removed from the reactor during the heating-up period. The values reported as oxidized lead, metallic lead, and sulphide lead represent the portion of the total lead content which is soluble in ammonium acetate, silver nitrate, and ferric chloride-sodium chloride solution, respectively.

VII.2 The A Series of Runs

VII.2.1 Rate Data

TABLE 22

RATE DATA FOR THE A SERIES OF RUNS

Run No. & Experimental Conditions	t	Wt. gain	W	x_{mid}	x_{end}	Rate
A.1	0	-	-			
				8.5		0.0032
-25 +36 # (B.S.S.)	6	0.2889	0.2889		17.0	
				21.8		0.0022
particles	11	0.1647	0.4536		26.7	
				32.1		0.0014
Sample wt. = 15 g.	20	0.1845	0.6381		37.6	
				43.0		0.00083
Temp. = 600 ± 3°C	35	0.1869	0.8250		48.5	
				53.5		0.00046
H_2 flow =	60	0.1728	0.9978		58.6	
				62.6		0.00030
5 l. s.t.p./min.	90	0.1345	1.1323		66.6	
				69.3		0.00020
P_{H_2} = 1.0 atm.	120	0.0916	1.2239		72.0	
				75.5		0.00013
	176	0.1104	1.3343		79.0	
A.2	0	-	-			
				8.55		0.0032
-25 +36 # (B.S.S.)	6	0.2918	0.2918		17.1	
				22.4		0.0020
particles	12	0.1817	0.4735		27.8	
				34.6		0.0012
Sample wt. = 15 g.	25	0.2332	0.7067		41.5	
				44.5		0.00068
Temp. = 600±5°C	35	0.1024	0.8091		47.5	
				52.6		0.00046
H_2 flow = 10 l. s.t.p./min.	60	0.1738	0.9829		57.7	
				61.4		0.00028
	90	0.1266	1.1095		65.0	
P_{H_2} = 1.0 atm.				67.9		0.00021
	120	0.0957	1.2052		70.8	

TABLE 22 (contd.)

Run No. & Experimental Conditions	t.	Wt. gain	W	x_{mid}	x_{end}	Rate
A.3				15.8		0.00715
	5	0.5375	0.5375		31.6	
-25 +36 # (B.S.S.) particles				38.25		0.0030
	10	0.2251	0.7626		44.9	
				49.0		0.00295
	15	0.2219	0.9045		53.1	
Sample wt. = 15g.				56.3		0.00143
	20	0.1070	1.0115		59.5	
Temp. = 700±4°C				65.5		0.0009
	35	0.2032	1.2147		71.5	
H_2 flow =				77.0		0.00051
5 l. s.t.p./min.	60	0.1918	1.4065		82.6	
				86.3		0.00028
p_{H_2} = 1.0 atm.	90	0.1250	1.5315		90.0	
				92.0		0.00014
	120	0.0649	1.5974		94.0	
				94.8		0.00010
	140	0.0296	1.6270		95.6	
				96.2		0.00007
	160	0.0218	1.6488		96.9	
				97.25		0.00006
	180	0.0173	1.6661		97.6	
				98.3		0.00005
	200	0.0154	1.6815		99.0	
				99.3		0.00004
	220	0.0118	1.6933		99.6	
				100.0		0.000035
	240	0.0105	1.7038		100.5	
				100.75		0.00004
	260	0.0123	1.7161		101.0	
A.4				18.0		0.0082
	5	0.6131	0.6131		36.0	
-25 +36 # (B.S.S.) particles				42.75		0.0031
	10	0.2308	0.8439		49.5	
				53.9		0.00197
	15	0.1477	0.9916		58.3	
Sample wt. = 15 g.				61.3		0.00137
	20	0.1026	1.0942		64.4	
Temp. = 700±5°C				70.0		0.00085
	35	0.1925	1.2867		75.6	

TABLE 22 (contd.)

Run No. & Experimental Conditions	t	Wt. gain	W	x_{mid}	x_{end}	Rate
A.4 (contd.)				79.9		0.00039
	60	0.1461	1.4328		84.3	
H_2 flow =				86.7		0.00019
10 l. s.t.p./min.	90	0.0831	1.5159		89.1	
				90.6		0.00011
	120	0.0502	1.5661		92.0	
A.5				16.85		0.0076
	5	0.5736	0.5736		33.7	
-25 +36 #				45.85		0.0055
(B.S.S.)	10	0.4121	0.9857		58.0	
particles				63.6		0.0026
	15	0.1927	1.1784		69.2	
Sample Wt. = 15g.				73.2		0.0018
	20	0.1321	1.3105		77.1	
Temp.= 800±5°C				81.7		0.0007
	35	0.1584	1.4689		86.4	
H_2 flow =				89.3		0.00027
5 l. s.t.p./min.	60	0.1001	1.5690		92.2	
				93.8		0.00013
p_{H_2} = 1.0 atm.	90	0.0566	1.6256		95.5	
				96.5		0.000065
	120	0.0295	1.6551		97.4	
				98.2		0.000059
	150	0.0265	1.6816		99.0	
A.6	5	1.0173	1.0173	29.85	59.7	0.0135
				68.85		0.0041
-25 +36 #	10	0.3083	1.3256		78.0	
(B.S.S.)				81.3		0.00153
particles	15	0.1147	1.4403		84.6	
				86.8		0.00096
Sample Wt. = 15g.	20	0.0724	1.5127		89.0	
				91.2		0.00051
Temp. = 800±2°C	30	0.0765	1.5892		93.4	
				95.0		0.00023
H_2 flow = 10 l. s.t.p./min.	45	0.0526	1.6418		96.6	
p_{H_2} = 1.0 atm.						

TABLE 22 (contd.)

Run No. & Experimental Conditions	t	Wt. gain	W	x_{mid}	x_{end}	Rate
A.7				9.5		0.0217
	1	0.3232	0.3232		19.0	
-25 +36 # (B.S.S.) particles				30.15		0.0127
	3	0.3804	0.7036		41.3	
Sample Wt. = 15g.				48.2		0.00784
	5	0.2347	0.9383		55.1	
Temp. = 800±5°C				65.0		0.00446
	10	0.3354	1.2737		74.9	
H_2 flow = 13 l. s.t.p./min.				79.1		0.00194
	15	0.1460	1.4197		83.4	
P_{H_2} = 1.0 atm.				85.7		0.00105
	20	0.0788	1.4985		88.0	
				90.5		0.00057
	30	0.0858	1.5843		93.0	
				94.8		0.00027
	45	0.0601	1.6444		96.6	
				97.5		0.00012
	60	0.0265	1.6709		98.4	
				98.7		0.00009
	70	0.0130	1.6839		99.0	
				99.15		0.00003
	80	0.0047	1.6886		99.3	
				99.45		0.000028
	90	0.0042	1.6928		99.6	
				99.7		0.00001
	100	0.0015	1.6943		99.8	
				99.0		0.00005
	107.5	0.0059	1.7002		100.0	
A.8				2.0		0.00073
	6	0.0666	0.0666		4.0	
-25 +36 # (B.S.S.) particles				6.55		0.00099
	12	0.0893	0.1559		9.1	
Sample Wt. = 15g.				17.0		0.00078
	35	0.2683	0.4242		24.9	
Temp. = 500±6°C				29.25		0.00039
	60	0.1466	0.5708		33.6	
H_2 flow = 10 l. s.t.p./min.				38.55		0.00019
	120	0.1700	0.7408		43.5	
P_{H_2} = 1.0 atm.				46.05		0.000096
	180	0.0866	0.8274		48.6	

TABLE 22 (contd.)

Run No. & Experimental Conditions	t	Wt. gain	W	x_{mid}	x_{end}	Rate
A.9				6.95		0.0158
	1	0.2368	0.2368		13.9	
-72 +100 # (B.S.S.) particles				21.25		0.0083
	3	0.2488	0.4856		28.6	
Sample Wt. = 15g.				32.5		0.0045
	5	0.1334	0.6190		36.4	
Temp. = 700±4°C				42.7		0.0029
	10	0.2164	0.8354		49.1	
H_2 flow = 10 l. s.t.p./min.				53.1		0.0018
	15	0.1380	0.9734		57.2	
				60.3		0.00137
	20	0.1024	1.0758		63.4	
p_{H_2} = 1.0 atm.				67.9		0.00104
	30	0.1559	1.2317		72.5	
				77.0		0.00067
	45	0.1508	1.3825		81.5	
				84.1		0.00041
	60	0.0926	1.4751		86.8	
				89.6		0.00021
	90	0.0952	1.5703		92.4	
				93.9		0.00011
	120	0.0493	1.6196		95.3	
A.10				7.75		0.0175
	1	0.2626	0.2626		15.5	
-72 +100 # (B.S.S.) particles				21.8		0.0072
	3	0.2173	0.4799		28.2	
Sample Wt. = 15g.				31.9		0.00425
	5	0.1272	0.6071		35.7	
Temp. = 700±2°C				42.8		0.00324
	10	0.2432	0.8503		50.0	
H_2 flow = 13 l. s.t.p./min.				54.8		0.0020
	15	0.1510	1.0013		59.5	
				64.0		0.00154
	20	0.1152	1.1165		68.5	
p_{H_2} = 1.0 atm.				73.4		0.00095
	35	0.2140	1.3305		78.3	
				82.9		0.00042
	60	0.1577	1.4882		87.5	
				89.5		0.00015
	90	0.0684	1.5566		91.5	
				92.0		0.00010
	100	0.0148	1.5714		92.5	

TABLE 22 (contd.)

Run No. & Experimental Conditions	t	Wt. gain	W	x_{mid}	x_{end}	Rate
A.10 (contd.)				92.75		0.000062
	110	0.0093	1.5807		93.0	
				93.2		0.000054
	120	0.0081	1.5888		93.4	
				93.6		0.00035
	130	0.0052	1.5940		93.9	
				94.1		0.00042
	140	0.0063	1.6003		94.2	
A.11				0.99		0.0011
	2	0.0335	0.0335		1.98	
-72 +100 # (B.S.S.) particles				3.32		0.0010
	5	0.0458	0.0793		4.66	
				7.68		0.0014
Sample Wt. = 15g.	10	0.1021	0.1814		10.7	
				16.3		0.0013
Temp. = 500±2°C	20	0.1904	0.3718		21.9	
				26.8		0.00074
H_2 flow = 10 l. s.t.p./min.	35	0.1672	0.5390		31.7	
				36.3		0.00043
	60	0.1597	0.6987		41.0	
P_{H_2} = 1.0 atm.				43.5		0.00018
	90	0.0832	0.7819		46.0	
				47.7		0.00013
	120	0.0575	0.8394		49.4	
				50.7		0.00010
	150	0.0449	0.8843		52.0	
				53.1		0.00008
	180	0.0370	0.9213		54.2	
A.12				9.75		0.0044
	5	0.3310	0.3310		19.5	
-72 +100 # (B.S.S.) particles				26.5		0.0023
	12	0.2391	0.5701		33.5	
				37.9		0.00125
Sample Wt. = 15g.	20	0.1494	0.7195		42.3	
				47.1		0.00072
Temp. = 600±4°C	35	0.1618	0.8813		51.9	
				56.4		0.00041
	60	0.1537	1.0350		60.9	

TABLE 22 (contd.)

Run No. & Experimental Conditions	t	Wt. gain	W	x_{mid}	x_{end}	Rate
A.12 (contd.)				64.45		0.00027
	90	0.1213	1.1563		68.0	
H_2 flow = 10				70.6		0.00020
l. s.t.p./min.	120	0.0890	1.2453		73.2	
				76.6		0.00013
P_{H_2} = 1.0 atm.	180	0.1164	1.3617		80.0	
				82.2		0.00008
	240	0.0724	1.4341		84.4	
A.13				16.85		0.019
	2	0.5736	0.5736		33.7	
-72 +100 #				40.6		0.0078
(B.S.S.)	4	0.2350	0.8086		47.5	
particles				52.3		0.00545
	6	0.1633	0.9719		57.1	
Sample Wt. = 15g.				63.5		0.00364
	10	0.2188	1.1907		70.0	
Temp. = 800±6°C				74.2		0.0020
	15	0.1483	1.3390		78.5	
H_2 flow = 13				80.9		0.00102
l. s.t.p./min.	20.	0.0767	1.4157		83.3	
				85.5		0.00054
P_{H_2} = 1.0 atm.	30	0.0818	1.4975		88.0	
				89.8		0.00032
	45	0.0715	1.5690		91.6	
				93.3		0.00013
	60	0.0479	1.6169		95.0	
				96.5		0.000114
	90	0.0513	1.6682		98.0	
				98.8		0.00005
	120	0.0232	1.6914		99.6	
A.14				0.70		0.00078
	2	0.0236	0.0236		1.40	
-52 +72 #				2.75		0.0010
(B.S.S.)	5	0.0456	0.0692		4.10	
particles				6.65		0.00117
	10	0.0880	0.1572		9.2	
Sample Wt. = 15g.				14.0		0.00107
	20	0.1614	0.3186		18.80	
Temp. = 500±4°C				23.3		0.00069

TABLE 22(contd.)

Run No. & Experimental Conditions	t	Wt. Gain	W	x_{mid}	x_{end}	Rate
A.14 (contd.)	35	0.1549	0.4735		27.80	
H_2 flow = 10 l. s.t.p./min.				31.1		0.00039
	60	0.1455	0.6190		36.4	
				39.3		0.00022
p_{H_2} = 1.0 atm.	90	0.0972	0.7162		42.2	
				44.0		0.00014
	120	0.0616	0.7778		45.8	
				48.0		0.000082
	180	0.0742	0.8520		50.2	
				51.65		0.000057
	240	0.0510	0.9030		53.1	
A.15	0		-			
				3.65		0.0041
-52 +72 # (B.S.S.)	2	0.1236	0.1236		7.3	
				12.3		0.0038
particles	5	0.1731	0.2967		17.4	
				22.5		0.0023
Temp. = 600±5°C	10	0.1735	0.4702		27.7	
				34.1		0.00145
Sample Wt.= 15g.	20	0.2171	0.6873		40.5	
				45.5		0.00076
H_2 flow = 10 l. s.t.p./min.	35	0.1713	0.8586		50.5	
				55.0		0.00042
	60	0.1572	1.0158		59.6	
p_{H_2} = 1.0 atm.				63.3		0.00028
	90	0.1240	1.1398		67.0	
				69.4		0.00018
	120	0.0822	1.2220		71.8	
				75.1		0.00012
	180	0.1087	1.3307		78.4	
A.16	0		-			
				7.55		0.0171
-52 +72 # (B.S.S.)	1	0.2570	0.2570		15.1	
				19.1		0.0091
particles	2	0.1368	0.3938		23.1	
				30.2		0.0054
Sample Wt. = 15g.	5	0.2420	0.6358		37.4	
				44.0		0.0029
Temp. = 700±5°C						

TABLE 22 (contd.)

Run No. & Experimental Conditions	t	Wt. gain	W	x_{mid}	x_{end}	Rate
A.16 (contd.)	10	0.2215	0.8573		50.5	
				54.6		0.0019
H_2 flow = 10 l. s.t.p./min.	15	0.1428	1.0001		58.8	
				61.9		0.0014
	20	0.1074	1.1075		65.0	
p_{H_2} = 1.0 atm.				69.7		0.00105
	30	0.1569	1.2644		74.4	
				81.7		0.00056
	60	0.2508	1.5152		89.0	
				92.3		0.00025
	90	0.1115	1.6267		95.6	
				97.1		0.00010
	120	0.0459	1.6726		98.5	
				98.8		0.000045
	140	0.0137	1.6863		99.1	
				99.5		0.000042
	160	0.0127	1.6990		99.9	
A.17	0					
				0.52		0.00059
-36 +52 # (B.S.S.) particles	2	0.0177	0.0177		1.04	
				2.10		0.00080
	5	0.0361	0.0538		3.16	
Sample Wt.= 15g.				5.6		0.00109
	10	0.0819	0.1357		7.96	
Temp. = 500±2°C				12.0		0.00092
	20	0.1384	0.2741		16.1	
H_2 flow = 10 l. s.t.p./min.				20.3		0.00064
	35	0.1448	0.4189		24.6	
				28.7		0.00037
	60	0.1408	0.5597		32.9	
p_{H_2} = 1.0 atm.				35.9		0.00022
	90	0.1008	0.6605		38.8	
				40.6		0.00014
	120	0.0629	0.7234		42.5	
				45.0		0.00009
	180	0.0848	0.8082		47.5	
A.18	0		-			
				3.25		0.0037
-36 +52 # (B.S.S.) particles	2	0.1109	0.1109		6.5	
				11.2		0.0036
	5	0.1630	0.2739		15.9	

TABLE 22(contd.)

Run No. & Experimental Conditions	t	Wt. gain	W	x_{mid}	x_{end}	Rate
A.18 (contd.)				21.2		0.0024
	10	0.1780	0.4519		26.6	
Sample Wt. = 15g.				32.9		0.00145
	20	0.2173	0.6692		39.3	
Temp. = 600±6°C				44.5		0.00079
	35	0.1771	0.8463		49.7	
H_2 flow = 10 l. s.t.p./min.				54.7		0.00046
	60	0.1711	1.0174		59.7	
				63.6		0.00029
p_{H_2} = 1.0 atm.	90	0.1330	1.1504		67.6	
				70.3		0.00021
	120	0.0937	1.2441		73.0	
				76.7		0.00014
	180	0.1242	1.3683		80.4	
A.19	0					
				6.45		0.0146
-36 +52 # (B.S.S.)	1	0.2186	0.2186		12.9	
				18.7		0.0066
particles	3	0.1974	0.4160		24.5	
				28.3		0.0044
Sample Wt.= 15g.	5	0.1331	0.5491		32.2	
				38.6		0.0029
Temp. = 700±8°C	10	0.2159	0.7650		45.0	
				49.0		0.0019
H_2 flow = 10 l. s.t.p./min.	15	0.1397	0.9047		53.1	
				56.1		0.0014
	20	0.1031	1.0078		59.1	
p_{H_2} = 1.0 atm.				63.6		0.0010
	30	0.1517	1.1595		68.1	
				71.2		0.00071
	40	0.1070	1.2665		74.4	
				78.6		0.00048
	60	0.1443	1.4108		82.8	
				86.6		0.00028
	90	0.1277	1.5385		90.4	
				92.0		0.00012
	120	0.0523	1.5908		93.5	
				94.8		0.000053
	180	0.0476	1.6384		96.1	

VII.2.2 General Data and Sample Compositions

The experimental conditions for these tests are set out in Table 22.

TABLE 23

GENERAL RESULTS FOR THE A SERIES OF TESTS

Run No.	Reduction period (min.)	Water formed (g.)	Weight loss (g.)	Total lead	Total zinc
A.1	176	1.3343	1.2708	38.35	8.65
A.2	120	1.2050	1.1579	38.20	9.70
A.3	260	1.7161	1.7506	41.60	5.80
A.4	120	1.5661	1.7890	38.6	7.94
A.5	150	1.6816	2.1088	40.5	4.4
A.6	45	1.6418	2.2225	40.1	4.0
A.7	107.5	1.7002	2.5325	39.3	3.65
A.8	180	0.8274	0.7867	39.4	9.65
A.9	120	1.6196	1.7036	39.3	7.43
A.10	140	1.6003	1.9000	38.9	5.70
A.11	180	0.9213	0.8142	39.4	7.90
A.12	240	1.4341	1.4400	38.1	8.25
A.13	120	1.6914	2.4989	38.6	3.70
A.14	240	0.9030	0.8933	37.2	10.20
A.15	180	1.3307	1.3594	36.8	9.55
A.16	160	1.6990	1.8154	38.9	6.90
A.17	180	0.8082	0.8003	36.8	10.0

TABLE 23 (contd.)

Run No.	Reduction period (min.)	Water formed (g.)	Weight loss (g.)	Total lead	Total zinc
A.18	180	1.3683	1.3780	37.9	9.1
A.19	180	1.6384	1.8303	38.6	6.9

VII.3 The C to E Series of Runs

VII.3.1 The C Series

Conditions

bed weight = 15 g.

particle size = -25 +36 # (B.S.S.)

temperature = 600 ± 5°C

P_{H_2} = 1 atm.

TABLE 24

RESULTS OF THE C SERIES OF TESTS

Run No.	Reductn. period (min.)	Water formed (g.)	Weight loss (g.)	Total lead	Total zinc	Oxid. lead	Metallic lead	Sulphide lead
C.8	2	0.1075	0.0884	41.0	10.1	38.6	-	1.4
C.1	5	0.2892	0.2776	39.2	10.1	33.4	4.4	1.9
C.2	11	0.4547	0.4409	39.1	9.9	26.8	11.1	2.2
C.3	20	0.6185	0.6197	39.0	9.7	21.1	16.0	2.3

TABLE 24 (contd.)

Run No.	Reductn. period (min.)	Water formed (g.)	Weight loss (g.)	Total lead	Total zinc	Oxid. lead	Metallic lead	Sulphide lead
C.4	35	0.8376	0.8579	39.7	9.9	16.5	18.5	2.3
C.5	60	0.9691	0.9975	38.6	9.4	12.5	22.8	2.3
C.6	90	1.1164	1.1766	40.2	9.2	10.5	25.3	2.3
C.7	240	1.4768	1.5511	39.6	8.2	6.6	29.0	3.9

VII.3.2 The D Series

Conditions

bed weight = 15 g.

size fraction = -52 +72 # (B.S.S.)

temperature = 700 ± 7°C

P_{H_2} = 1.0 atm.

TABLE 25

RESULTS OF THE D SERIES OF TESTS

Run No.	Reductn. period (min.)	Water formed (g.)	Weight loss (g.)	Total lead	Total zinc	Oxid. lead	Metallic lead	Sulphide lead
D.1	1	0.2478	0.2855	38.2	9.65	34.0	2.1	1.7
D.2	3	0.5016	0.4843	38.2	9.70	27.0	7.8	1.7
D.3	7	0.7167	0.6922	38.4	9.70	20.7	14.1	2.7

TABLE 25 (contd.)

Run No.	Reductn. period (min.)	Water formed (g.)	Weight loss (g.)	Total lead	Total zinc	Oxid. lead	Metallic lead	Sulphide lead
D.4	15	1.0657	1.0254	38.3	9.40	11.7	22.3	3.4
D.5	30	1.2169	1.2237	38.4	9.35	6.9	26.4	3.8
D.6	60	1.4937	1.6000	38.5	7.95	3.6	28.0	5.8

VII.3.3 The E Series

Conditions

bed weight = 15 g.

size fraction = -52 +72 # (B.S.S.)

temperature = 500 ± 4°C

P_{H_2} = 1.0 atm.

TABLE 26

RESULTS OF THE E SERIES OF TESTS

Run No.	Reductn. period (min.)	Water formed (g.)	Weight loss (g.)	Total lead	Total zinc	Oxid. lead	Metallic lead	Sulphide lead
E.1	12	0.2026	0.1946	39.2	10.3	34.2	2.50	1.7
E.2	24	0.4012	0.3566	38.2	10.0	29.0	6.40	1.7
E.3	45	0.5435	0.4933	38.6	10.1	24.1	12.0	1.9
E.4	90	0.7337	0.6728	38.0	9.9	18.6	16.0	3.7

VII.3.4 The F Series

Conditions

bed weight = 15 g.

size fraction = -52 +72 # (B.S.S.)

P_{H_2} = 0.91 atm.

TABLE 27

RESULTS OF THE F SERIES OF TESTS

Run No.	Temp. °C	Reductn. Time (min.)	Weight loss (g.)	Total lead	Total zinc	Oxid. lead	Metallic lead	Sulphide lead
F.1	700	1	0.3024	38.4	9.42	34.3	1.6	0.8
F.2	700	3	0.5207	38.0	9.32	28.3	7.1	1.4
F.3	700	7	0.6854	38.2	9.74	22.20	12.8	1.3
F.4	700	11	0.7771	38.4	9.65	18.0	17.1	1.2
F.5	600	2	0.1580	39.0	9.60	35.5	0.2	1.6
F.6	600	11	0.4342	39.0	9.80	26.0	9.0	2.3
F.7	600	20	0.5554	38.6	9.84	21.0	14.2	2.3

APPENDIX VIII

Results - Fluidized Bed Reactor

VIII.1 General Conditions and Notation

The chemical and physical properties of the various size fractions are given in Section 5.2, and the basis used to calculate the overall per cent reduction is discussed in Section 6.5.2. The hydrogen flow rate is expressed in l. s.t.p./min., and as a fraction of the theoretical minimum fluidizing velocity, V_{mf}. The values of V_{mf} for the various particle sizes and system conditions are presented in Section 7.3. The reported uncertainty in the temperature measurement is the maximum variation from the set point observed during the run, and, in general, the temperature fluctuations are less than the reported values.

"t" is the time in minutes at which the gas-meter pointer passed each $\frac{1}{4}$ ft^3 increment of makeup hydrogen. "W" is the weight in grams of water formed by reaction between two successive time measurements, t_1 and t_2, calculated from the volume of hydrogen consumed by reaction. The term "Rate" is an abbreviation for the overall reaction rate, the units being g. H_2O/min., g. sinter.

"x_{mid}" is the overall per cent reduction of the sample at the mid-point of the interval of measurement, and "x_{end}" is the per cent reduction at time "t" minutes.

VIII.2 Rate Data TABLE 28

RATE DATA FOR THE B SERIES OF RUNS

Run No. & Experimental Conditions	t	W	x_{end}	x_{mid}	Rate
B.1	0	-	-	3.6	0.008
-52 +72 # (B.S.S.) particles	1.02	4.1	7.25	10.0	0.00142
Flowrate = 114 l. s.t.p./min. or 7.8 V_{mf}	5.47	3.16	12.80	14.65	0.001
Temp. = 500±5°C	9.47	2.06	16.50	19.10	0.00114
Bed Wt. = 500 g.	14.70	2.97	21.70	24.10	0.00095
	20.43	2.72	26.50	28.50	0.00069
	27.06	2.27	30.50	32.30	0.00057
	34.16	2.02	34.10	35.75	0.00047
	42.36	1.91	37.40	38.45	0.00026
	51.13	1.16	39.50	40.30	0.00020
	60.31	0.91	41.10	41.65	0.00013
	70.08	0.63	42.20	42.85	0.00011
	80.01	0.57	43.30	43.65	0.00009
	90.13	0.45	44.0	44.30	0.00007
	100.46	0.36	44.6	44.85	0.00005
	110.94	0.27	45.1	45.30	0.000038
	121.57	0.20	45.5	45.45	0.000007
	132.49	0.04	45.60	45.60	-
	143.51	-	45.60	45.70	0.000016
	154.38	0.09	45.8	45.80	-
	165.40	-	45.8		
B.2	0	-	-	7.4	0.0162
	1.03	4.20	14.8		

TABLE 28 (contd.)

Run No. & Experimental Conditions	t	W	x_{end}	x_{mid}	Rate
B.2 (contd.)				22.4	0.0062
-52 +72 # (B.S.S.) particles	3.85	4.32	30.0	36.5	0.0036
Flowrate = 114 l. s.t.p./min. or 8.6 V_{mf}	7.98	3.68	43.0	47.9	0.0018
Temp. = 600±5°C	14.0	2 78	52.8	55.8	0.00083
Bed Wt. = 250 g.	22.22	1.71	58.8	61.7	0.00080
	30.52	1.66	64.6	67.1	0.00064
	39.34	1.41	69.6	71.4	0.00042
	48.96	1.02	73.2	74.3	0.00022
	59.48	0.59	75.4	75.65	0.000049
	70.95	0.14	75.9	77.65	0.00042
	80.58	1.02	79.4	80.2	0.00016
	91.43	0.43	81.0	81.45	0.00009
	102.66	0.25	81.9	82.25	0.00007
	113.98	0.20	82.6	82.8	0.00004
	125.38	0.11	83.0	83.05	0.00002
	136.98	0.07	83.1	83.1	0.000002
	148.71	0.005	83.1	83.1	-
	160.47	-	83.1		
B.3	0	-	-	6.7	0.014
-52 +72 # (B.S.S.) particles	1.1	3.90	13.4	21.7	0.0074
Flowrate = 114 l. s.t.p./min. or 8.6 V_{mf}	3.58	4.60	30.0	36.8	0.0037
	7.78	3.85	43.6	49.25	0.0022
	13.50	3.20	54.9		

TABLE 28(contd.)

Run No. & Experimental Conditions	t	W	x_{end}	x_{mid}	Rate
B.3 (contd.)				58.7	0.0011
	21.60	2.16	62.5		
Temp. = 600±10°C				65.45	0.00071
	30.88	1.66	68.4		
Bed Wt. = 250 g.				71.2	0.00064
	40.36	1.57	74.0		
				76.15	0.00049
	50.56	1.25	78.3		
				80.0	0.00037
	61.31	1.0	81.7		
				83.4	0.00035
	72.13	0.95	85.1		
				86.6	0.00029
	83.33	0.82	88.1		
				89.1	0.00020
	95.06	0.59	90.1		
				90.85	0.00013
	107.19	0.41	91.6		
				92.1	0.00008
	119.69	0.25	92.6		
				92.8	0.000044
	132.46	0.14	93.0		
				93.1	0.000014
	145.42	0.045	93.2		
				93.25	0.000007
	158.47	0.023	93.3		
				93.3	-
	171.53	0	93.3		
B.4	0	-	-		
				8.5	0.017
-52 +72 # (B.S.S.) particles)	1.12	4.80	17.0		
				24.2	0.006
	3.87	4.07	31.4		
				37.5	0.0037
Flowrate = 114 l. s.t.p./min., or 8.6 V_{mf}	7.68	3.46	43.6		
				48.55	0.0023
	12.55	2.82	53.5		
				57.4	0.0015
Temp. = 600±10°C	18.53	2.18	61.3		
				64.1	0.00091
Bed Wt. = 250 g.	25.53	1.59	66.9		
				68.9	0.00061
	33.20	1.17	71.0		
				72.5	0.0004

TABLE 28 (contd.)

Run No. & Experimental Conditions	t	W	x_{end}	x_{mid}	Rate
B.4 (contd.)	41.53	0.82	73.9		
				75.2	0.00035
	49.96	0.75	76.6		
				78.3	0.00049
	67.99	0.98	80.0		
				80.05	0.000077
	77.39	0.018	80.1		
				80.1	0.000059
	86.86	0.014	80.1		
				80.1	0.000046
	96.36	0.011	80.1		
				80.2	0.00038
	105.91	0.091	80.3		
				80.4	0.00014
	115.56	0.034	80.5		
				80.6	0.00019
	125.19	0.045	80.7		
				80.8	0.00028
	134.76	0.068	80.9		
				80.95	0.00002
	144.45	0.005	81.0		
				81.0	-
	154.15	-	81.0		
B.5	0	-	-		
				4.85	0.0073
-52 +72 # (B.S.S.) particles	1.50	5.50	9.7		
				14.10	0.0070
	2.93	4.97	18.5		
				22.6	0.0045
Flowrate = 76 l. s.t.p./min. or 5.75 V_{mf}	5.00	4.65	26.75		
				30.5	0.0029
	7.95	4.23	34.20		
				37.6	0.0022
Temp. = 600±5°C	11.48	3.85	41.0		
				44.2	0.0017
Bed Wt. =500 g.	15.68	3.62	47.4		
				50.2	0.0013
	20.63	3.25	53.0		
				55.3	0.0008
	26.83	2.61	57.6		
				59.6	0.00064
	33.80	2.25	61.6		

TABLE 28 (contd.)

Run No. & Experimental Conditions	t	W	x_{end}	x_{mid}	Rate
B.5 (contd.)				63.6	0.0006
	41.0	2.14	65.5		
				67.2	0.00055
	48.4	2.04	69.0		
				70.7	0.0005
	56.07	1.91	72.5		
				73.8	0.00038
	64.39	1.59	75.3		
				76.4	0.00029
	73.29	1.30	77.5		
				78.4	0.00022
	82.62	1.02	79.3		
				80.1	0.00020
	92.19	0.95	81.0		
				82.2	0.00029
	101.06	1.30	83.4		
				83.9	0.00015
	111.09	0.73	84.5		
				85.0	0.00011
	121.44	0.59	85.6		
				85.9	0.00008
	132.11	0.43	86.3		
				86.6	0.00006
	143.01	0.32	87.0		
				87.1	0.000033
	154.18	0.18	87.2		
				87.35	0.000016
	165.56	0.091	87.5		
				87.55	0.00008
	177.03	0.045	87.6		
				87.6	0.00004
	188.53	0.022	87.6		
				87.65	-
	200.05	-	87.7		
B.6	0	-	-		
				5.55	0.0102
-52 +72 # (B.S.S.) particles	1.23	6.30	11.1		
				15.6	0.0068
	2.73	5.09	20.1		
				24.4	0.00485
Flowrate = 92 l. s.t.p./min., or 7.0 V_{mf}	4.75	4.89	28.7		
				32.7	0.0037
	7.70	4.53	36.8		
				40.4	0.0021

TABLE 28 (contd.)

Run No. & Experimental Conditions	t	W	x_{end}	x_{mid}	Rate
B.6 (contd.)	11.63	4.14	44.0	47.4	0.0017
Temp. = 600±5°C	16.20	3.88	50.9	54.0	0.0013
Bed Wt. = 500 g.	21.67	3.52	57.1	59.7	0.00088
	28.47	3.00	62.4	64.7	0.00066
	36.30	2.59	67.0	69.0	0.00052
	44.96	2.27	71.0	72.8	0.00046
	54.09	2.09	74.6	76.1	0.00034
	64.19	1.70	77.6	78.1	0.00031
	74.56	1.59	80.5	81.8	0.00027
	85.76	1.50	83.1	83.9	0.00015
	97.83	0.93	84.7	85.3	0.00011
	110.50	0.68	86.0	86.4	0.000068
	123.80	0.455	86.9	87.05	0.000047
	137.38	0.320	87.2	87.4	0.00015
	151.51	0.11	87.6	87.6	0.000003
	165.86	0.023	87.6	87.6	-
	180.28	-	87.6		
B.7	0	-	-	6.25	0.013
-52 +72 # (B.S.S.) particles)	1.09	7.10	12.5	17.0	0.0095
	2.16	5.09	21.5	25.65	0.0053
Flowrate = 114 l. s.t.p./min., or 8.65 V_{mf}	3.94	4.70	29.8	33.6	0.0033
	6.51	4.27	37.35	40.6	0.0023

TABLE 28 (contd.)

Run No. & Experimental Conditions	t	W	x_{end}	x_{mid}	Rate
B.7 (contd.)	9.84	3.75	44.0	47.1	0.0019
Temp. = 600^{+}-5°C	13.64	3.59	50.3	53.1	0.0015
Bed Wt. = 500 g.	18.07	3.25	56.0	58.3	0.00098
	23.54	2.68	60.7	62.7	0.00075
	29.72	2.30	64.8	66.6	0.00059
	36.44	1.98	68.4	69.9	0.00051
	43.51	1.80	71.5	73.0	0.00042
	50.98	1.57	74.4	75.7	0.00043
	58.38	1.61	77.1	78.1	0.00025
	66.80	1.05	79.0	80.0	0.00031
	74.85	1.25	81.1	81.9	0.00020
	83.58	0.885	82.8	83.5	0.00017
	92.53	0.775	84.2	84.65	0.00014
	101.70	0.63	85.1	85.45	0.00014
	110.82	0.66	86.4	86.9	0.00013
	120.04	0.61	87.5	87.9	0.00010
	129.46	0.50	88.3	88.6	0.000086
	139.03	0.41	89.0	89.4	0.00008
	148.66	0.39	89.8	90.1	0.00007
	158.33	0.36	90.4	90.6	0.00008
	167.91	0.39	90.8	91.2	0.0008
	177.51	0.39	91.5	91.5	-
	187.84	-	91.5		

TABLE 28 (contd.)

Run No. & Experimental Conditions	t	W	x_{end}	x_{mid}	Rate
B.8	0	-	-		
				9.45	0.024
-52 +72 # (B.S.S.) particles	0.90	10.70	18.9		
				23.45	0.0074
	2.30	5.15	28.0		
				32.3	0.0048
Flowrate = 131 l. s.t.p./min., or 10.0 V_{mf}	4.33	4.90	36.6		
				40.6	0.0030
	7.38	4.52	44.6		
				48.1	0.0022
Temp. = 600±5°C	11.23	4.21	52.1		
				55.4	0.0015
Bed Wt. = 500 g.	16.15	3.80	58.8		
				61.8	0.0011
	22.18	3.38	64.9		
				67.0	0.00061
	30.45	2.52	69.1		
				70.9	0.00042
	40.08	2.02	72.8		
				74.4	0.00034
	50.43	1.75	76.0		
				77.2	0.00027
	61.48	1.48	78.4		
				79.5	0.00021
	73.21	1.23	80.7		
				81.5	0.00015
	85.64	0.95	82.4		
				83.2	0.00014
	98.16	0.91	84.0		
				84.6	0.00011
	111.21	0.73	85.2		
				85.6	0.00008
	124.73	0.54	86.1		
				86.5	0.00005
	138.80	0.34	86.9		
				87.0	0.00003
	153.12	0.23	87.1		
				87.25	0.000014
	167.75	0.10	87.4		
				87.45	0.000007
	182.55	0.05	87.5		
				87.5	-
	197.47	-	87.5		

TABLE 28 (contd.)

Run No. & Experimental Conditions	t	W	x end	x mid	Rate
B.9	0	-	-		
				9.2	0.0186
-52 +72 # (B.S.S.)	1.12	10.40	18.4		
				22.7	0.012
particles	1.95	4.95	27.1		
				31.2	0.008
Flowrate = 114 l. s.t.p./min.,	3.13	4.64	35.3		
				39.1	0.0054
or 9.6 V_{mf}	4.71	4.28	42.9		
				46.2	0.0039
Temp. = 700±10°C	6.71	3.91	49.6		
				52.7	0.0028
Bed Wt. = 500 g.	9.18	3.48	55.9		
				58.6	0.0021
	12.06	3.09	61.3		
				63.3	0.0013
	15.61	2.30	65.4		
				67.2	0.0011
	19.61	2.12	69.0		
				70.5	0.00078
	24.06	1.73	72.0		
				73.7	0.0008
	28.46	1.77	75.4		
				76.2	0.00039
	33.69	1.02	77.1		
				78.0	0.00038
	38.94	1.00	78.9		
				79.6	0.00030
	44.41	0.82	80.3		
				80.9	0.00023
	50.06	0.64	81.5		
				82.0	0.00019
	55.81	0.55	82.4		
				82.7	0.00013
	61.76	0.39	83.0		
				83.2	0.00009
	67.83	0.27	83.5		
				83.8	0.00010
	73.88	0.30	84.1		
				84.1	0.000016
	80.21	0.05	84.2		
				84.2	-
	86.58	-	84.2		

TABLE 28 (contd.)

Run No. & Experimental Conditions	t	W	x_{end}	x_{mid}	Rate
B.10	0	-	-		
				5.6	0.0118
-52 +72 # (B.S.S.)	1.07	9.5	11.2		
				15.1	0.0119
particles	1.85	6.95	19.3		
				22.2	0.0058
Flowrate = 114 l. s.t.p./min., or 8.65 V_{mf}	3.00	5.03	25.2		
				28.0	0.0042
	4.52	4.82	30.9		
				33.6	0.0035
Temp. = 600±5°C	6.32	4.66	36.4		
				39.0	0.0024
Bed Wt. = 750 g.	8.72	4.32	41.5		
				44.0	0.0021
	11.39	4.16	46.4		
				48.6	0.0016
	14.59	3.86	50.9		
				53.0	0.0012
	18.51	3.47	55.0		
				56.8	0.00093
	22.93	3.18	58.7		
				60.3	0.00075
	27.95	2.84	62.0		
				63.5	0.00062
	33.45	2.57	65.0		
				66.5	0.00055
	39.27	2.39	67.9		
				69.1	0.00048
	45.42	2.21	70.4		
				71.7	0.00049
	51.55	2.23	73.1		
				74.2	0.00038
	58.25	1.89	75.4		
				76.3	0.00032
	65.30	1.68	77.2		
				78.1	0.00029
	72.52	1.59	79.0		
				79.8	0.00025
	80.37	1.48	80.7		
				81.3	0.00014
	88.84	0.89	81.9		
				82.2	0.00011
	97.64	0.70	82.5		
				82.9	0.000084
	106.69	0.57	83.4		
				83.6	0.000058

TABLE 28 (contd.)

Run No. & Experimental Conditions	t	W	x_{end}	x_{mid}	Rate
B.10 (contd.)	116.02	0.41	83.8		
				84.0	0.00042
	125.54	0.30	84.2		
				84.3	0.00028
	135.11	0.27	84.5		
				84.5	0.00019
	144.94	0.14	84.6		
				84.6	0.000006
	154.89	0.045	84.7		
				84.7	0.000003
	164.91	0.023	84.8		
				84.8	0.0000015
	174.95	0.011	84.8		
				84.8	-
	185.0	-	84.8		
B.11	0	-	-		
				4.4	0.0084
-52 +72 # (B.S.S.) particles	1.18	9.90	8.7		
				11.0	0.00505
	2.21	5.20	13.3		
				15.6	0.0052
Flowrate = 114 l. s.t.p./min., or 8.65 V_{mf}	3.21	5.23	17.9		
				20.1	0.0042
	4.43	5.11	22.4		
				24.6	0.0032
Temp. = 600±10°C	5.98	4.95	26.8		
				28.9	0.0026
Bed Wt. = 1000 g.	7.83	4.82	31.0		
				33.0	0.0019
	10.20	4.60	35.1		
				37.0	0.0015
	13.10	4.35	38.9		
				40.8	0.00125
	16.42	4.14	42.6		
				44.3	0.00104
	20.19	3.93	46.0		
				47.6	0.00081
	24.64	3.62	49.2		
				50.6	0.00060
	29.97	3.20	52.1		
				53.3	0.000465
	36.07	2.84	54.5		
				55.7	0.00041

TABLE 28(contd.)

Run No. & Experimental Conditions	t	W	x_{end}	x_{mid}	Rate
B.11 (contd.)	42.52	2.68	57.0	58.0	0.00037
	49.37	2.50	59.1	60.0	0.00028
	57.00	2.14	61.0	61.9	0.00027
	64.80	2.07	62.8	63.7	0.00026
	72.65	2.05	64.6	65.5	0.00023
	80.83	1.89	66.4	67.2	0.00022
	89.08	1.84	68.0	68.7	0.00019
	97.78	1.64	69.5	70.1	0.00018
	106.61	1.59	70.8	71.4	0.00015
	115.91	1.36	72.0	72.5	0.00012
	125.68	1.14	73.0	73.4	0.00010
	135.73	1.00	73.9	74.2	0.000078
	146.16	0.82	74.6	74.9	0.000056
	157.06	0.61	75.2	75.4	0.000040
	168.28	0.45	75.6	75.7	0.000028
	179.85	0.32	75.9	76.0	0.000013
	191.73	0.16	76.1	76.1	0.000006
	203.75	0.07	76.2	76.2	0.000002
	215.93	0.02	76.2	76.2	-
	228.15	-	76.2		
B.12	0	-	-	4.7	0.0095
-25 +36 # (B.S.S.) particles	1.20	5.30	9.4	14.5	0.0053
	3.02	4.80	19.6		

TABLE 28 (contd.)

Run No. & Experimental Conditions	t	W	x_{end}	x_{mid}	Rate
B.12 (contd.)				23.6	0.0036
	5.52	4.50	27.5		
Flowrate = 144 l. s.t.p./min., or 3.1 V_{mf}				31.1	0.0025
	8.77	4.12	34.8		
				38.1	0.0017
	12.93	3.68	41.3		
Temp. = 600±5°C				44.2	0.0013
	18.00	3.23	47.0		
Bed Wt. = 500 g.				49.5	0.00097
	23.85	2.84	52.0		
				54.1	0.00070
	30.68	2.39	56.3		
				58.2	0.0006
	37.97	2.16	60.0		
				61.6	0.00044
	46.06	1.77	63.2		
				64.5	0.00034
	54.74	1.48	65.8		
				66.9	0.00028
	63.86	1.27	68.0		
				68.8	0.00020
	73.64	0.96	69.7		
				70.4	0.00019
	83.44	0.93	71.2		
				72.4	0.00027
	92.59	1.25	73.5		
				74.4	0.00020
	102.34	0.96	75.3		
				75.9	0.00016
	112.41	0.82	76.6		
				77.3	0.00016
	122.51	0.80	78.1		
				78.7	0.00014
	132.76	0.73	79.4		
				80.1	0.00015
	142.91	0.77	80.8		
				81.3	0.00012
	153.36	0.64	81.9		
				82.4	0.00012
	163.83	0.61	83.0		
				83.5	0.00011
	174.36	0.59	84.0		
				84.5	0.00010
	184.98	0.55	85.0		
				85.4	0.00008

TABLE 28 (contd.)

Run No. & Experimental Conditions	t	W	x_{end}	x_{mid}	Rate
B.12 (contd.)	195.81	0.43	85.9		
				86.1	0.000062
	206.86	0.34	86.3		
				86.5	0.000037
	218.19	0.21	86.6		
				86.6	0.0000086
	229.85	0.05	86.7		
				86.7	-
	241.59	-	86.7		
B.13	0	-	-		
				7.3	0.014
-36 +52 # (B.S.S.) particles	1.18	8.3	14.7		
				18.8	0.0055
	2.88	4.68	22.9		
				26.6	0.0033
Flowrate = 132 l. s.t.p./min., or 5.45 V_{mf}	5.43	4.18	30.3		
				33.8	0.0026
	8.40	3.93	37.2		
				40.6	0.0023
Temp. = 600±8°C	11.63	3.78	44.0		
				47.0	0.00017
Bed Wt. = 500 g.	15.53	3.38	49.9		
				52.4	0.0013
	20.18	2.95	55.0		
				57.2	0.0009
	25.66	2.45	59.4		
				61.2	0.00069
	31.74	2.11	63.1		
				64.8	0.00062
	38.06	1.95	66.5		
				68.0	0.00052
	44.74	1.75	69.6		
				71.0	0.00042
	51.84	1.50	72.4		
				73.9	0.00053
	58.49	1.77	75.5		
				76.7	0.00035
	65.92	1.32	77.8		
				78.8	0.00028
	73.72	1.09	79.8		
				80.4	0.00018
	82.05	0.77	81.0		
				81.6	0.00016

TABLE 28 (contd.)

Run No. & Experimental Conditions	t	W	x_{end}	x_{mid}	Rate
B.13 (contd.)	90.52	0.68	82.3		
				82.8	0.00015
	99.07	0.63	83.4		
				83.9	0.000136
	107.73	0.59	84.4		
				84.8	0.00011
	116.53	0.50	85.2		
				85.6	0.00011
	125.36	0.49	86.0		
				86.5	0.00010
	134.24	0.45	87.0		
				87.3	0.000087
	143.24	0.39	87.6		
				87.9	0.00008
	152.29	0.36	88.2		
				88.3	0.000039
	161.61	0.18	88.5		
				88.6	0.000019
	171.08	0.09	88.7		
				88.7	0.000008
	180.65	0.04	88.8		
				88.8	0.000004
	190.25	0.02	88.9		
				88.9	-
	199.90	-	88.9		
B.14	0	-	-		
				6.8	0.0125
-72 +100 # (B.S.S.) particles	1.23	7.7	13.6		
				18.2	0.0077
	2.58	5.2	22.8		
				27.2	0.0053
Flowrate = 92 l. s.t.p./min., or 11.6 V_{mf}	4.48	5.0	31.6		
				35.6	0.0040
	7.73	4.52	39.6		
				43.5	0.00245
Temp. = 600±5°C	11.31	4.39	47.4		
				50.7	0.0014
	16.76	3.75	54.0		
				56.8	0.00091
	23.79	3.20	59.6		
				61.8	0.00057
	32.67	2.54	64.1		
				65.9	0.00042

TABLE 28(contd.)

Run No. & Experimental Conditions	t	W	x_{end}	x_{mid}	Rate
B.14 (contd.)	42.69	2.07	67.7	69.4	0.00036
	53.34	1.91	71.1	72.7	0.00033
	64.29	1.79	74.4	75.5	0.00023
	76.37	1.41	76.6	77.6	0.00016
	89.50	1.02	78.6	79.4	0.00014
	102.92	0.91	80.2	80.9	0.00010
	116.90	0.73	81.6	81.9	0.000068
	131.53	0.50	82.3	82.5	0.000030
	146.93	0.23	82.7	82.8	0.0000025
	162.90	0.02	82.9	82.9	-
	178.93	-	82.9		
B.15	0	-		8.2	0.0228
-36 +52 # (B.SS.) particles	0.82	9.30	16.4	20.3	0.0094
	1.88	4.98	25.2	29.4	0.0065
Flowrate = 132 l.s.t.p./min., or 6.05 V_{mf}	3.33	4.73	33.6	37.2	0.0036
	5.63	4.16	40.9	44.0	0.0023
Temp, = 700$^{+}_{-}$8°C	8.78	3.62	47.2	50.1	0.0018
Bed Wt. = 500 g.	12.42	3.30	53.1	56.1	0.0016
	16.27	3.14	59.0	61.3	0.00114
	20.90	2.64	63.6	65.6	0.0009
	26.02	2.32	67.7	69.7	0.0008
	31.40	2.14	71.6	73.1	0.0006

TABLE 28(contd.)

Run No. & Experimental Conditions	t	W	x_{end}	x_{mid}	Rate
B.14 (contd.)	42.69	2.07	67.7	69.4	0.00036
	53.34	1.91	71.1	72.7	0.00033
	64.29	1.79	74.4	75.5	0.00023
	76.37	1.41	76.6	77.6	0.00016
	89.50	1.02	78.6	79.4	0.00014
	102.92	0.91	80.2	80.9	0.00010
	116.90	0.73	81.6	81.9	0.000068
	131.53	0.50	82.3	82.5	0.000030
	146.93	0.23	82.7	82.8	0.0000025
	162.90	0.02	82.9	82.9	-
	178.93	-	82.9		
B.15	0	-		8.2	0.0228
-36 +52 # (B.SS.) particles	0.82	9.30	16.4	20.3	0.0094
	1.88	4.98	25.2	29.4	0.0065
Flowrate = 132 l.s.t.p./min., or 6.05 V_{mf}	3.33	4.73	33.6	37.2	0.0036
	5.63	4.16	40.9	44.0	0.0023
Temp, = 700$^{+}_{-}$8°C	8.78	3.62	47.2	50.1	0.0018
Bed Wt. = 500 g.	12.42	3.30	53.1	56.1	0.0016
	16.27	3.14	59.0	61.3	0.00114
	20.90	2.64	63.6	65.6	0.0009
	26.02	2.32	67.7	69.7	0.0008
	31.40	2.14	71.6	73.1	0.0006

TABLE 28 (contd.)

Run No. & Experimental Conditions	t	W	x_{end}	x_{mid}	Rate
B.15 (contd.)	37.30	1.80	74.6		
				76.0	0.00051
	43.52	1.59	77.4		
				78.6	0.00043
	50.02	1.41	79.9		
				80.9	0.00031
	56.99	1.09	81.9		
				82.6	0.00025
	64.22	0.91	83.4		
				83.9	0.00013
	72.07	0.52	84.4		
				84.7	0.00010
	80.10	0.41	85.1		
				85.2	0.000043
	88.48	0.18	85.4		
				85.4	0.000009
	97.05	0.04	85.5		
				85.45	0.000005
	105.67	0.02	85.5		
				85.0	-
	114.30	-	85.5		
B.16	0	-	-		
				6.2	0.0155
-25 +36 # (B.S.S.) particles	0.92	7.0	12.4		
				16.3	0.0079
	2.04	4.41	20.2		
				23.8	0.0062
Flowrate = 163 l. s.t.p./min., or 3.86 V_{mf}	3.36	4.11	27.4		
				30.6	0.0042
	5.08	3.64	33.8		
				36.6	0.0030
Temp. = 700±10°C	7.20	3.16	39.4		
				42.0	0.0027
Bed Wt. = 500 g.	9.45	3.00	44.6		
				47.1	0.0023
	11.88	2.80	49.6		
				51.8	0.00187
	14.56	2.50	54.1		
				56.3	0.00187
	17.24	2.50	58.5		
				60.6	0.0018
	19.97	2.43	62.7		
				63.8	0.0017

TABLE 28 (contd.)

Run No. & Experimental Conditions	t	W	x_{end}	x_{mid}	Rate
B.16 (contd.)	22.75	2.36	67.0		
				69.0	0.0016
	25.63	2.27	71.0		
				73.0	0.0017
	28.41	2.36	75.0		
				76.0	0.0005
	32.38	1.00	76.9		
				77.5	0.00039
	36.48	0.80	78.2		
				78.8	0.00030
	40.71	0.64	79.4		
				79.8	0.00022
	49.39	0.57	81.3		
				81.8	0.00025
	53.71	0.54	82.3		
				82.6	0.00020
	58.11	0.45	83.0		
				83.5	0.00028
	62.39	0.59	84.1		
				84.4	0.00018
	66.81	0.41	84.7		
				85.0	0.00013
	71.33	0.30	85.3		
				85.3	-
	76.10	-	85.3		

BIBLIOGRAPHY

1. Perry, J. (Editor). (1950). Chemical Engineer's Handbook, 3rd ed. p.310. New York: McGraw-Hill.
2. Butts, A. (1943). "Metallurgical Problems", 2nd ed. p.377. New York: McGraw-Hill.
3. Osborn, C.J. (1950). Journal of Metals. 188, p.600
4. Richardson, F.D. and Jeffes, J.H.E. (1948). J. Iron and Steel Inst. 160, p.261
5. Blaskett, D.R. (1958). International Sintering Symposium, Trans. A.I.M.M.E. p.61.
6. Woods, S.E. and Harris, C.F. (1958). International Sintering Symposium, Trans. A.I.M.M.E. p.196
7. Manson, W. McA. (1958). International Sintering Sumposium, Trans. A.I.M.M.E. p.160.
8. Bogan, L.C. and Worner, H.K. (1958). International Sintering Symposium, Trans. A.I.M.M.E. p.94.
9. Matthew, I.G. (1959). Ph. D. Thesis, University of Adelaide.
10. Kitchener, J.A. and Ignatowicz, S. (1951). Trans. Faraday Soc. 47, p.1278.
11. Gomez, R.M. (1960). M. Sc. Thesis, University of Adelaide.
12. Oldright, G. and Miller, V. (1932). U.S. Bureau of Mines Report of Investigation 3183.
13. McIntosh, D.H. (1927). Univ. of Utah Bull. 17, p.8.
14. Zawadski, J. et al. (1926) Roczniki Chem. 6, p.236
15. Edström, J.O. (1953). J. Iron Steel Inst. 175, p.289
16. Stalhane, B. and Malmberg, T. (1930). Jernkontorets Ann., 114, p.600

BIBLIOGRAPHY (contd.)

17. Ezz, S.Y. (1960) Trans. Metallurgical Soc. A.I.M.E., 218, p.709

18. Lloyd, W.A. and Amundson, N.R. (1960). Ind. Eng. Chem. 53, No.1, p.19

19. Dalla Lana, I.G. and Amundson, N.R. (1960). Ind. Eng. Chem. 53, No.1, p.22

20. Olmer, F. (1943). J. Phys. Chem. 47, p.313

21. Parravano, G. (1952). J. Am. Chen. Soc. 74, p.1194

22. Baba, H. (1956). Bull. Chem. Soc. of Japan 29, p.789

23. Pease, R.N. and Taylor, H.S. (1921). J. Am. Chem. Soc. 43 , p.2179

24. Benton, A.F. and Emmett, P.H. (1924) J. Am. Chem. Soc. 46, p.2728

25. Gadsby, J., Hinshelwood, C.N. and Sykes, K.W. (1946) Proc. Royal Soc. (Lond.) A187 p.129

26. Kivnick, A. and Hixson, A. (1952). Chem. Eng. Prog. 48, p.394

27. Lewis, W., Gilliland, E., and Reed, W. (1949). Ind. Eng. Chem. 41, p.1227

28. Lewis, W., Gilliland, E., and McBride, G. (1949). Ind. Eng. Chem., 41, p.1213

29. Johnstone, H., Batchelor, J., and Shen, C. (1955). J. Am. Inst. Chem. Eng. 1, p.318

30. Lewis, W., Gilliland, E., and Sweeney, M. (1951). Chem. Eng. Prog. 47, p.251

31. Culver, R.V., Hamdorf, C.J., and Spooner, E.C.R. (1958). J. Appl. Chem., 8, p.820

32. Collee, R. (1956). Analytica Chimica Acta 14, No.5, p.430

33. Krossin, E. (1948). Zeitschrift für Erzgebau und Metallhuttenweisen 1, No.6,p.167

BIBLIOGRAPHY (contd.)

34. Oldright, G. & Miller, V. (1929). U.S. Bureau of Mines, Report of Investigation No. 2943.

35. Low, A., Weinig, A., and Schoder, W. (1948). "Technical methods of ore analysis", p.287. New York: Wiley.

36. Read, N. Broken Hill Associated Smelters Technical Report, Investigation 4, No.3.

37. McIntosh, D. (1927). Univ. of Utah Bull. 17, p.8.

38. Gilliland, et al. (1949). Ind. Eng. Chem. 41, p.1191-6

39. Kettenring, K.M., et. al. (1950). Chem. Eng. Prog., 46, p.139

40. Morse, R.D., et al. (1951). Ind. Eng. Chem. 43, p.1220-6

41. Askin, J.W., et al. (1951). Chem. Eng. Prog. 47, p.401-4

42. Gilliland, E.R., et al. (1952). Ind. Eng. Chem. 44, p.218-24

43. Van Heerden, C., (1952). J. Appl. Chem. Suppl. Issue 1, p.7-17

44. Leva, M., et al. (1951). Bureau of Mines, U.S. Govt. Printing Office Bulletin 504.

45. Matheson, G.L., et al., (1949). Ind. Eng. Chem. 41, p.1099-104

46. Parent, J.D., et al. (1947). Chem. Eng. Prog. 43, p. 429-36

47. Othmer, D.F. (1956). Fluidisation. Reinhold Publ. Corpn., New York.

48. Lewis, W.K. (1955). Mechanism of fluidisation of powders in gases. Royal Institute.

49. Carman, P. (1937). Trans. Inst. Chem. Eng. 15, p.150

50. Leva, M., Grummer, M., Weintraub, M., and Polchick, M. (1948). Chem. Eng. Prog. 44, p.619

51. Miller, C., and Logwinuck, A. (1951). Ind. Eng. Chem. 43, p.1220

BIBLIOGRAPHY (contd.)

52. Van Heerden, C., et al. (1952). Chem. Eng. Science 1, p.37

53. Cathala, J. (1953). Chem. Eng. Science 2, p.273

54. Othmer, C.F. op. cit. p.53

55. Culver, R.V., Hamdorf, C.J., and Spooner, E.C.R. (1958). J. Appl. Chem., 8, p.810

56. Skapski, A. and Dabrowski, J. (1932). Z. Electrochem. 38, p.365

57. Toomey, R., and Johnstone, H. (1952). Chem. Eng. Prog. 48, p.220

58. Scott, W.W., and Furman, N.H. (1939). "Standard Methods of Chemical Analysis" Technical Press: London. p.500-514, 530-532 and 800-801

59. Ezz, S.Y., and Wild, R. (1960). J. Iron Steel Inst., p.211

60. Mostowitsch, W. (1907). Metallurgie 4, p.654

61. Perry, J. op. cit. p.151

62. Ward, D.H. (1959). M.E. Thesis, University of Adelaide

63. Hamdorf, C.J. (1957). Ph. D. Thesis, University of Adelaide

64. Leva, M. (1957). Chem. Eng. 64, No.11, p.266

65. Shen, C., and Johnstone, H. (1955). J. Am. Inst. Chem. Eng. 1, p.349

66. Perry, J. op. cit. p.1019

67. Korn, A. (1951) Chem. Eng. 57, No.3, p.108

68. Brown, G., and associates. (1950). "Unit Operations", p.79. New York: McGraw-Hill.

69. Lapple, C., and Shepherd, C. (1940). Ind. Eng. Chem. 32, p.605

70. Steinour, H. (1944). Ind. Eng. Chem. 36, p.618

71. Steinour, H. (1944). Ind. Eng, Chem. 36, p.840

72. Steinour, H. (1944). Ind. Eng. Chem. 36, p.901

BIBLIOGRAPHY (contd.)

73. Hariu, O., and Molstad, M. (1949). Ind. Eng. Chem. 41, p.1148

74. Belden, D., and Kassel, L. (1949). Ind. Eng. Chem. 41, p.1174

75. Voght, E., and White, R. (1948). Ind. Eng. Chem. 40, p.1731

76. Clarke, R., et al. (1952). Trans. Inst. Chem. Eng. 30, p.209

77. Cramp, W., and Priestley, A. (1924). Engineering 137, p.34

78. Sittig, M. (1953). Chem. Eng. 60, No.5, p.219

79. Gregory, S. (1952). J. Appl. Chem. 2, Suppl. Issue No.1, S1.

80. Sadler, A. (1949). Chem. Eng. 56, No.5, p.110

81. Farbar, L. (1949). Ind. Eng. Chem. 41, p.1184

82. Anon. (1951). Ind. Chem. 27, p.496

83. Pinkus, O. (1952). J. Appl. Mech. 19, p.425

84. Lapple, C. (1951). Chem. Eng. 58, No.5, p.144

85. Stairmand, C. (1951). Trans. Inst. Chem. Eng. 29, p.356

86. Evans, P., and Kepper, H. (1952). J. Appl. Chem. 2, Suppl. Issue No.1, S33.

87. Perry, J. op. cit. (1950).

88. Stoever, H. (1941). "Applied Heat Transmission", 1st ed. p.103 New York: McGraw-Hill.

89. McAdams, W. (1954). "Heat Transmission, 3rd ed. New York: McGraw-Hill.

90. Colburn, A. (1951). Proc. Inst. Mech. Eng. 164, p.448

91. Ward, D.H. (1959). op. cit. p.45

92. Lewis, W., Gilliland, E., and Bauer, W. (1949). Ind. Eng. Chem. 41, p.1104